DGK Veröffentlichungen der DGK

Ausschuss Geodäsie der Bayerischen Akademie der Wissenschaften

Reihe C | Dissertationen | Heft Nr. 927

Chaiyaporn Kitpracha

The Improvement of VLBI Tropospheric Modeling with a Dense GNSS Network

München 2024

Bayerische Akademie der Wissenschaften

ISSN 0065-5325 ISBN 978-3-7696-5339-7

Diese Arbeit ist gleichzeitig veröffentlicht in:
DepositOnce – Forschungsdaten und Publikationen der Technischen Universität Berlin
https://doi.org/10.14279/depositonce-19110, Berlin 2023 und
GFZpublic – Publikationsdatenbank Helmholtz-Zentrum Potsdam Deutsches GeoForschungsZentrum GFZ
https://doi.org/10.48440/gfz.b103-23045, Potsdam 2023

DGK Veröffentlichungen der DGK

Ausschuss Geodäsie der Bayerischen Akademie der Wissenschaften

Reihe C Dissertationen Heft Nr. 927

The Improvement of VLBI Tropospheric Modeling with a Dense GNSS Network

Von der Fakultät VI – Planen Bauen Umwelt
der Technischen Universität Berlin
zur Erlangung des akademischen Grades
Doktor-Ingenieur (Dr.-Ing.)
genehmigte Dissertation

von

Chaiyaporn Kitpracha, M. Eng.

München 2024

Bayerische Akademie der Wissenschaften

ISSN 0065-5325 ISBN 978-3-7696-5339-7

Diese Arbeit ist gleichzeitig veröffentlicht in:

DepositOnce – Forschungsdaten und Publikationen der Technischen Universität Berlin
https://doi.org/10.14279/depositonce-19110, Berlin 2023 und
GFZpublic – Publikationsdatenbank Helmholtz-Zentrum Potsdam Deutsches GeoForschungsZentrum GFZ
https://doi.org/10.48440/gfz.b103-23045, Potsdam 2023

Adresse der DGK:

Ausschuss Geodäsie der Bayerischen Akademie der Wissenschaften (DGK)

Alfons-Goppel-Straße 11 ● D – 80 539 München

Telefon +49 - 331 - 6264 1685 ● E-Mail post@dgk.badw.de

http://www.dgk.badw.de

Prüfungskommission:

Vorsitzender: Prof. Dr. Jürgen Oberst

Referent: Prof. Dr. Dr. h. c. Harald Schuh

Korreferenten: Prof. Dr. Chris Rizos (UNSW Sydney, Australien)
Prof. Dr. Chalermchon Satirapod (Chulalongkorn University)
Prof. Dr. Jens Wickert

Tag der mündlichen Prüfung: 18.08.2023

ISSN 0065-5325 ISBN 978-3-7696-5339-7

Zusammenfassung

Die vier geodätischen Raumverfahren VLBI (Very Long Baseline Interferometry), GNSS (Global Navigation Satellite System), SLR (Satellite Laser Ranging) und DORIS (Doppler Orbitography and Radiopositioning Integrated by Satellite) liefern Beiträge zum besseren Verständnis des Erdsystems. Ihre Datensätze sind von zentraler Bedeutung für die Realisierung eines präzisen terrestrischen Referenzrahmens (ITRF). Da die einzelnen Messtechniken Stärken und Schwächen für die TRF-Bestimmung aufweisen, werden die Datensätze kombiniert mit dem Ziel, die Schwächen auszugleichen. Der aktuelle ITRF, der Internationale Terrestrische Referenzrahmen 2020 (ITRF2020), ist eine Lösung, die kombinierte Stationskoordinaten an den Kollokationsstationen unter Verwendung lokaler Verbindungsvektoren (local ties), d.h. den Abstandsvektoren zwischen den jeweiligen Referenzpunkten, und kombinierte EOP (Erdorientierungsparameter) liefert. Das globale geodätische Beobachtungssystem (GGOS) stellt an die Lage des Ursprungs des ITRF die wissenschaftlich begründete Genauigkeitsanforderung von 1 mm. Die ITRF2020-Genauigkeit erfüllt diese Vorgabe jedoch nicht ganz. Um dieses Ziel zu erreichen, sind daher innovative Ansätze zu entwickeln.

Die geodätischen Raumverfahren VLBI und GNSS, die Signale im Mikrowellenfrequenzspektrum nutzen, liefern an den Kolokationsstationen Beobachtungsdaten unter den gleichen atmosphärischen Bedingungen. Die Verknüpfung atmosphärischer Parameter kann daher ebenfalls im Ausgleichungsprozess eingesetzt werden. Ähnlich wie die Stationskoordinaten können diese Parameter auch miteinander verknüpft, also kombiniert, werden. Die Verknüpfung troposphärischer Parameter wird als „tropospheric tie“ bezeichnet. Im Gegensatz zu den lokal ties, die mit Totalstationen oder anderen Messgeräten am Referenzpunkt des jeweiligen Sensors gemessen werden, können die troposphärischen ties nur mittels Modellrechnungen bestimmt werden. Dabei werden gegenwärtig zwei verschiedene Ansätze verfolgt. Zum einen erfolgt die Berechnung mittels eines analytischen Modells auf der Grundlage meteorologischer Daten, die aus unterschiedlichen Quellen stammen, beispielsweise meteorologische Sensoren am Messstandort, numerische Wettermodelle (NWM) oder empirische meteorologische Modelle. Zum anderen wird die Methode der Strahlverfolgung (ray tracing) durch ein vom NWM abgeleitetes Brechungsindexfeld eingesetzt. Diese nur aus Modellen berechneten troposphärischen ties weisen notwendigerweise eine begrenzte Genauigkeit auf. Für höhere Genauigkeiten müssen weitere systematische Effekte berücksichtigt werden, die zu Abweichungen zwischen den beobachteten troposphärischen Parametern und den troposphärischen ties führen.

Um diese systematischen Effekte zu untersuchen, werden in dieser Arbeit troposphärische Parameter verglichen, die in GNSS- und VLBI-Analysen berechnet wurden. Die Ergebnisse zeigen, dass signifikante Abweichungen in der vertikalen Signallaufzeitverzögerung (zenith total

delay, ZTD) durch instrumentelle Effekte des GNSS-Verfahrensverursacht werden, insbesondere durch Elevations-abhängige Laufzeitvariationen und Verwendung einer Abdeckvorrichtung „radom“. Abweichungen der horizontalen Gradienten werden hingegen nicht durch das Instrument beeinflusst, sondern durch Mehrwegeffekte, die sich insbesondere auf Beobachtungen bei geringen Elevationswinkeln auswirken. In dieser Studie wird bei VLBI-Messungen kein systematischer Effekt, der instrumentelle Ursachen hat, beobachtet. Der systematische Effekt in den troposphärischen Parametern, der auf das Instrument zurückzuführen ist, wird im Folgenden als „instrumental bias“ bezeichnet. Für die Überprüfung der Hypothese, dass der instrumental bias überwiegend durch instrumentelle Effekte der von GNSS-Beobachtungen abgeleiteten ZTD-Parametern verursacht ist, wurde ein GNSS-Kollokationsexperiment durchgeführt. Die Ergebnisse des Experiments bestätigen diese Hypothese. Des Weiteren zeigt sich, dass der instrumental bias der horizontalen Gradienten, die von GNSS-Beobachtungen bei niedrigen Elevationen abgeleitet wurden, auf multi-pathing zurückzuführen ist. Um den instrumental bias in den ZTD-Parametern zu bestimmen, wurde ein weiteres GNSS-Kollokationsexperiment realisiert. Hierbei wurden Unterschiede in der Phasenzentrumsposition der verschiedenen Antennentypen mittels eines höhenverstellbaren Antennenmasts bis auf wenige Millimeter ausgeglichen. Während der Messung konnte die Position der Antennenreferenzpunkte erfolgreich innerhalb eines Bereichs von 2 mm gehalten werden. Die verbleibenden Abweichungen in den abgeleiteten troposphärischen Parametern sind daher nicht auf troposphärische Effekte sondern lediglich auf instrumentelle Ursachen zurückzuführen.

Möglichkeiten und Grenzen der tropospheric ties werden in dieser Studie durch eine Kombination von VLBI- und GNSS-Beobachtungsdaten auf Normalgleichungsebene (NEQ) untersucht. Die Verwendung von tropospheric ties zeigt signifikante Effekte auf die Kombination von VLBI bzw. GNSS. Eine VLBI-Intratechnikkombination zweier Teleskope an der Kollokationsstation Hobart, Australien, während der CONT14-Messkampagne führt zu einer Genauigkeitssteigerung bezüglich der Stationskoordinaten und der troposphärischen Parameter. Die Untersuchung der tropospheric ties zeigt, dass sie eine Alternative zu den local ties darstellen, z.B. wenn diese fehlerbehaftet sind, insbesondere in der vertikalen Komponente. Die Ergebnisse zeigen, dass VLBI den größten Nutzen aus der Kombination von troposphärischen Parametern mit tropospheric ties zieht, sowohl bei den Stationskoordinaten als auch bei den troposphärischen Parametern. Es wird untersucht, welche zeitliche Auflösung für die Anwendung der tropospheric ties geeignet ist. Die Ergebnisse zeigen ähnliche Resultate für alle Szenarien, sowohl für Stationskoordinaten als auch für troposphärische Parameter. Zum ersten Mal wird eine Kombination von GNSS und VLBI unter Verwendung der tropospheric ties mit einer Korrektur des instrumental bias durchgeführt. Die Ergebnisse zeigen eine signifikante Verbesserung der Stationskoordinaten, insbesondere bei VLBI. Darüber hinaus wird durch die Anwendung der tropospheric ties mit der instrumental bias-Korrektur die Diskrepanz zwischen den local ties und den Ergebnissen aus den geodätischen Raumverfahren deutlich verringert. Bei den troposphärischen Parametern kann durch die Anwendung der instrumental bias-Korrektur jedoch keine Verbesserung nachgewiesen werden. Auch die Folgen der Gewichtung der tropospheric ties wird untersucht. Die Ergebnisse zeigen, dass sich eine hohe Gewichtung positiv auf die Verwendung der tropospheric ties auswirkt. Allerdings müssen systematische Effekte berücksichtigt werden, um eine Verschlechterung der kombinierten Lösung

zu vermeiden. Es ist wichtig darauf hinzuweisen, dass für die Verwendung der tropospheric ties ein vollständiger Satz an local ties erforderlich ist, da die tropospheric ties nicht die Rangdefizite im NEQ-System ausgleichen können.

Abstract

Space geodetic techniques contribute significantly to enhancing our understanding of the Earth system. These techniques include Very Long Baseline Interferometry (VLBI), Global Navigation Satellite System (GNSS), Satellite Laser Ranging (SLR), and Doppler Orbitography and Radiopositioning Integrated by Satellite (DORIS). The primary objective of these space geodetic techniques is to establish an accurate Terrestrial Reference Frame (TRF). Since each technique has its strengths and weaknesses, a combination of space geodetic techniques is employed to overcome the weaknesses in TRF determination. The current TRF, known as the International Terrestrial Reference Frame 2020 (ITRF2020), is determined with a combination of space geodetic techniques through station coordinate parameters at the co-location sites using local ties, which represent the difference between the station coordinates of a space geodetic technique at a co-location site. According to the scientific-driven requirements of the Global Geodetic Observing System (GGOS), the TRF needs to be established with an accuracy level of 1 mm. However, the ITRF2020 has not yet reached this scientific requirement. Therefore, another perspective needs to be investigated in order to reach the scientific-driven requirement for TRF determination.

Microwave-based space geodetic techniques, such as VLBI and GNSS, observe under the same atmospheric conditions and are also included as a parameter in the adjustment process. Therefore, similar to station coordinates, this parameter can also be combined using ties. The ties for tropospheric parameters are referred to as "tropospheric ties". Unlike the local ties, which are directly measured using a total station or other distance measurements at the reference point of the space geodetic technique, tropospheric ties can only be derived through a model. Currently, two different approaches can be used to derive tropospheric ties. The first approach involves using an analytical model with meteorological data from different sources, such as meteorological sensors at the site, a Numerical Weather Model (NWM), and an empirical meteorological model. The second approach involves using the ray-tracing technique through a refraction field of NWM. However, since tropospheric ties can only be derived from the model, their accuracy is limited. To improve their accuracy, it is necessary to address the systematic effects that cause a discrepancy between the observed tropospheric parameter differences and tropospheric ties.

This thesis investigates this discrepancy using the GNSS and VLBI intra/inter technique comparison of tropospheric parameters. The results indicate that the discrepancy is caused by the GNSS instrument, specifically the antenna and radome, in zenith total delay (ZTD) differences. On the other hand, the horizontal gradient difference is affected by multipath effects that occur at low-elevation observations, rather than the instrument. This study observes no systematic effect in VLBI due to the instrument. The systematic effect in

tropospheric parameters due to the instrument is referred to as instrumental bias. To prove this hypothesis, a GNSS co-location site experiment was conducted. The experiment reveals that the instrumental bias in GNSS-derived ZTD parameters originates from the instrument. Furthermore, the bias in GNSS-derived horizontal gradients comes from the multipath effect that occurs at low-elevation observations. To address the instrumental bias, another GNSS co-location experiment was conducted. This experiment employed a vertical steering pole to minimize the height difference of various antenna phase centers to a few millimeters level during antenna changing. The experiment successfully kept the reference point position for each experiment antenna at the same position within a 2 mm level. Thus, the remaining bias in GNSS-derived tropospheric parameters is attributed to the instrumental bias.

This study demonstrates the capability and limitations of tropospheric ties through a combination of VLBI and GNSS on the Normal Equation (NEQ) level. The combination of VLBI and GNSS with tropospheric ties shows a prominent improvement in station coordinates and tropospheric parameters. A VLBI intra-technique combination during CONT14 demonstrated improvements in station coordinates and tropospheric parameters for two telescopes at the Hobart co-location site. Tropospheric ties demonstrate a capability as alternative ties when the local ties are of poor quality, particularly the height component. The results indicate that VLBI received the most benefit when combining tropospheric parameters with tropospheric ties in both station coordinates and tropospheric parameters. The study of proper temporal resolution for applying tropospheric ties was investigated. The results show similar results for all scenarios in both station coordinates and troposphere parameters. For the first time, a combination of GNSS and VLBI utilizing tropospheric ties with an instrumental bias correction is performed. The results show a significant improvement in station coordinates, particularly in VLBI. Furthermore, applying tropospheric ties with an instrumental bias correction considerably reduces the discrepancy between local ties and the space geodetic technique solution. However, there is no improvement in tropospheric parameters from using instrumental bias correction for tropospheric ties. The study also evaluates the impact of weighting tropospheric ties. The results indicate that strong weight provides the most benefit from using tropospheric ties. Nevertheless, systematic effects must be addressed to avoid degradation in the combined solution. It is important to note that one full set of local ties, i.e., both horizontal and vertical components, is necessary to use tropospheric ties since they cannot fulfill rank deficiencies in the NEQ system.

Acknowledgements

I am extremely grateful to all those who have supported and contributed to the completion of this Ph.D. thesis.

First and foremost, I would like to express my deep appreciation to my supervisor, Prof. Dr.-Ing. Dr. h.c. Harald Schuh, for offering me the opportunity to carry out my doctoral studies as a member of the VLBI group at GFZ Potsdam, for providing guidance throughout the course of my work, for facilitating solid research, and for granting me the freedom to pursue my course of studies, as well as providing financial support for conducting doctoral studies. I am also indebted to Dr. Robert Heinkelmann for his fascinating ideas in conducting research and creating a framework for the dissertation, unwavering guidance, encouragement, and invaluable feedback throughout this journey in both my personal and academic life. My gratitude extends to Emeritus Prof. Dr. Chris Rizos for agreeing to evaluate this thesis, providing insightful and constructive feedback, and becoming a part of the defense committee. I am also grateful to Prof. Dr. Chalermchon Satirapod for agreeing to evaluate this thesis, becoming a part of the defense committee, and providing invaluable support and solid knowledge in Geodesy, especially GNSS, during my bachelor's and master's studies, as well as his encouragement and invaluable support to continue a doctoral study in Geodesy. I would like to thank the German Academic Exchange Service (DAAD) for providing the scholarship for my doctoral studies as well as all the necessary support in daily life and financial support in my doctoral studies. All these supports have been crucial to the success of my doctoral studies.

My work at GFZ gave me access to the geoscientific community and exposed me to a host of stimulating ideas, some of which were developed further in the framework of my dissertation. I would like to thank Dr. Benjamin Männel for providing support, knowledge, and invaluable guidance in GNSS data processing, as well as guidance and insightful comments for my publication. I am also indebted to Dr. Markus Ramatschi for supporting the conducting of two GNSS co-location experiments, which is a crucial part of my dissertation, as well as my publication. I would like to thank Dr.-Ing. Kyriakos Balidakis for his idea, insightful feedback, solid knowledge of atmospheric delay, as well as providing atmospheric data from the Numerical Weather Model, which is important for my dissertation and publication. I would also like to acknowledge Dr. Georg Beyerle for his support and guidance in VLBI data analysis with PORT, as well as guidance in functional development for a certain investigation for my dissertation. I am also grateful to Dr. Florian Zus for providing the ray-tracing atmospheric data for an investigation in my dissertation. I want to thank Sylvia Magnussen (IT specialist) for providing solutions to several technical issues instantaneously. I am also grateful to my colleagues in the GNSS and VLBI groups at GFZ who have provided me with valuable insights

and advice throughout this journey. Their support and camaraderie have been an essential source of motivation for me.

I would like to acknowledge the valuable services of ECMWF and VMF Data Server, from which I retrieved data, and the continuous efforts of all the IVS and IGS components over many years for providing high-quality data.

Last but not least, I would like to thank all my friends for their support during my studies. I want to say a heartfelt "thank you" to my parents Supachai and Wanee for their unconditional love, and financial support throughout my life. I want to thank my Danuthida for her encouragement, support, and love. I could not have done it without you.

Lastly, I would like to express my deep appreciation to the countless individuals who have contributed to the advancement of knowledge in my field of study. I am proud to have contributed to this collective effort, and I hope that my work will contribute to further progress in the years to come. I extend my heartfelt gratitude to all the participants who generously shared their time and expertise to make this research possible. This thesis would not have been possible without the contributions and support of each and every one of you, and for that, I am truly grateful.

Table of Contents

List of Figures

List of Tables

Abbreviations

BDS BeiDou Navigation Satellite System

CODE Centre for Orbit Determination in Europe
CPO Celestial Pole Offset
CRF Celestial Reference Frame

DORIS Doppler Orbitography and Radiopositioning Integrated by Satellite

ECEF Earth-centered, Earth-fixed
ECMWF European Centre for Medium-Range Weather Forecasts
EOP Earth Orientation Parameters
ERP Earth Rotation Parameters

GFZ GeoForschungsZentrum
GGOS Global Geodetic Observing System
GLONASS Globalnaya Navigatsionnaya Sputnikova Sistema (The Russian GNSS system)
GNSS Global Navigation Satellite System
GPS The US Navstar Global Positioning System
GPT2 Global Pressure and Temperature model 2
GPT3 Global Pressure and Temperature model 3

ICRF International Celestial Reference Frame
ICRF3 The International Celestial Reference Frame 3
IERS International Earth Rotation and Reference Systems Service
IGS International GNSS service
ITRF International Terrestrial Reference Frame
ITRF2020 International Terrestrial Reference Frame 2020

LLR Lunar Laser Ranging
LOD Length of the Day

MTT The MIT Temperature mapping function

NAVIC Navigation with Indian Constellation
NEQ Normal Equation
NNR No-Net Rotation
NNT No-Net Translation

PNT Positioning, Navigation, and Timing

PORT Potsdam Open-source Radio interferometry Tool

PSD Power Spectral Density

PWLF Piecewise Linear Function

PWV Precipitate Water Vapor

QZSS Japanese Quasi-Zenith Satellite System

SLR Satellite Laser Ranging

TAGPT3 Tropospheric ties Analytical model based on meteorological data from GPT3

TAMET Tropospheric ties Analytical model based on meteorological data from METeorological sensor

TANWM Tropospheric ties Analytical model based on meteorological data from NWM

TAVM3 Tropospheric ties Analytical model based on meteorological data from VMF3

TEC Total Electron Content

TGE East-west component of horizontal gradients

TGN North-south component of horizontal gradients

TR Ray-traced tropospheric ties

TRF Terrestrial Reference Frame

UT1 Universal Time

VGOS VLBI Global Geodetic Observing System

VLBI Very Long Baseline Interferometry

VMF1 Vienna Mapping Functions 1

VMF3 Vienna Mapping Functions 3

WM Weighted Mean

WSTD Weighted Standard Deviation

ZHD Zenith Hydrostatic Delay

ZTD Zenith Total Delay

ZWD Zenith Wet Delay

1 Introduction

1.1 Introduction

Space geodetic techniques consist of observational and computational instruments and methods that provide the solution to a geodetic problem using precise measurements of artificial or natural bodies. These space geodetic techniques include Global Navigation Satellite Systems (GNSS), Very Long Baseline Interferometry (VLBI), Satellite Laser Ranging (SLR), Lunar Laser Ranging (LLR), and Doppler Orbitography and Radiopositioning Integrated by Satellite (DORIS). The most important contributions of space geodetic techniques are the establishment and maintenance of high-accuracy terrestrial and celestial reference frames, the monitoring of Earth's rotation, the study of atmospheric activity, the determination of Earth's gravity field, and the determination of satellite orbits. These techniques are essential for precise positioning and navigation, understanding the dynamics of the Earth's interior and atmosphere, studying the state and variability of the atmosphere, gaining insights into the distribution of mass within the Earth, and enabling satellite-based applications such as navigation, Earth observation, and communication (Altamimi et al., 2016). Table 1.1 indicates which space geodetic technique can be utilized to determine geodetic parameters. For instance, VLBI is capable of determining the full set of Earth Orientation Parameters (EOP). It provides the rotation of the Earth, i.e., UT1-UTC, in absolute terms, and Celestial Pole Offset (CPO), i.e. precession/nutation, with long-term stability, which are valuable information regarding interactions within the Earth system on the transformation between the Celestial Reference Frame (CRF) and the Terrestrial Reference Frame (TRF) (Schuh and Böhm, 2013). Due to deficiencies in the orbit modeling, the satellite techniques GNSS, SLR, and DORIS can only determine the Length of the Day (LOD) and CPO in terms of time derivatives. However, the dynamics of the orbits enable the measurement of the Earth's gravity field by satellite techniques, although this is limited to the low-degree spherical harmonic coefficients (Sośnica, 2014), whereas VLBI is a purely geometrical technique and thus can not contribute to the determination of the Earth's gravity field (Thaller, 2008).

Microwave-based space geodetic techniques, such as VLBI, GNSS, and DORIS, are subjected to atmospheric propagation effects. Regarding atmospheric effects, the atmosphere layers that caused propagation effects are the troposphere, which extends up to approximately 20 km, and the ionosphere, where the density of free electrons and ions is sufficient to cause the propagation of microwave signals over distances between 60 and 2000 km, depending on location and time (Böhm et al., 2013). In terms of the ionosphere, it is a dispersive medium for microwave-based space geodetic techniques. In the ionosphere layer, microwave signals are affected proportionally by the inverse square of their frequencies. Important information for dealing with ionospheric delay is the Total Electron Content (TEC), which is the line integral of electron density along a given ray path (Alizadeh et al., 2013). The ionospheric delay is typically eliminated by a dual frequency ionosphere-free linear combination in VLBI and GNSS techniques for geodetic applications (Kouba and Héroux, 2001; Schuh and Behrend, 2012). Regarding the troposphere delay, this delay is independent of the frequencies of the microwave techniques; therefore, it is impossible to eliminate the tropospheric delay by utilizing multiple frequencies, as was done for the ionosphere. For geodetic applications, the tropospheric delay is typically separated into a dry component and a wet component, each of which is handled separately. The hydrostatic component is a consequence of the total density of air and can be precisely modeled using an empirical model (c.f., Saastamonien model (Saastamoinen, 1972) or the Hopfield model (Hopfield, 1969)) along with atmospheric pressure at the station (Schuh and Böhm, 2013; Subirana et al., 2013a). In contrast, the wet component is challenging to predict empirically due to the high spatial and temporal variability of precipitated water vapor in the troposphere. The wet component varies from a few millimeters at the poles to approximately 40 centimeters over the equatorial regions (Nilsson et al., 2013). To achieve centimeter or sub-centimeter accuracy positioning with microwave-based space geodetic techniques, the wet part is typically determined as the Zenith Wet Delay (ZWD) parameters to correct this effect. Therefore, the parameter estimation process introduces a high correlation between height coordinates, receiver clock offsets, and ZWD (Kouba and Héroux, 2001; Schuh and Böhm, 2013; Subirana et al., 2013a). However, due to the high correlation between ZWD and height coordinates, the effect of ZWD would decrease the stability of the vertical coordinates due to the variability of ZWD. Therefore, a precise ZWD is required to stabilize the height coordinates. To increase the precision of the ZWD parameters, an inter-technique combination of GNSS and VLBI was investigated. Numerous studies, such as Krügel et al. (2007), Diamantidis et al. (2021), and Wang et al. (2022), demonstrated conclusively that a combination of GNSS and VLBI improved the stability of the height coordinates. However, such a combination is only possible at co-location sites between techniques. GNSS and VLBI experience tropospheric effects in the same way, thus demonstrating good agreement between two space geodetic techniques (Puente et al., 2021).

According to the scientific requirements of the Global Geodetic Observing System (GGOS) in establishing TRF, the TRF-defining datum, namely origin, orientation, and scale, of 1 mm accuracy and 0.1 mm/year stability are required (Gross et al., 2009). Individual space geodetic techniques cannot achieve this objective on their own, as their contributions to the determination of TRF have varying strengths and weaknesses. Therefore, it is recommended to combine them in order to achieve the GGOS objective. In order to combine space geodetic

techniques, it is essential to determine their relationship. Local ties, for example, establish the relationship between station coordinates. In general, local ties, which are measured distances between space geodetic techniques' reference points, are provided to combine station coordinates parameters between space geodetic techniques. This method is employed in the determination of the International Terrestrial Reference Frame (ITRF) (Altamimi et al., 2016). In addition, global parameters, such as EOP, are combined directly because they are assumed to be comparable regardless of satellite techniques or geometric techniques. Another geodetic parameter that can be combined is troposphere parameters by utilizing "tropospheric ties". Similar to local ties, tropospheric ties are the differences between tropospheric parameters of the space geodetic technique. Details regarding tropospheric ties will be provided in Section 3.2. Combining tropospheric parameters improves the product derived from space geodetic techniques, particularly when combining VLBI and GNSS. Numerous studies demonstrate the improvement of space geodetic techniques-derived products when combining tropospheric parameters. For instance, Kitpracha et al. (2022) demonstrated the combination of three VLBI parallel networks during the continuous VLBI observation campaign in 2017 (CONT17) and the benefits of combining tropospheric parameters on VLBI-derived station coordinates and tropospheric parameters. The combination of tropospheric parameters on the observation level and its benefit on the TRF and Earth Rotation Parameters (ERP) derived from VLBI and GNSS were demonstrated by Diamantidis et al. (2021); Wang et al. (2022). As demonstrated by Balidakis et al. (2020), combining tropospheric parameters also mitigates the effects of systematic errors introduced by local ties. Therefore, it is beneficial to combine tropospheric parameters in order to improve the estimated parameters from space geodetic techniques, which is essential for space geodesy and related applications.

As mentioned earlier, to combine single-space geodetic technique solutions for determining the global TRF, it is necessary to establish a relationship between non-identical parameters, such as station coordinates and tropospheric parameters (Glaser et al., 2019). In the case of station coordinates, the local ties provide a direct link between the station coordinates of different co-located stations. However, this might not be the case for tropospheric parameters because the estimated parameters may be defined differently depending on the analysis center or software. For instance, one may directly estimate the ZWD, while others may estimate the Zenith Total Delay (ZTD) correction. Therefore, one must exercise caution when applying tropospheric ties during the combination process. Furthermore, many effects are likely to cause a discrepancy between tropospheric ties and observed tropospheric parameter differences. For instance, Kitpracha et al. (2020) analyzed long time series (10 years) of the differences in tropospheric parameters at the Wettzell co-location site using three different GNSS observations (e.g., L1, L2, and the ionosphere-free linear combination of dual-frequency, L3) to estimate tropospheric parameters. They found that an instrumental bias causes a significant bias in tropospheric parameter differences, especially in ZTD. In addition, they found that the instrumental changes caused significant jumps in the time series of the differences in the tropospheric parameters. To improve the geodetic parameters derived from a combination of VLBI and GNSS utilizing tropospheric ties, it is necessary to investigate these effects.

This study aims to clarify the discrepancy between tropospheric ties and observed tropospheric parameter differences in VLBI and GNSS and to propose a calibration method

for an instrumental bias. This thesis also demonstrates how the interaction of tropospheric ties can impact the estimation of station coordinates and tropospheric parameters during the combination of space geodetic techniques. It also discusses the capability and limitations of tropospheric ties in the combination process. The effect of a weighting of tropospheric ties is also investigated. In addition, the impact of applying the instrumental bias correction to tropospheric ties is investigated. Chapter 2 provides an overview of VLBI and GNSS techniques, including the discussion of their differences and similarities. Chapter 3 provides an overview of tropospheric effects and tropospheric ties theory. In addition, an intra/inter-technique comparison of VLBI and GNSS is presented, along with a discussion of the systematic effects found in observed tropospheric parameter differences. Chapter 4 describes two GNSS-colocation experiments and the instrumental bias calibration method derived from these experiments. Furthermore, this chapter demonstrates the approach of combining VLBI and GNSS on the normal equation (NEQ) level, utilizing local and tropospheric ties. Additionally, this chapter provides a detailed investigation into the impact of tropospheric ties during the combination process, including their capabilities and limitations. In addition, a description of the dataset employed in the combination is provided in this chapter. Chapter 5 demonstrates the impact of using tropospheric ties on the geodetic parameters, i.e., station coordinates and tropospheric parameters, obtained from the combination of VLBI and GNSS, as well as a discussion of the results. Chapter 6 provides the conclusion and outlook.

Parameter type		VLBI	GNSS	SLR	DORIS	LLR
CRF	**Quasar positions**	**X**				
	Orbits (satellites, moon)		**X**	**X**	**X**	**X**
EOP	**Celestial Pole Offsets**	**X**				**X**
	Celestial Pole Offset rates	**X**	**X**	**X**	**X**	**X**
	UT1-UTC	**X**				
	LOD	**X**	**X**	**X**	**X**	**X**
	Polar motion	**X**	**X**	**X**	**X**	**X**
TRF	**Station positions**	**X**	**X**	**X**	**X**	**X**
	Geocenter		**X**	**X**	**X**	**X**
	Gravity field		**X**	**X**	**X**	**X**
Atmosphere	**Troposphere**	**X**	**X**		**X**	
	Ionosphere	**X**	**X**		**X**	

Table 1.1: Different characteristics of space geodetic techniques which contribute to the determination of geodetic parameters (modified from (Rothacher, 2002))

1.2 Objectives

- ✓ This research aims to study the characteristics of tropospheric ties and evaluate the performance of the tropospheric ties derivation approaches as well as their uncertainties.
- ✓ Investigate the systematic effects, such as instrumental bias, which results in the discrepancy between tropospheric ties and observed tropospheric parameter differences in VLBI and GNSS through a comparison.
- ✓ Proving any systematic effects founded from VLBI and GNSS intra/inter-technique comparison and propose a founded systematic effect calibration through a novel co-location experiment.
- ✓ Demonstrate the benefit of applying tropospheric ties on geodetic parameters, such as station coordinate and tropospheric parameter in the combination of VLBI and GNSS, as well as its limitations. Moreover, a proper weighting of tropospheric ties in the combination is discussed.
- ✓ Investigate an improvement due to applying instrumental bias correction in tropospheric ties.

2

Space geodetic techniques

The following chapter provides an overview of the microwave space geodetic techniques, GNSS and VLBI, as well as their advantages and disadvantages. Chapter 2.1 describes VLBI, including the fundamental, technical, and observation equations in detail. In addition, the benefits of VLBI and its relevance in geodesy are described in this chapter. Chapter 2.2 provides a general overview of GNSS, including its technical aspects and measurement principles. The details of the observations equation for two primary measurements are presented, along with the systematic effects that occur in their observations. In addition, the application and benefits of GNSS are described. Lastly, Chapter 2.3 describes the strengths and limitations of each technique.

2.1 Very Long Baseline Interferometry

Very Long Baseline Interferometry (VLBI) is one of the four main space geodetic techniques that are purely geometrical. Initially devised as a tool for radio astronomy in the mid-1960s, VLBI swiftly garnered recognition for its potential in geodetic applications. In 1969, VLBI found its potential in geodesy, astrometry, and clock synchronization, demonstrating baseline length accuracies within the range of 2-5 meters and 1 arcsecond for radio source positioning (Schuh and Behrend, 2012). Notably, in 1972, experiments employing the Mark I system achieved a formal error of approximately 70 mm for baseline length, with overall accuracy falling within the range of a few decimeters. By the end of the century, formal errors for the finest global baselines had been reduced to under 1 mm, with accuracies ranging from 5-10 mm. This accomplishment represents a nearly 100 times improvement in accuracy over a quarter-century, primarily attributed to the introduction of the bandwidth synthesis method in the early 1980s to increase the recorded effective bandwidth. Since the 1970s, VLBI has proven to be an essential technique for determining precise coordinates and monitoring Earth rotation and orientation (Schuh and Behrend, 2012).

VLBI is a microwave-based measurement system that determines the difference in signal arrival time from celestial radio sources by cross-correlation. Geodetic VLBI typically employs quasars as radio sources, although satellite beacons have also been employed (Schuh and

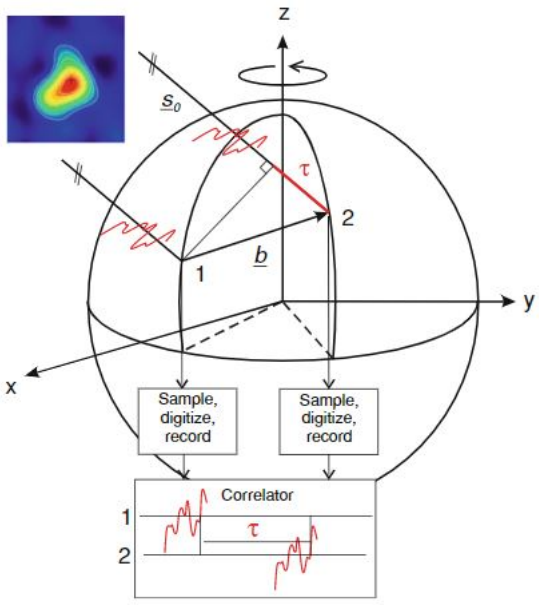

Figure 2.1: The geometric principle of VLBI from Schuh and Böhm (2013).

Böhm, 2013). Two types of measurements are used in VLBI, namely group and phase delays. Phase delays are commonly used in astronomical application, while group delays are mainly used in geodetic application. Therefore, the details of phase delays are not considered in this thesis. However, more information can be found in Sovers et al. (1998). Typically, VLBI radio telescopes with diameters between 10-30 m are used in geodetic VLBI applications. The current geodetic VLBI system frequencies are in the radio spectrum in S and X bands (around 2.3 and 8 GHz).

The principle of VLBI is straightforward. As shown in Figure 2.1, two VLBI radio telescopes receive radio signals in the form of plane wavefronts from extragalactic objects along the unit vector pointing to the radio source $\underline{s}_0$, and they are separated by the baseline vector $\underline{b}$. The reception time difference or time delay τ is calculated between two VLBI radio telescopes. When considering only the pure geometry, the relationship between the geometric delay τ_g, the direction to the radio source s_0, the baseline vector $\underline{b}$, and the speed of light c can be expressed as follows (Schuh and Behrend, 2012):

$$\tau_g = -\frac{\underline{b} \cdot \underline{s}_0}{c} \tag{2.1}$$

The baseline vector $\underline{b}$ is composed of two position vectors, r_1 and r_2, representing the locations of two VLBI radio telescopes. These position vectors are defined in the Earth-centered, Earth-fixed (ECEF) coordinate system, and they incorporate the terrestrial reference frame as well as the inertial reference frame transformation matrix. This transformation matrix R_{EOP} is described by Earth Orientation Parameters (EOP), which consists of CPO, Earth rotation, and polar motion. Thus, Equation 2.1 can be expressed by:

$$\tau_g = -\frac{R_{EOP}(r_1 - r_2).s_0}{c} \tag{2.2}$$

The group delay (time delay) τ is measured by cross-correlation processing data from two or more telescopes. The data at individual VLBI radio telescopes are recorded and time-tagged with very stable frequency standards, such as active hydrogen masers. These recorded data, along with the precise timing data, are digitally recorded and transmitted to a specialized VLBI correlator facility designed for cross-correlation processing. The cross-correlation analysis is performed to determine the time delay between the two digital bitstreams by identifying the point at which they exhibit the highest degree of alignment. To accomplish this, it is necessary to account for the effects of Earth's rotation on the positions of the stations over the integration period. For instance, adjustments must be made to consider the additional path length that the planar wavefront must traverse after reaching point 1 and before reaching point 2 due to the Earth's movement during this interval. The relative delay at which the peak of the cross-correlation function occurs provides a group delay τ (Cannon, 1999). The description of the entire cross-correlation processing will be omitted and it is referred to well-defined literature, e.g., Sovers et al. (1998); Whitney (2000).

In reality, the group delay is corrupted by several systematic effects that have to be taken into account, such as gravitational effects, atmospheric effects, etc. According to Schuh and Behrend (2012), the VLBI fundamental equation can be expressed following:

$$\tau = \tau_g + \delta_{clk} + \delta_{ab} + \delta_{tro} + \delta_{ion} + \delta_{disp} + \delta_{inst} + \delta_{rel} \tag{2.3}$$

where τ_g is geometric delay from Eq. 2.2. δ_{ab} contribute to diurnal and annual aberration. δ_{clk} is a clock synchronization error between telescopes. δ_{inst} is a contribution to the signal delay arising from the propagation delays through on-site cable runs and other instrumentation. δ_{tro} refers to the effects due to the atmospheric propagation delays of Earth's troposphere. δ_{ion} refers to the effects due to the atmospheric propagation delays on Earth's ionosphere. δ_{disp} refers to site displacement effects, such as ocean and atmosphere loading effects. δ_{rel} is a correction due to special and general relativistic effects. Normally, the ionospheric effects can be dealt with in the first order by using two different frequencies, i.e. utilizing a linear combination of group delay measurements at S- and X- bands.

Geodetic VLBI plays an important role in geodesy and related fields. One important role is the precise determination of the Earth Orientation Parameters (EOPs). VLBI measurements of quasars and extragalactic radio sources enable the determination of parameters such as the Universal time (UT1) and celestial pole offsets in a long-term sense (Schuh and Behrend, 2012). In addition, VLBI has played a crucial role in maintaining the International Celestial Reference Frame (ICRF) and ITRF because only VLBI can access both radio sources and station coordinates. VLBI has a significant advantage in determining the ITRF scale because it only depends on the speed of light c, as opposed to satellite-based techniques (Schuh and Böhm, 2013). This enables VLBI to provide a stable scale for the global terrestrial reference frame (Blewitt, 2015; Schuh and Böhm, 2013). VLBI has also been instrumental in monitoring tectonic plate motions and crustal deformation. By determining the precise baseline of VLBI radio telescopes across the continent and observing their relative motions, researchers can gain valuable insights into the dynamics of the Earth's crust. This information is vital for understanding seismic hazards and mitigating natural disasters. Moreover, VLBI has enabled the determination of various geodynamic and astronomical parameters, including the Love

numbers h and l for the Shida number (Krásná et al., 2013). Additionally, the long-term time series of VLBI zenith wet delays are of interest to meteorologists for studying climate processes on Earth. Moreover, they can be utilized to validate troposphere parameters from other space geodetic techniques (Teke et al., 2011). Geodetic VLBI can also observe gravitational deflection caused by massive bodies in the solar system (Schuh and Behrend, 2012).

In accordance with the scientific requirements outlined by the Global Geodetic Observation System (GGOS) (Plag et al., 2009), the existing S/X system, often referred to as the legacy system, falls short of meeting these scientific requirements. Consequently, this shortcoming in the legacy system has led to the development of a next-generation VLBI system known as VLBI2010 or VLBI Global Geodetic Observing System (VGOS). VLBI2010 or VGOS, representing the forefront of VLBI technology, is presently undergoing active development. This innovative system has been meticulously engineered to observe a wide broadband frequency range spanning from 2 to 14 GHz. Furthermore, the antenna is designed with a reduced diameter of 12 m, accompanied by a high data acquisition rate of 8 Gbps or higher, in contrast to the legacy system. These advancements enable the new system to achieve rapid slew rates and enhance sky sampling capabilities, resulting in a substantially increased volume of observations and a significant reduction in error components compared to the legacy system. With this innovative design, it is anticipated that this future system will attain a remarkable accuracy level of 1 mm (Schuh and Behrend, 2012).

Despite this, it is unlikely that VLBI alone can achieve 1 mm accuracy in ITRF determination, as there are numerous factors involved, such as station distribution, source structure, and atmospheric effect. Later, the strengths and weaknesses of VLBI will be discussed.

2.2 Global Navigation Satellite Systems

GNSS is a state-of-the-art satellite-based positioning, navigation, and timing (PNT) system that uses electromagnetic waves traveling at the speed of light to determine a user's position on Earth. These electromagnetic waves operate within the radio spectrum, specifically within the 1.2 to 1.6 GHz range, which falls within the L-band. This frequency range has been deliberately chosen for GNSS signals due to several advantageous factors. Firstly, it allows for measurements with a satisfactory level of precision. Secondly, it facilitates the design of relatively uncomplicated user equipment. Lastly, these signals are not significantly attenuated by the atmosphere under typical weather conditions. Within this frequency range, GNSS signals exhibit a wavelength spanning approximately 19 to 25 cm. Similar to early radio navigation systems like Transit, GNSS systems transmit signals across multiple frequencies to compensate for ionospheric delays in their measurements (Langley et al., 2017). Nowadays, the GNSS constellations include the US Navstar Global Positioning System (GPS), the Russian Globalnaya Navigatsionnaya Sputnikova Sistema (GLONASS), the European Galileo, the Chinese BeiDou (BDS), the Japanese Quasi-Zenith Satellite System (QZSS), and the Navigation with Indian Constellation (NAVIC).

The GNSS system is composed of three segments. The first is the space segment, which includes satellites orbiting in space. The second is the control segment, which is responsible

for monitoring and managing the satellites. The third segment is the user segment, which receives signals from the satellites in space and calculates the user's position on the Earth's surface. Figure 2.2 illustrates the architecture of the GNSS system.

The primary functions of the space segment involve generating and transmitting signals, as well as storing and broadcasting the navigation message provided by the control segment. The precision of these transmissions is ensured by highly accurate atomic clocks onboard the satellites. GNSS space segments consist of constellations of satellites, ensuring there are enough satellites for users to consistently access a minimum of four satellites from any location on Earth at any given time. Satellites are equipped with various structures and mechanisms to maintain their orbital paths, communicate with the control segment, and transmit signals to receivers. One critical component in GNSS is the satellite clocks, which use atomic clocks known for their exceptional stability, such as rubidium, cesium, and hydrogen maser clocks.

The GNSS control segment is another crucial part of the system, responsible for control and maintaining the space segment. It consists of a network of ground stations with the primary duty of tracking satellites and collecting information about their condition and the arrangement of the satellite constellation. This collected data is used for determining key parameters like satellite ephemeris and clock evolution, among others. These parameters are then used to update the navigation messages for all the satellites. Furthermore, the control segment is responsible for ensuring the stability of the GNSS time scale.

The user segment involves GNSS receivers on the ground, at sea, in the air, and even in space, which are responsible for receiving GNSS signals, determining pseudoranges and other observables, and then solving navigation equations to determine the coordinates and deliver highly accurate time information. A standard GNSS receiver is composed of essential components, such as an antenna with preamplification, a radio frequency module, a microprocessor, an intermediate-precision oscillator, a power supply unit, storage for data, and a user interface. The determined position is referenced to the antenna's phase center.

The specific information for each GNSS constellation, including the characteristics of the satellites, the control segment, and the mechanism of the GNSS receiver can be found in well-established literature, such as Teunissen and Montenbruck (2017).

A fundamental principle of GNSS is measuring the signal propagation time from the satellite to the receiver, which is then multiplied by the speed of light c, to determine the distance. GNSS observations typically consist of three types of measurements: pseudorange, carrier phase, and Doppler measurements (Langley et al., 2017). Pseudorange is a standard observation in positioning and navigation, with a precision at the decimeter level. It is determined by calculating the difference between the time of signal transmission and reception, and scaling it by the speed of light. Carrier phase is determined by measuring the beat frequency between the transmitted signal and a frequency generated by the receiver at the time of reception. This measurement is much more precise than pseudorange measurement (typically two orders of magnitude higher) (Subirana et al., 2013a) and is therefore used in high-precision applications. Doppler measurement observes the rate of change in range caused by the frequency shift at the receiver, which is known as the Doppler effect. The determination of pseudorange observable (time of flight) and Doppler shift is done simultaneously, but Doppler shift is not considered for geodetic data analysis, whereas the pseudorange observable is exploited for the determination

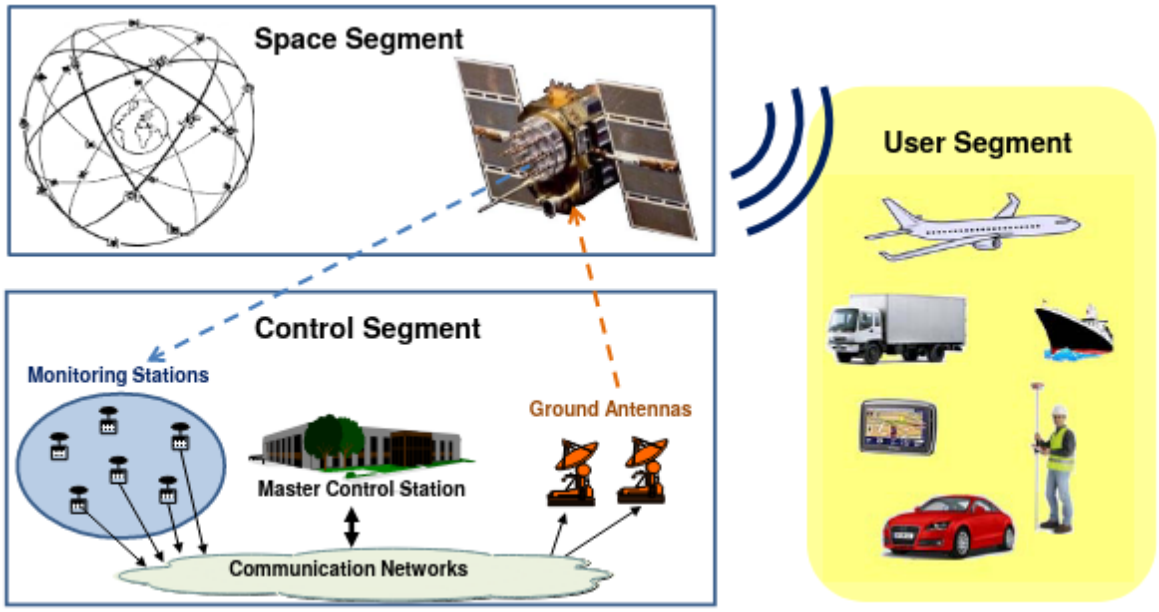

Figure 2.2: The GNSS is comprised of three key segments: the space segment, the control segment, and the user segment. This figure is taken from Subirana et al. (2013b).

of geodetic parameters. However, GNSS measurements are affected by various systematic effects that cause an additional delay to the GNSS measurements, such as signal propagation effects due to the atmosphere, satellite and receiver clock errors, etc. Therefore, to take all necessary systematic effects into account, the GNSS pseudorange observation equation R_r^s can be expressed as:

$$R_r^s = \rho_r^s + (\delta t_r - \delta t_s)c + \delta_{tro} + \delta_{ion} + \delta_{disp} + \delta_{rel} + \epsilon, \tag{2.4}$$

where c represents the speed of light, and subscripts r and superscripts s indicate the receiver and satellite, respectively. The GNSS signal emission time and reception time are denoted by t_s and t_r, respectively. δt_r and δt_s denote the receiver and satellite clock offsets from the GNSS system time. δ_{tro} and δ_{ion} are the tropospheric and ionospheric effects. δ_{rel} denotes the relativistic effects, while δ_{disp} accounts for site displacement effects, such as ocean and atmosphere loading effects. Finally, ϵ represents the unmodeled effects and other small effects. The geometric distance between the satellite and receiver is denoted by ρ_r^s, which is given by the following equation:

$$\rho_r^s = \sqrt{(x_s - x_r)^2 + (y_s - y_r)^2 + (z_s - z_r)^2} \tag{2.5}$$

where the satellite coordinates (x_s, y_s, z_s) and the receiver coordinates (x_r, y_r, z_r) are typically both given in the ECEF coordinate system (Xu and Xu, 2016).

Similarly, the carrier phase observation equation (ϕ_r^s) is presented as:

$$\phi_r^s = \rho_r^s + (\delta t_r - \delta t_s)c + \lambda N_r^s + \delta_{tro} - \delta_{ion} + \delta_{disp} + \delta_{rel} + \epsilon, \tag{2.6}$$

where λ represents the carrier wavelength, and N_r^s is the integer carrier phase ambiguity number. The observation equations 2.4 and 2.6 can be formulated not only for GNSS

fundamental frequency but also for any linear combination. Depending on which linear combination is used, some terms might disappear from the equation. For example, the geometric distance ρ_r^s disappears in the case of the geometry-free linear combination or δ_{ion} in the case of the ionosphere-free linear combination. Forming differences between stations or satellites is also beneficial since it removes some parameters from the equations. Although the full derivation of the fundamental equation and details about different linear combinations and forming differences are omitted here, they can be found in well-established literature such as Odijk (2017).

GNSS provides position measurements with accuracies ranging from meters to millimeters through sophisticated data analysis employing the equations mentioned above. GNSS has a wide range of applications across various domains, including the mass market, civil and military sectors, and scientific research. One of the most common uses of GNSS is in everyday navigation, including car and other transportation modes, marine vessel navigation, aviation, and aircraft control, such as approach and landing at airports. GNSS also facilitates the tracking of individuals, vehicles, and aircraft, with GNSS-derived positions relayed through supplementary communication channels, like mobile phones or dedicated devices, for Search and Rescue operations. One of the earliest high-precision applications of GNSS involved surveying and geodesy using carrier-phase measurements, enabling the establishment of precise coordinates and geodetic markers. These carrier-phase measurements subsequently found utility in other fields, such as machine control, aerial photogrammetry, and high-precision agriculture. Furthermore, carrier-phase measurements are employed for precise orbit determination in the new generation of Low-Earth orbit satellites equipped with GNSS receivers. GNSS also provides precise clock parameters (see Equation 2.6), enabling its use in global synchronized timing systems, particularly for time-tagging in financial trades. Additionally, GNSS timing is instrumental in the telecommunication industry for synchronizing mobile phone networks.

Furthermore, GNSS plays a pivotal role in Earth system monitoring through the extensive GNSS networks of continuously operating tracking stations. It is used to assess long-term tectonic plate motion, monitor Earth surface phenomena like landslides and volcanic activity, and aid in accurate earthquake predictions, potentially saving lives. GNSS also serves as an invaluable tool for atmospheric sensing by analyzing the effects of GNSS signals as they passage through the ionosphere and lower atmosphere. This allows for mapping the ionosphere's variable electron content and quantifying water vapor levels in the troposphere. Several national weather services rely on GNSS-derived water vapor measurements to enhance weather forecasts (De Haan et al., 2019). GNSS also aids in comprehending ionospheric processes, which is crucial given their potential of bad weather in the ionosphere to disrupt communication, navigation, and power systems. By examining the impact of earthquakes and tsunamis on ionospheric electron density, GNSS-based ionospheric sensing can contribute to tsunami warning systems (Langley et al., 2017). The GNSS demonstrates its potential in climate monitoring through ground-based and radio occultation GNSS data, particularly in monitoring precipitate water vapor (PWV) trends and temperature structure, which are important in the study of global warming (Jones, 2020).

In the field of geodesy, GNSS plays a key role in determining the International Terrestrial Reference Frame (ITRF) with sub-centimeter accuracy, marking a significant achievement in

the field. However, GNSS alone cannot achieve the millimeter-level accuracy required by the Global Geodetic Observing System (GGOS) or the estimation of a full set of Earth Orientation Parameters (EOP). The limitations of GNSS are further discussed in the following subsection.

2.3 Similarities and differences between VLBI and GNSS

It is worthwhile to provide some insights into the similarities and differences between VLBI and GNSS techniques. By considering the observation equations (Equation 2.3 and Equation 2.6), both methods yield various products through data analysis. Table 1.1 enumerates common and distinct products offered by both VLBI and GNSS. For instance, station coordinates and velocities derived from VLBI and GNSS are jointly employed to realize the ITRF.

Concerning data analysis, GNSS analysis can be conducted either in real-time or through post-processing, contingent upon the specific application. Conversely, VLBI data analysis is exclusively carried out through post-processing, owing to the limitations of correlation centers. Furthermore, GNSS allows continuous observations throughout a campaign or as part of a permanent tracking network, whereas VLBI observations occur on a weekly basis, typically once or twice a week.

In the view of the realization of ITRF, VLBI offers a distinct advantage over GNSS owing to its extensive historical record of measurements, tracing back to the early 1970s. In contrast, GNSS commenced observations in the 1990s with the introduction of GPS (Schuh and Böhm, 2013). VLBI stands as the sole technique with access to quasars, enabling the establishment of a stable CRF. Additionally, VLBI facilitates the comprehensive observation of Earth Orientation Parameters (EOP) (Schuh and Böhm, 2013), whereas satellite-based techniques like GNSS can only contribute to the Earth Rotation Parameters (ERP), comprising Length-of-Days (LOD) and polar motion. Furthermore, VLBI significantly contributes to the scale of the ITRF as the precise group delay done in the time domain are convert to the distance just applying the speed of light (Schuh and Behrend, 2012). In contrast, GNSS falls short in providing a stable scale for the ITRF due to uncertainties in their antenna phase center definition (Villiger et al., 2020). Since VLBI is a purely geometric technique, it lacks access to the geocenter and gravity field, unlike GNSS, which can access these through satellite orbits. Consequently, GNSS contributes to establishing the ITRF origin along with other satellite-based technique, e.g. SLR. GNSS holds an advantage in terms of spatial coverage, as the equipment is compact and easily deployable globally. In contrast, VLBI radio telescopes are costly and require specific environmental conditions for installation. Figure 2.4 illustrates the global GNSS network, operated by the International GNSS Service (IGS), comprising over 500 stations. On the other hand, VLBI comprises a network of 40 radio telescopes around the globe, as depicted in Figure 2.3, coordinated by the International VLBI Service for Geodesy and Astrometry (IVS). This contrast underscores GNSS's superiority in network geometry, with coverage in all parts of the world, while the primary orientation of the VLBI network is focused the northern hemisphere. This may introduce a bias in the TRF realization if VLBI is employed as the datum for the network.

Since VLBI and GNSS are microwave-based techniques, they are susceptible to tropospheric effects (as demonstrated by Eqs. 2.3 and 2.6). These effects are typically treated as parameters

in data analysis. Tropospheric parameters derived from VLBI and GNSS observations are also essential products contributing to the development of meteorological models and providing an independent validation method for climate time series (Heinkelmann et al., 2011). GNSS serves as a valuable tool in atmospheric sensing due to its ability to provide continuous data and a reasonable view of the sky. This enables the generation of continuous time series for meteorological parameters, especially Precipitable Water Vapor (PWV). However, GNSS equipment is prone to change after extended use, resulting in discontinuities in GNSS time series products, which limit long-term studies. In contrast, the VLBI reference point remains stable throughout the history of observations, offering an advantage in long-term PWV monitoring, a crucial aspect for climate studies. Additionally, both VLBI and GNSS are affected by ionospheric effects, which can be mitigated by employing a linear combination of two frequency observations. Both techniques are also utilized to study ionospheric effects, particularly as ground-based Total Electron Content (TEC) measurements. Nevertheless, given GNSS's advantages in terms of global coverage and continuous data, it is preferred over VLBI, as demonstrated by the community's preference for using GNSS to operationally derive a global map of TEC and to study space weather-related phenomena.

In conclusion, GNSS are employed across a wide range of applications, not only for navigation but also for scientific and other high-precision purposes. In contrast, VLBI is primarily utilized for scientific research. A robust GNSS network with continuous data provides GNSS with a significant advantage as a valuable tool in numerous scientific fields and spatial applications. However, the long-term stability of VLBI is one of its advantages over GNSS, as VLBI does not require frequent equipment changes like GNSS. Therefore, VLBI can be employed to calibrate certain GNSS-derived products, enhancing their long-term stability, which is essential for many studies, such as total water vapor content monitoring. Furthermore, concerning the realization of the ITRF, VLBI and GNSS exhibit distinct strengths and weaknesses in determining global TRF parameters such as EOP, scale, and origin. Therefore, the current approach in the ITRF realization combines VLBI and GNSS observations with other space geodetic techniques (SLR and DORIS) to maximize their strengths and compensate for the weaknesses of each technique.

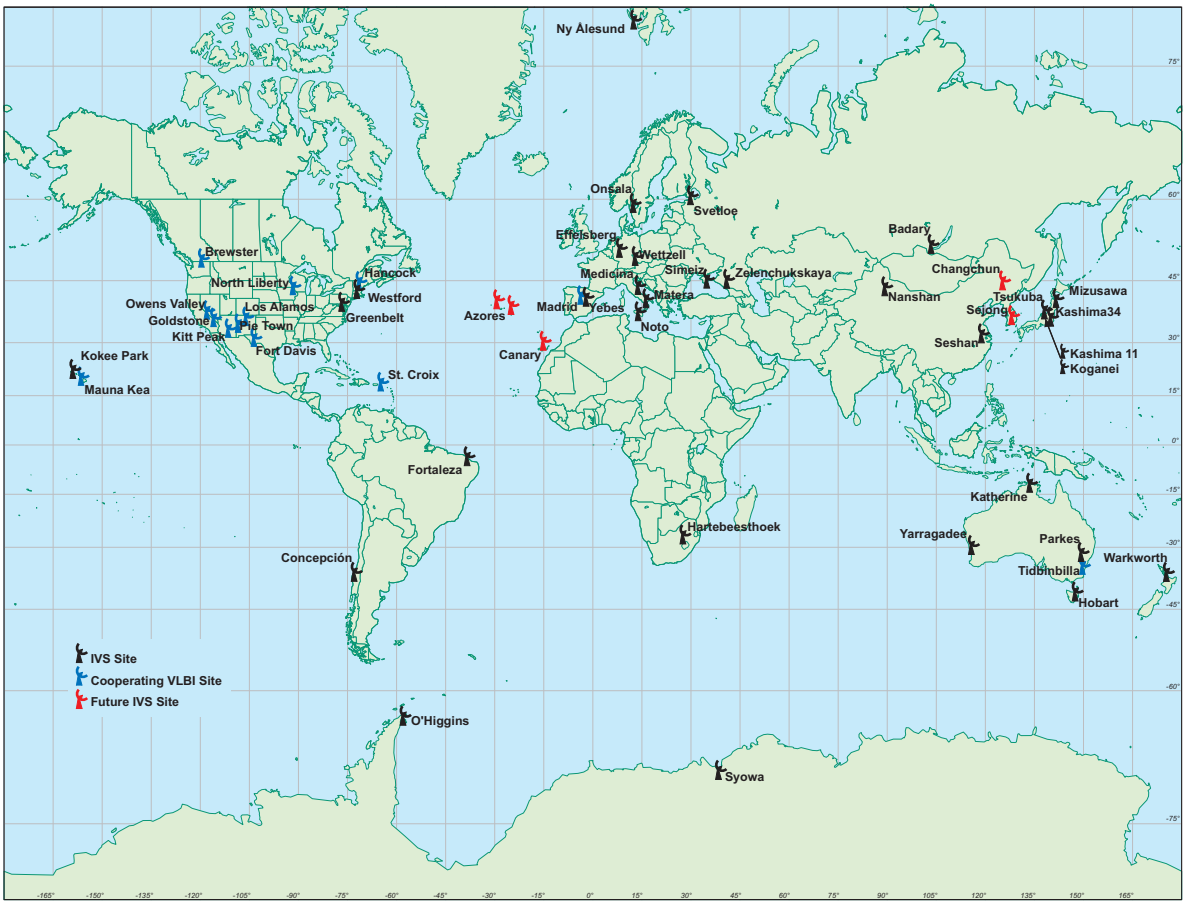

Figure 2.3: Locations of the 40 VLBI radio telescopes in the global network of the IVS (Courtesy from IVS).

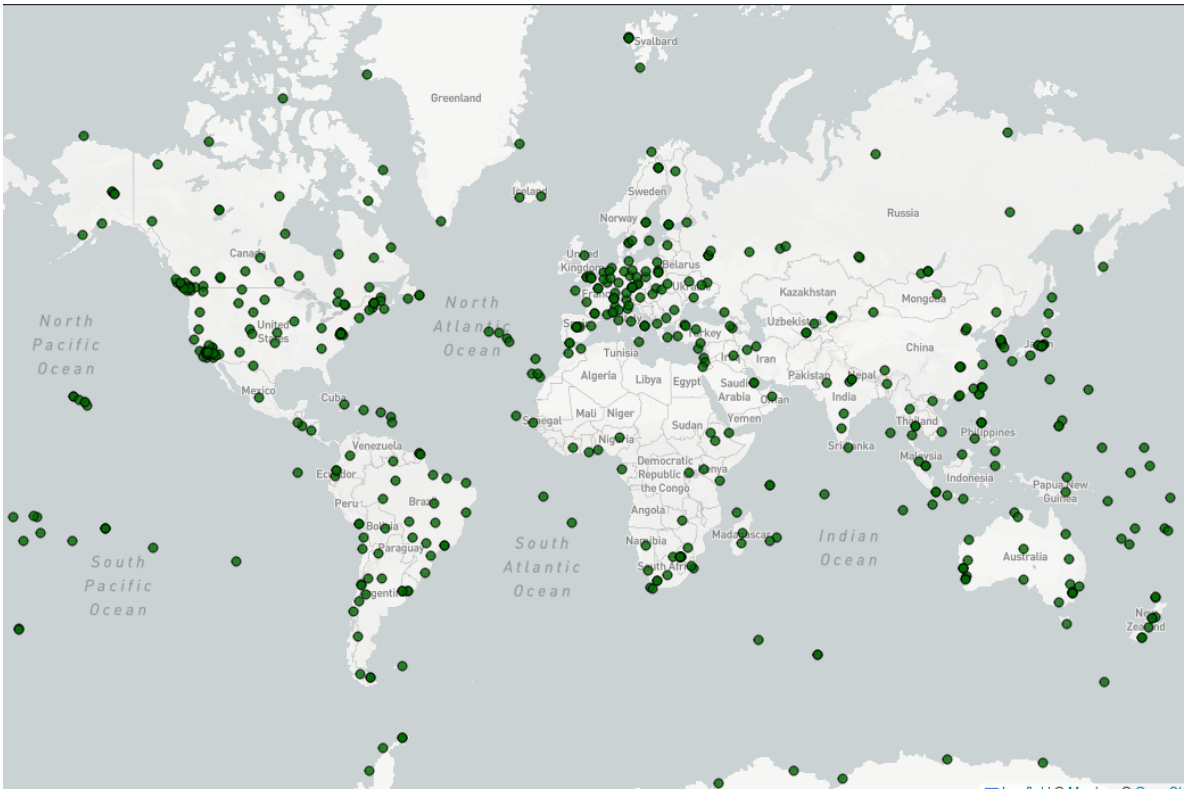

Figure 2.4: Locations of the more than 500 GNSS stations of the global tracking network of the IGS as of September 2023 (Courtesy from IGS).

3

The comparison of space geodetic technique's atmospheric delay

The following chapter describes the influence of the troposphere on GNSS and VLBI observations. Several aspects will be discussed in the upcoming chapters. Chapter 3.1 focuses on the effect of the troposphere on microwave-based space geodetic techniques, such as GNSS and VLBI. Additionally, the chapter explains how to model the tropospheric effect and parameterize it for data analysis. In Chapter 3.2, an overview of "tropospheric ties" is provided, which is the most crucial information for combining tropospheric parameters and the primary subject of this thesis. The chapter describes various approaches to derive tropospheric ties and their characteristics. Furthermore, Chapter 3.3 discusses the discrepancies between the tropospheric ties model and those obtained from space geodetic techniques. Chapter 3.3.1 presents a GNSS intra-technique comparison of tropospheric parameters at co-location sites. It also includes a discussion of effects that are not associated with the theory of tropospheric ties. In Chapter 3.3.2, a VLBI intra-technique comparison is discussed. Finally, Chapter 3.3.3 provides a comparison of GNSS and VLBI tropospheric parameters and a discussion of their results.

3.1 Impact of tropospheric effects on VLBI and GNSS.

The troposphere, the lowest layer of Earth's atmosphere, comprises approximately 80% of the atmosphere's mass and contains 90% of its water vapor and aerosols. Its lower boundary is the Earth's surface, and it extends up to 20 kilometers above sea level, as shown in Figure 3.1, although its height varies depending on the location (Hobiger and Jakowski, 2017). The troposphere is responsible for causing refraction on electromagnetic signals in the microwave frequency range due to dry gases and water vapor, which leads to significant delays in signal propagation of microwave-based space geodetic techniques, such as VLBI and GNSS, a phenomenon known as tropospheric delays. Unlike the ionosphere, the troposphere is a non-dispersive medium at VLBI and GNSS carrier frequencies, which implies that multi-frequency

combinations cannot be used to eliminate the troposphere's effects. Tropospheric delays consist of two components: the hydrostatic and the wet components. The hydrostatic component, which results from tropospheric dry gases, accounts for 90% of the total delay and can be accurately predicted with an empirical model, such as the Saastamonien model (Saastamoinen, 1972), based on the pressure value at the site. Hobiger and Jakowski (2017) demonstrated that the hydrostatic component's variation is minimal, about 1% within a few hours. The wet component, which primarily consists of water composites in the atmosphere, such as water vapor and condensed water in the form of clouds, contributes less to the tropospheric effect. However, it is difficult to determine the wet component with precision using an empirical model, given the high spatial and temporal variability of water vapor and weather conditions. The wet component's variation differs depending on location, varying by a few millimeters at the poles and up to 40 cm in equatorial regions (Nilsson et al., 2013). Currently, deriving an empirical model of the wet part remains challenging.

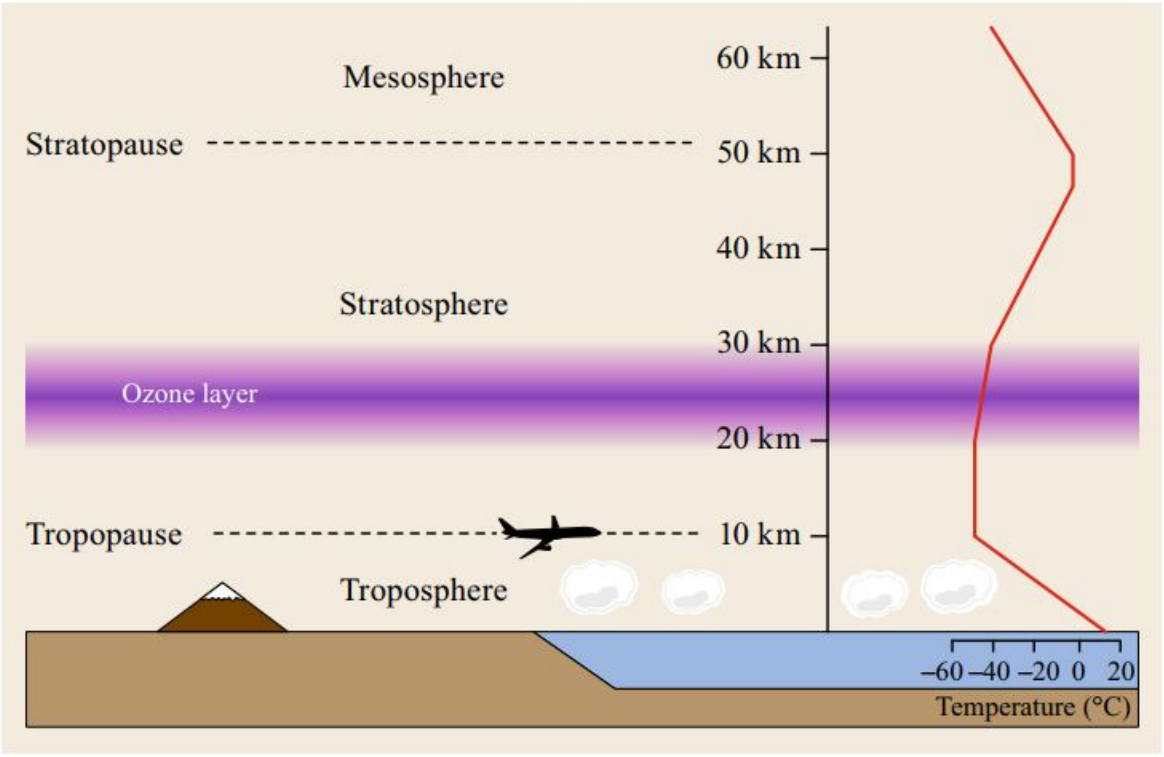

Figure 3.1: The Earth's atmospheric layers, indicating their respective altitudes above the surface. The troposphere represents the lowest layer, succeeded by the stratosphere and mesosphere. Adapted from Hobiger and Jakowski (2017).

The tropospheric effects $\rho_{tro}(e)$ at an elevation angle e is represented in the zenith direction product ρ^z_{tro} along with an elevation-dependent mapping function $mf(e)$:

$$\rho_{tro}(e) = \rho^z_{tro}.mf(e) \tag{3.1}$$

As mentioned above, the tropospheric effect consists of two parts. The hydrostatic part in the zenith direction refers to the Zenith Hydrostatic Delay (ZHD). The wet part in the zenith

direction is introduced as Zenith Wet Delay (ZWD). The combination of two parts refers to Zenith Total Delay (ZTD). This relationship can be expressed as:

$$\rho_{tro}^{z} = \rho_{zhd} + \rho_{zwd} \tag{3.2}$$

In space geodetic data analysis, the ZHD is easily modeled using surface pressure measurements. However, the ZWD cannot be precisely determined with meteorological information at the surface. Therefore, it is commonly determined as a parameter in the data analysis. To derive ZHD, various empirical models are available for calculation, such as the Saastamonien model (Saastamoinen, 1972) and the modified Hopfield model (Hopfield, 1969). According to the current conventions of the International Earth Rotation and Reference Systems Service (IERS) (Petit and Luzum, 2010), the Saastamonien model is recommended to determine ZHD in data analysis. The Saastamonien model for ZHD derivation can be expressed as:

$$\rho_{zhd} = 0.0022768 \frac{p_0}{(1 - 0.00266\cos(2\theta) - 0.28 \times 10^{-6} h_0)}, \tag{3.3}$$

where p_0 is the surface pressure in hPa, and θ and h_0 are the latitudes and orthometric (or ellipsoidal) heights of the station. As previously mentioned, surface pressure is a crucial parameter to determine ZHD. An error of 1 hPa in surface pressure causes an error of 2.3 mm at sea level, which affects station coordinates, especially the height component, estimated from space geodetic techniques. To achieve the scientific-driven requirement by the Global Geodetic Observing System (GGOS), a pressure accuracy of 0.05 hPa is required (Nilsson et al., 2013). To acquire accurate pressure values, a pressure sensor is recommended to be installed at the site. If a pressure sensor is not available at the site, values retrieved from Numerical Weather Models (NWM) or empirical models can be used (Elgered and Wickert, 2017; Nilsson et al., 2013; Schuh and Böhm, 2013). For the latter choice, the most prominent models are UNB3m (Leandro et al., 2006), Global Pressure and Temperature 2 (GPT2) (Lagler et al., 2013), and Global Pressure and Temperature 3 (GPT3) (Landskron and Böhm, 2018). According to the current IERS conventions, GPT2 is recommended as an empirical model for data analysis. However, wet delays cannot be accurately predicted using an empirical model despite providing accurate meteorological information. For less precise applications, an empirical model may be used to derive ZWD. For instance, the Saastamonien model is based on an assumption derived from the ideal gas law, as shown in Equation 3.4:

$$\rho_{zwd} = 0.0022768\,(1255 + 0.05T_0)\,\frac{p_{w0}}{T_0}, \tag{3.4}$$

where p_{w0} is the water vapor pressure at the surface and T_0 is the temperature at the surface. Both quantities can be obtained from meteorological sensors at the site, similar to surface pressure data. Typically, the meteorological sensor does not directly provide the water vapor pressure, but rather the relative humidity. However, the relative humidity can be converted to water vapor pressure by using the Magnus equation (Alduchov and Eskridge, 1996) to obtain the saturated water vapor pressure Es:

$$Es = 6.1094 \cdot \exp^{(\frac{17.625.T}{T+243.04})} \tag{3.5}$$

where T is the temperature in degree Celsius (°C). Subsequently, the water vapor pressure is calculated using the relationship of the relative humidity, the saturated water vapor pressure, and the water vapor pressure:

$$f = \frac{p_{w0}}{Es} \cdot 100 \tag{3.6}$$

where f is the relative humidity in %. If no surface meteorological measurement is available from the sensor, it can also be directly extracted from NWM or using empirical models, such as GPT2 or GPT3. Additionally, the ZWD can be extracted from NWM without relying on any models provided by sources like the station-wise Vienna Mapping Functions 1 (VMF1) (Boehm et al., 2006). However, the ZWD still needs to be estimated in data analysis for high-accuracy applications, such as geodesy.

It is worth noting that all empirical models mentioned above are provided in the zenith direction. However, the actual observations is refered to slant direction. Therefore, it is required to project the delays in zenith angle to an observed angle (see Figure 3.2). It is necessary to have an essential information for projecting delays in the zenith angle to the observed angle. This information is referred to as mapping functions. The mapping function

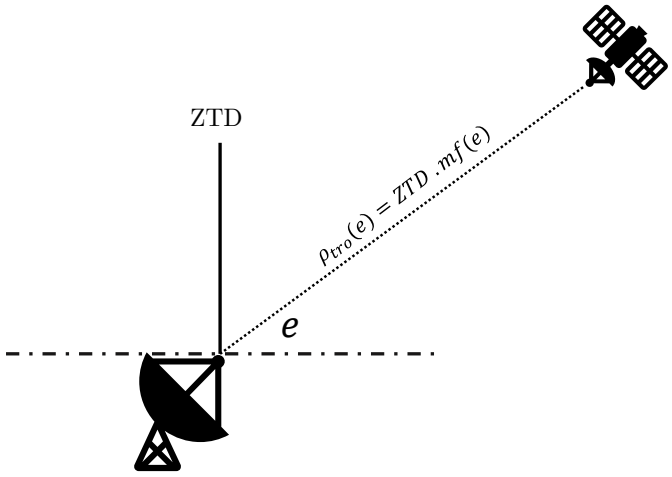

Figure 3.2: The relationship between ZTD and the tropospheric delay at the observed angle. The mapping function $mf\,(e)$ provides essential information to convert ZTD into the tropospheric delay at the observed angle.

has been extensively studied and developed in the past. Marini (1972) proposed the derivation of mapping function with the continued fraction form, which is independent of the azimuth of observations, as demonstrated in Equation 3.7. This continued fraction form is widely used in the analysis of space geodetic techniques nowadays.

$$mf\,(e) = \frac{1 + \frac{a}{1+\frac{b}{1+c}}}{sin\,(e) + \frac{a}{sin(e)+\frac{b}{sin(e)+c}}} \tag{3.7}$$

As demonstrated by the mapping function in continued fraction form (Eq. 3.7), it requires the coefficients a, b, and c. Consequently, numerous researchers have developed coefficients for the

mapping function. The most prominent analytical function is the MIT Temperature mapping function (MTT) proposed by Herring (1992) based on the continued fraction form. However, the MTT mapping function coefficients are highly dependent on temperature (Elgered and Wickert, 2017), resulting in numerous improvements in the derivation of mapping function coefficients that are independent of temperature. According to current IERS conventions (Petit and Luzum, 2010), the VMF1 is recommended for the analysis of space geodetic techniques because it provides the highest accuracy. The VMF1 is derived from ray-tracing through refractivity profiles of an NWM at 3 degrees for the hydrostatic and wet components. The VMF1 provides a discrete time series of coefficient a with time resolutions of 6 hours. The c coefficients, on the other hand, are provided by an empirical function. The literature regarding mapping functions can be found in many geodesy-related works, e.g., Elgered and Wickert (2017).

It is important to note that errors in mapping functions can impact the estimated station height coordinate. Schuh and Böhm (2013) and Nilsson et al. (2013) conducted a simulation study to investigate the impact of an incorrect mapping function and pressure values. For instance, errors of 0.1 and 0.01 in the wet and hydrostatic mapping functions at a 5° elevation angle lead to a station height error of 4 mm.

As previously discussed, zenith delays and mapping functions are based on the assumption of azimuthal symmetry of the neutral atmosphere at the site. However, due to regional climatic and meteorological phenomena, the delays at a given elevation angle will vary depending on the azimuth. In high-precision applications, such as geodesy, the horizontal gradients must be estimated alongside tropospheric delays to account for this effect. Therefore, the full correction term of tropospheric effects can be expressed as follows:

$$\rho_{tro}(a,e) = mf_h(e)\,\rho_{zhd} + mf_w(e)\,\rho_{zwd} + mf_{grad}(e)\,.\,[G_N cos(a) + G_E sin(a)]\,, \qquad (3.8)$$

where a is the observed azimuth direction, and G_N and G_E are north and east gradients, respectively.

Nowadays, there are two models for the horizontal gradients available in the analysis of space geodetic techniques. These models were developed by MacMillan (1995) and Chen and Herring (1997). The horizontal gradient mapping functions provided by these two models are different. MacMillan (1995) utilized $cot(e)$ for the gradient mapping function $mf_{grad}(e)$, whereas Chen and Herring (1997) used $\frac{1}{sin(e)tan(e)+C}$ for the gradient mapping function $mf_{grad}(e)$. The coefficient C is suggested to be 0.0031 and 0.0007 for the hydrostatic and wet parts, respectively. For the estimation of total gradients, Chen and Herring (1997) recommends using $C = 0.0032$. A more detailed description of gradients can be found in the current IERS conventions or Nilsson et al. (2013).

3.2 Tropospheric ties model

Section 2.3 shows that each technique shares parameters that can be estimated together to improve the geodetic solutions derived from space geodetic techniques. In the combination process, station coordinates are one of the most frequently used parameters. Local ties are the fundamental information that establishes a relationship between station coordinates using space

geodetic techniques, and they are commonly used in the determination of ITRF (Altamimi et al., 2016). Tropospheric parameters are another common type of parameter that can be used. Similar to station coordinates, it is essential to provide the necessary information regarding the relationship between tropospheric parameters. This information is referred as *tropospheric ties*.

Tropospheric ties are the expected differences between atmospheric parameters of space geodetic techniques, particularly microwave-based techniques (Bock et al., 2010; Poutanen and Rózsa, 2020; Teke et al., 2011). As shown in Figure 3.3, these expected differences are primarily due to the height difference between the reference points of the microwave space geodetic technique. In addition, other factors such as differences in observing frequency and the configuration of the observing system may also contribute to the differences (Bock et al., 2010). According to IAG Commission 1's terms of reference (JWG 1.1.1: Intra- and Inter-Technique Atmospheric Ties), zenith delays and gradients are currently considered a component of tropospheric ties. For the sake of convenience, this study refers to the zenith delays component as tropospheric ties and the gradient delays component as gradient ties.

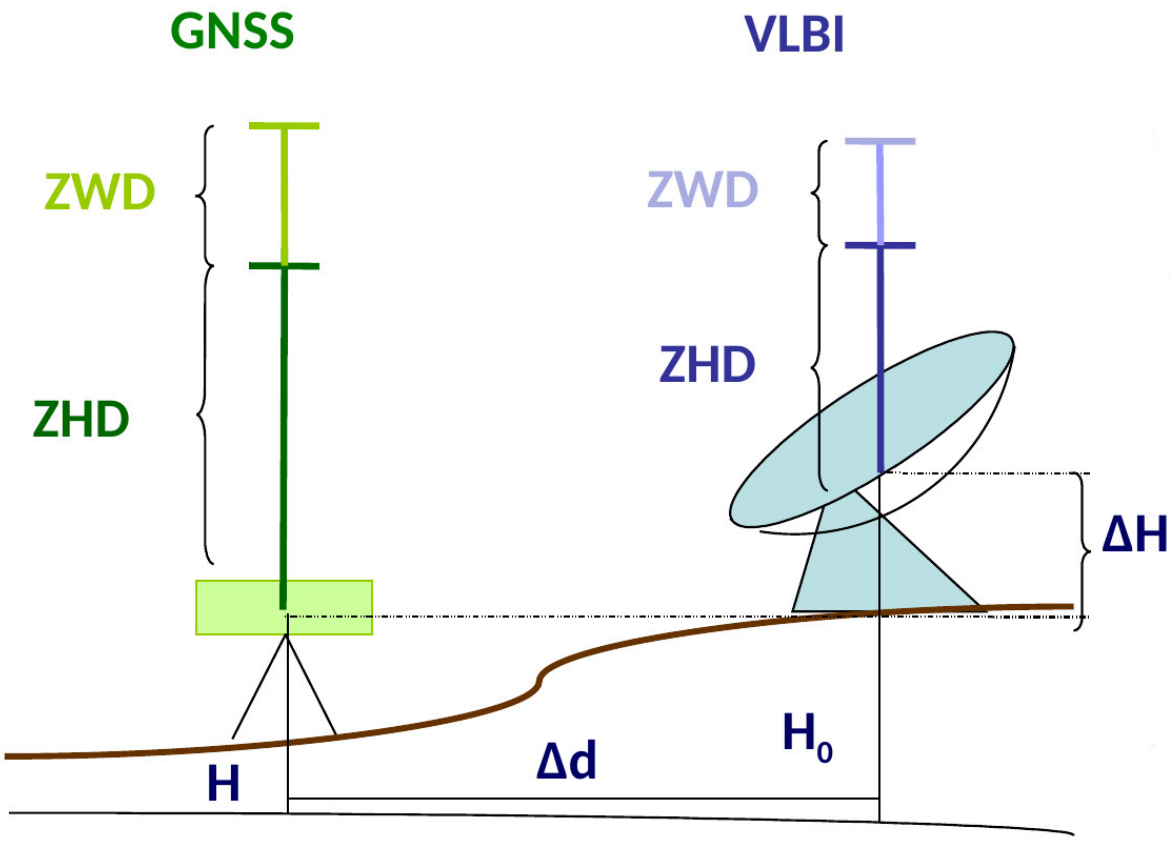

Figure 3.3: Illustration of the concept of tropospheric ties. The concept of tropospheric ties is the expected difference in tropospheric parameters due to the position differences between the reference points of the space geodetic technique (an example of VLBI and GNSS co-location site), primarily different in height coordinates, at co-location site. (Courtesy from Robert Heinkelmann).

3.2.1 Zenith delay ties (tropospheric ties)

There are currently several methods for determining tropospheric ties. As demonstrated in Eqs. 3.9 and 3.10, Teke et al. (2011) and Rothacher et al. (2011) proposed a method of deriving the difference between the hydrostatic and wet components based on the Saastamonien model (Saastamoinen, 1972). Furthermore, since the pressure values must be calculated at the reference point of the geodetic instrument, the height difference between the meteorological sensor and the geodetic instrument must be taken into account. This pressure-height dependence is given by Brunner and Rüeger (1992) and is expressed in Eq. 3.11.

$$\Delta ZHD = \frac{0.0022768(p - p_0)}{1 - 0.00266\cos(2\theta) - 0.28 \times 10^{-6} H_0} \tag{3.9}$$

$$\Delta ZWD = \frac{-2.789 e_0}{T_0^2} \left(\frac{5383}{T_0} - 0.7803 \right) \gamma (H - H_0) \tag{3.10}$$

$$p = p_0 \left(1 - \frac{\gamma (H - H_0)}{T_0} \right)^{\frac{g}{\gamma R_L}} \tag{3.11}$$

H_0 and θ refer to the reference height in meters and latitude of the reference station, respectively. The e_0, p_0, and T_0 denote the water vapor pressure in hPa, air pressure in hPa, and temperature in Kelvin at the reference station. H and p represent the height and pressure at the co-located station. The value of the average temperature lapse rate γ is $-0.0065\,\mathrm{K/m}$. The specific gas constant, R_L, is approximately equal to 287.058 $m^2 s^{-2} K^{-1}$.

Bock et al. (2010) and Thaller (2008) described the use of the "rule of thumb" based on surface pressure theory. For example, a difference in height of 10 meters corresponds to approximately a 3 mm difference in the tropospheric parameters, particularly the hydrostatic component. In addition to deriving tropospheric ties using an empirical model, Heinkelmann et al. (2016) proposed using ray-tracing in the tropospheric ties derivation based on an NWM. At the reference point, the ray-traced tropospheric parameters are determined and the differences are extracted. The principles of ray-tracing can be found in well-established literature, such as Zus et al. (2014).

The characteristics of tropospheric ties from analytical equations (see Eqs. 3.9, 3.10) (TA) and ray-traced tropospheric ties (TR) on ZHD and ZWD components are assessed in this study. Five years of data (2008-2013) from various VLBI and GNSS co-location sites are utilized. The ray-traced tropospheric ties were obtained from ray-traced ZHD and ZWD at the reference point position provided by the station-wise Vienna Mapping Function 3 (VMF3) (Landskron and Böhm, 2018), and then their differences were examined. Additionally, since the analytical equation relies on meteorological data, tropospheric ties from the analytical equation based on three different meteorological data are assessed. Firstly, the pressure, temperature, and water vapor pressure at the site provided by Global Pressure and Temperature Model 3 (GPT3) (Landskron and Böhm, 2018) and European Centre for Medium-Range Weather Forecasts (ECMWF) operational NWM, which are provided in station-wise VMF3, as well as height differences between the two antenna reference point positions were used as input for analytical equations. These are referred to as TAGPT3 and TAVM3. Similarly, tropospheric ties from the analytical equations utilizing meteorological data provided by the meteorological

sensor (TAMET) at the VLBI radio telescope were computed. Unlike GPT3 and NWM, the meteorological sensor does not provide water vapor pressure directly but instead provides relative humidity. Thus, the relative humidity was converted to water vapor pressure using the Magnus equation in this study.

The results show that TR, TAVM3, TAGPT3, and TAMET exhibit good agreement in both ZHD and ZWD ties at the Wettzell co-location site (WETTZELL-WTZR), Germany, where the height difference is small (3.5 m) and the atmospheric conditions are calm. Figure 3.5 demonstrates that TR, TAVM3, and TAMET account for sub-daily variations of the atmosphere, while TAGPT3 does not show sub-daily variation. Additionally, sub-daily variation is higher during summer than winter in ZWD ties. Similarly, the Tsukuba co-location site (TSUKUB32-TSKB), which represents an extreme case in terms of atmospheric conditions with a height difference of 18.6 m, exhibits similar results, as shown in Figure 3.6. However, the magnitude of tropospheric ties at this site is approximately four times and two times higher than at the Wettzell co-location site for ZHD and ZWD ties, respectively. Furthermore, annual signals are present in both ZHD and ZWD ties for TR, TAVM3, TAGPT3, and TAMET at both co-location sites. During the summer, TAGPT3 and TAVM3 show disagreement with TR and TAMET. The magnitude of ZHD and ZWD ties increases with height differences, as shown in Figure 3.7. However, the magnitude of ZWD ties increases less than that of ZHD ties. Additionally, Figure 3.8 illustrates the power spectral density (PSD) of the TAVM3 estimated from the Lomb-Scargle periodogram (Lomb, 1976; Scargle, 1982) over a five-year time span. The figure displays annual signals at four different co-location sites: Hobart, Australia; Tsukuba, Japan; Wettzell, Germany; and Kokee Park, USA. The results indicate that the Tsukuba co-location site exhibits the strongest annual signal compared to the other co-location sites, particularly in ZWD ties.

The magnitude of tropospheric ties depends on the height difference between the reference point positions of two space geodetic technique instruments. The magnitude of tropospheric ties is mainly observed in the ZHD ties, while the variation, especially the annual variation, is predominantly evident in the ZWD ties. The ZHD ties are primarily correlated with the height difference between the two reference point positions. The variation of tropospheric ties, especially in ZWD ties, is affected by the atmospheric conditions at the site and the height differences. This is illustrated by the co-location sites at Tsukuba and Kokee, where the atmospheric conditions are humid, but the height difference of KOKEE-KOKB (9.5 m) is smaller than TSUKUB32-TSKB (18.6 m). The Tsukuba co-location site exhibits a stronger annual signal compared to the Kokee Park co-location site. These demonstrate that tropospheric ties are dependent on both height differences and time. The four different tropospheric tie models show good agreement in this study, particularly during winter when the atmospheric conditions are calm. However, for the co-location site where the atmospheric conditions are humid and the height difference is high, such as Tsukuba, Japan, TAGPT3 and TAVM3 exhibit disagreement compared to TR and TAMET on ZWD ties during the summer. This discrepancy is attributed to the meteorological data from the GPT3 and NWM, which make assumptions about the atmosphere during model generation. As a result, TAGPT3 and TAVM3 may not accurately predict the variability of atmospheric conditions during this period. On the other hand, TR and TAMET are derived based on precise atmospheric conditions at

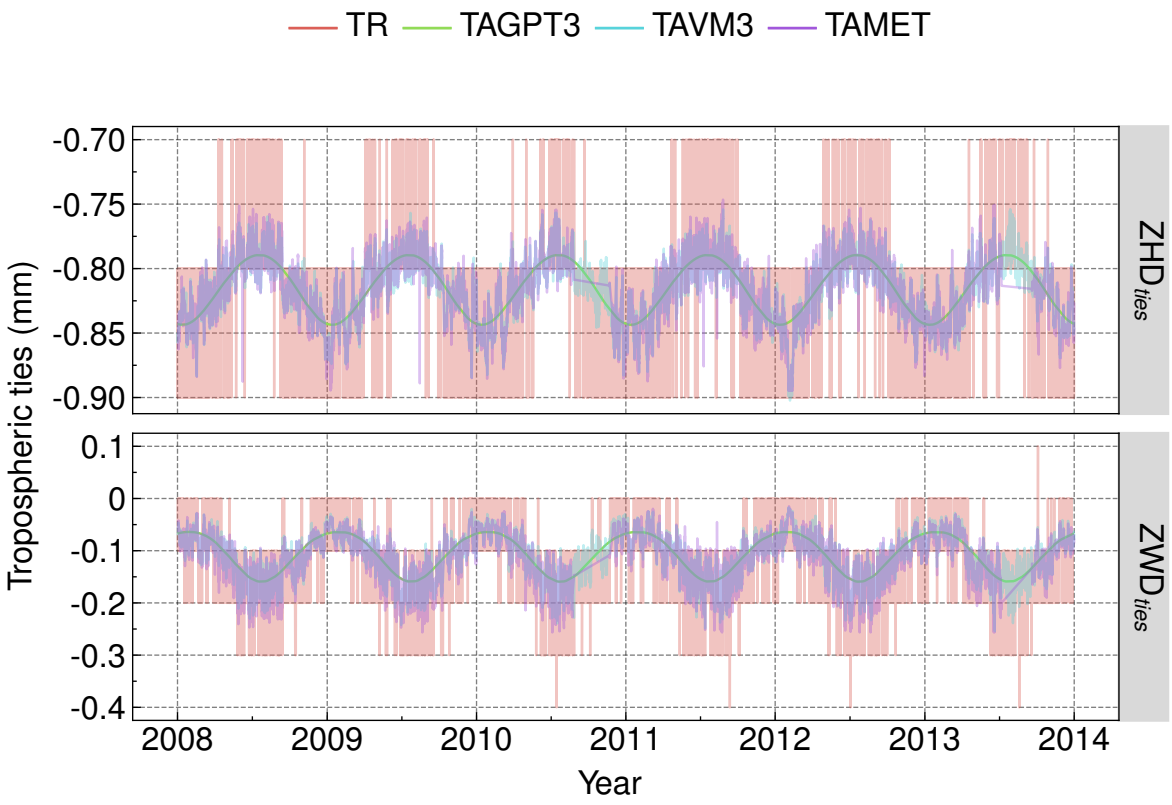

(a) A five-year time series of four different tropospheric tie models for both ZHD (top) and ZWD (bottom) components. Both subfigures (a) and (b) share the same legend.

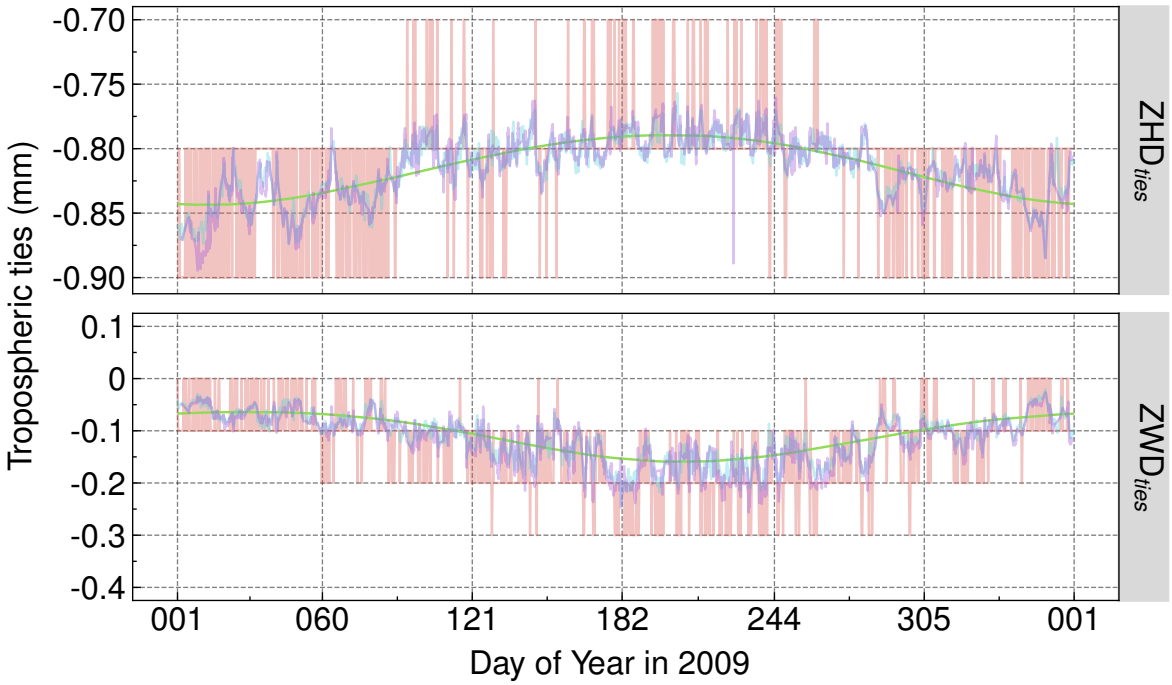

(b) A one-year snapshot from a five-year time series in 2009 for a comparison of four different tropospheric tie models for both ZHD (top) and ZWD (bottom) components. Both subfigures (a) and (b) share the same legend.

Figure 3.4: A comparison of four different tropospheric tie models at the Wettzell co-location site between 2008 and 2014, with a height difference of 3.5 m. The acronym TR refers to the ray-traced tropospheric ties, while TAVM3, TAGPT3, and TR refer to tropospheric ties obtained from analytical models based on meteorological data from VMF3, GPT3, and a meteorological sensor on-site, respectively.

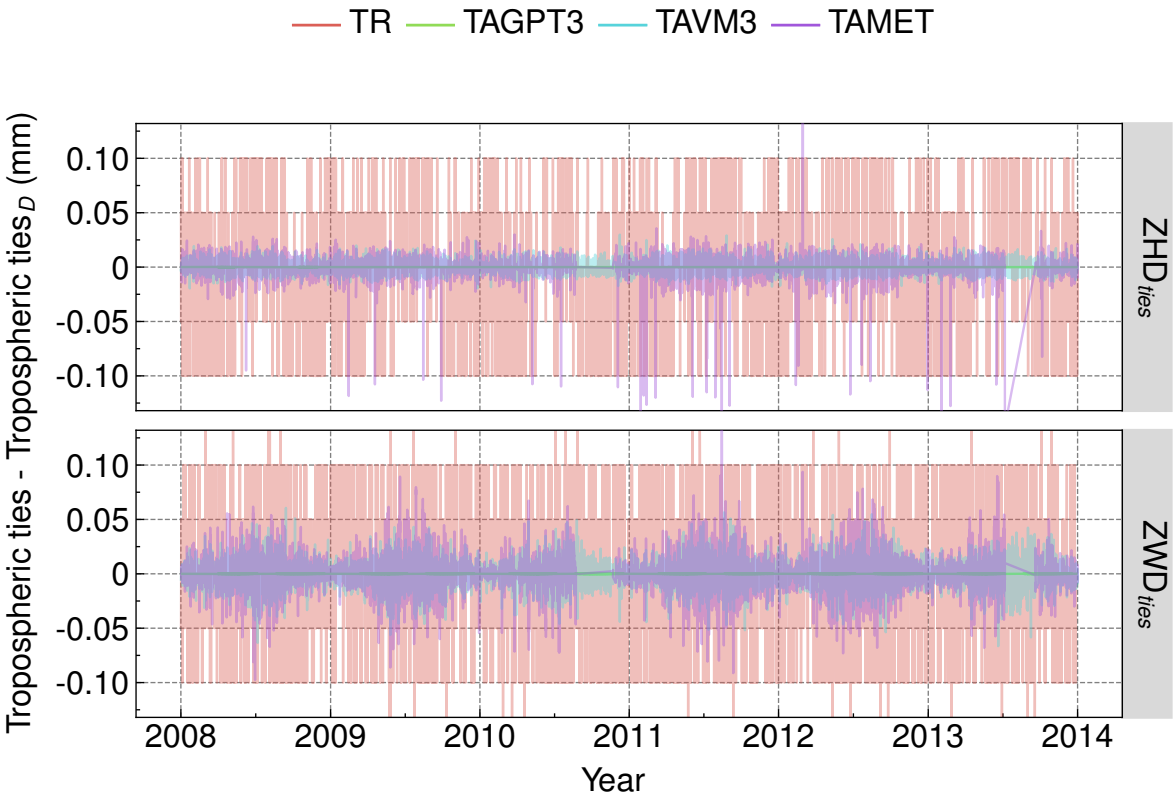

(a) A five-year time series of a comparison of tropospheric ties and daily median tropospheric ties for both ZHD (top) and ZWD (bottom) components. Both subfigures (a) and (b) share the same legend.

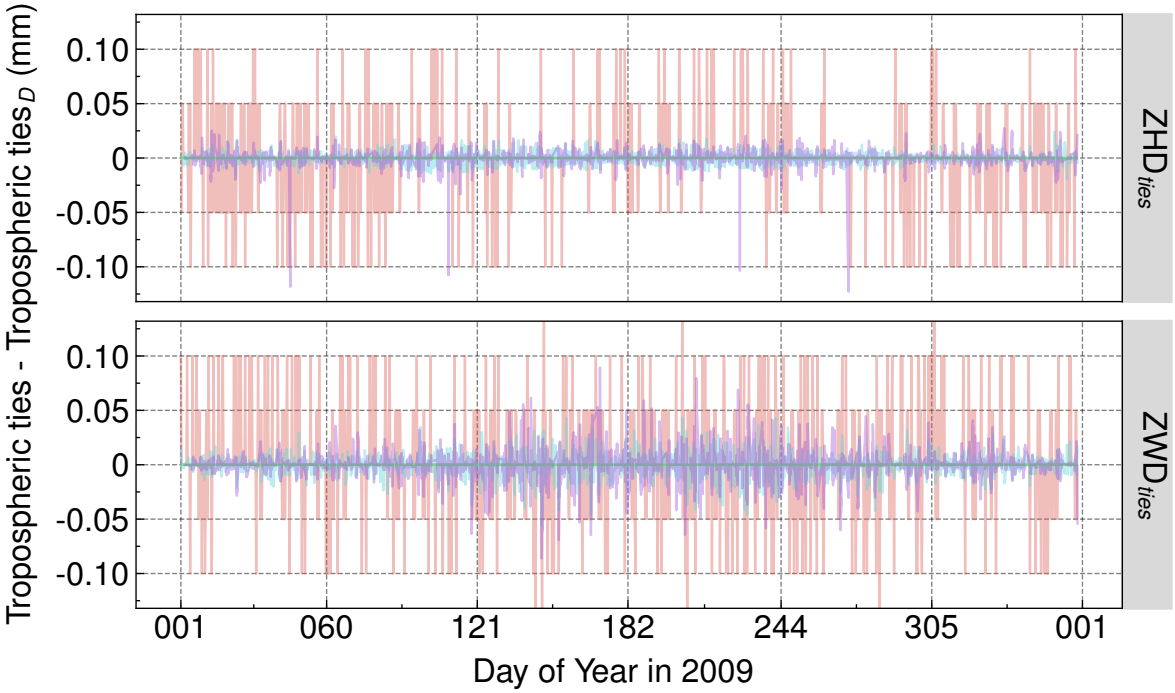

(b) A one-year snapshot from a five-year time series in 2009 for a comparison of tropospheric ties and daily median tropospheric ties for both ZHD (top) and ZWD (bottom) components. Both subfigures (a) and (b) share the same legend.

Figure 3.5: A comparison of tropospheric ties and daily median tropospheric ties for TR, TAVM3, TAGPT3, and TAMET at the Wettzell co-location site. TAGPT3 exhibits no sub-daily variation compared to the other models. Furthermore, the variation shows a higher magnitude during the summer months compared to winter.

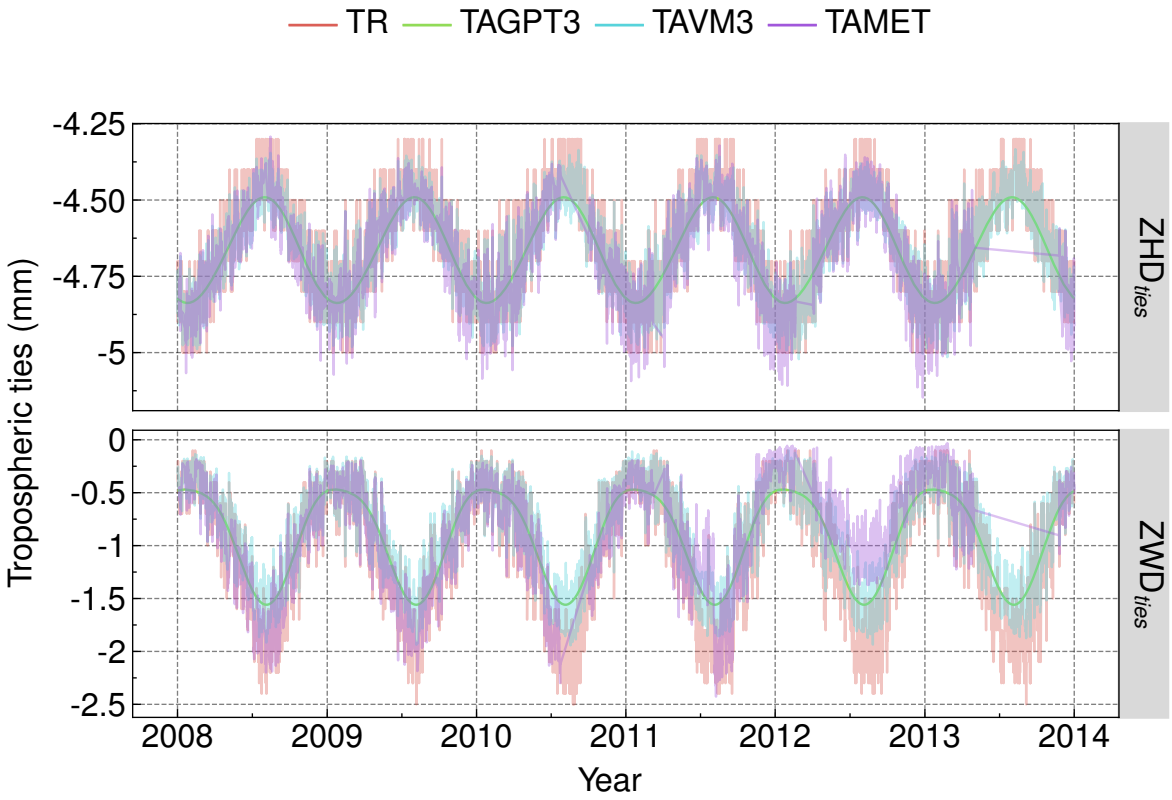

(a) A five-year time series of four different tropospheric tie models for both ZHD (top) and ZWD (bottom) components. Both subfigures (a) and (b) share the same legend.

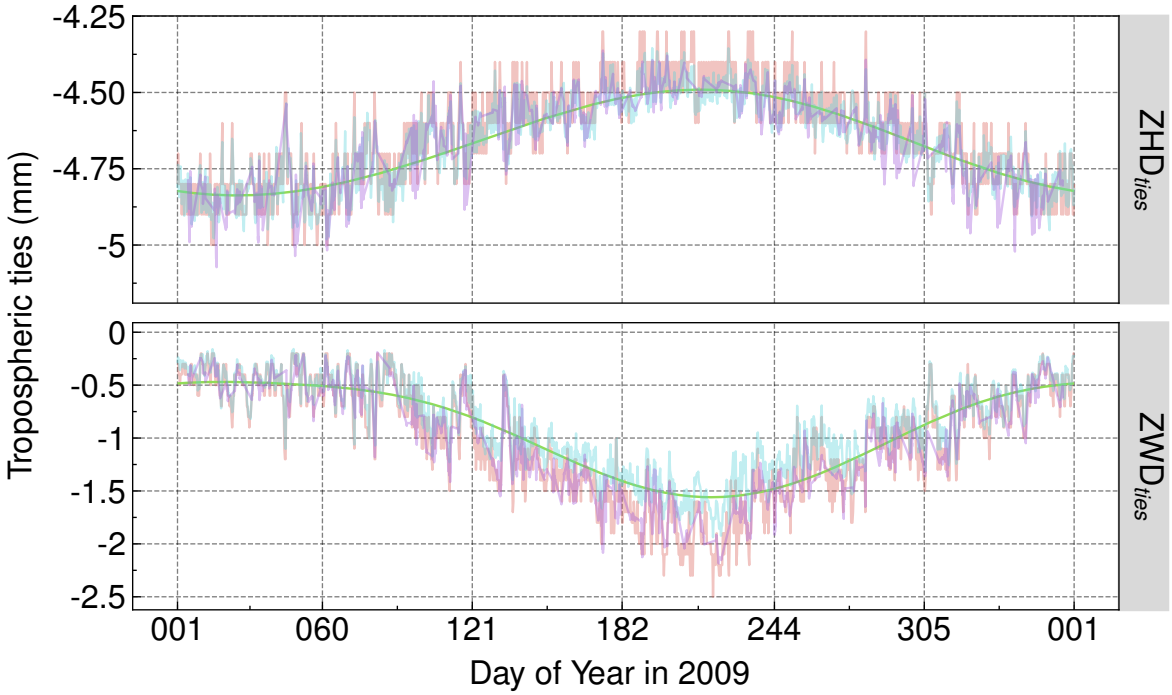

(b) A one-year snapshot from a five-year time series in 2009 for a comparison of four different tropospheric tie models for both ZHD (top) and ZWD (bottom) components. Both subfigures (a) and (b) share the same legend.

Figure 3.6: Tropospheric ties between VLBI and GNSS at Tsukuba, Japan (18.6 m height difference), derived from TR, TAVM3, TAGPT3, and TAMET from 2008 to 2014. The acronym TR refers to the ray-traced tropospheric ties, while TAVM3, TAGPT3, and TAMET refer to tropospheric ties obtained from analytical models based on meteorological data from VMF3, GPT3, and a meteorological sensor on-site, respectively.

the site, showing promising performance in deriving tropospheric ties when the atmospheric conditions are humid. Moreover, TAGPT3 does not exhibit sub-daily variation compared to TR, TAVM3, and TAMET because the GPT3 model only considers annual and semi-annual variations. Since the temporal resolution of tropospheric ties depends on meteorological data, the advantage of the analytic model is not limited by temporal resolution, unlike ray-tracing technique, which relies on the temporal resolution of a Numerical Weather Model (NWM). In contrast, ray-tracing technique derives values from precise atmospheric conditions and the reference point of the geodetic instrument, whereas analytic models rely on various atmospheric assumptions, such as the specific gas constant and extrapolation of pressure values.

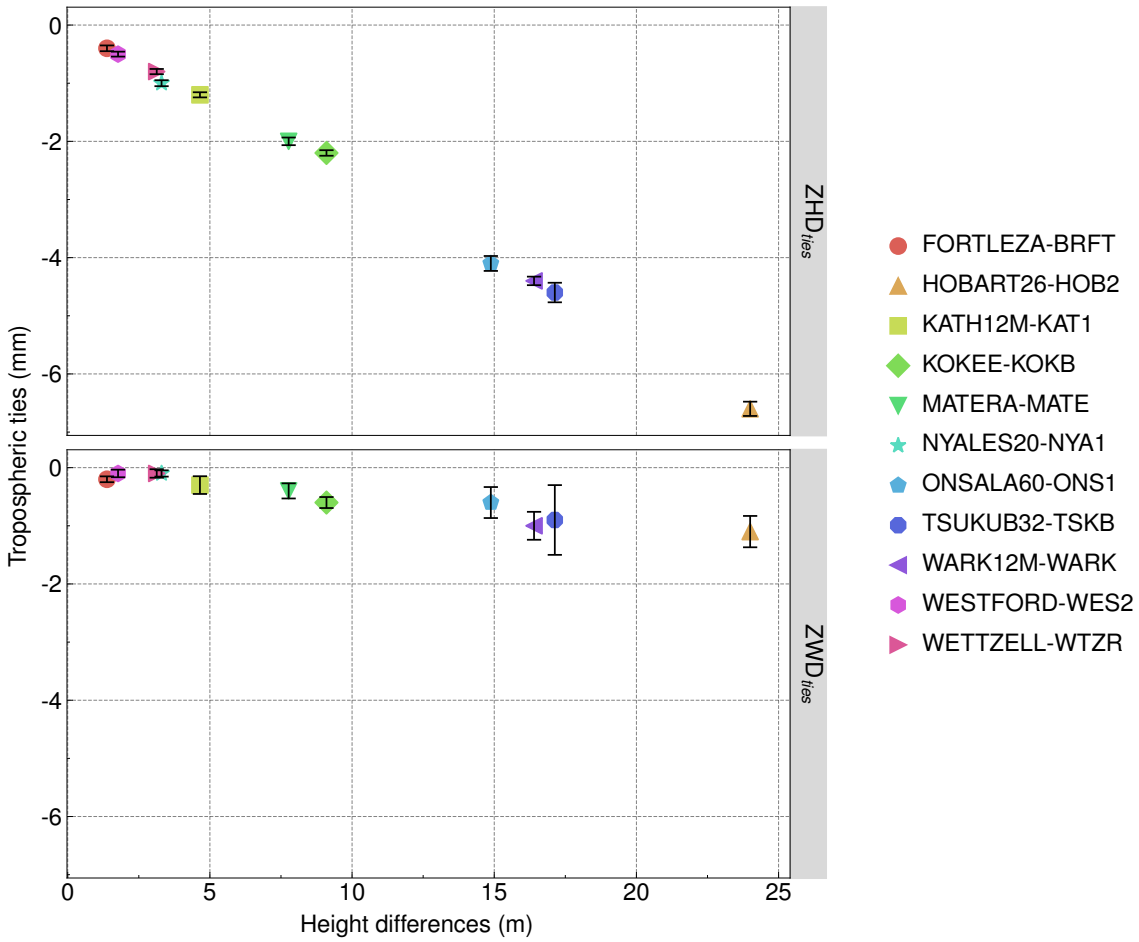

Figure 3.7: A comparison of the median tropospheric ties for ZWD (top) and ZHD (bottom) components is presented against the height differences between VLBI and GNSS reference point positions at eleven VLBI and GNSS co-location sites. The tropospheric ties were derived from TAVM3.

Moreover, the study presents a formal error assessment of the tropospheric ties. For this purpose, five VLBI and GNSS co-location sites were selected, where information regarding the uncertainty of meteorological data from the meteorological sensor is available in the VLBI station log file (as shown in Table 3.1). Unfortunately, the uncertainties of meteorological information from NWM and GPT3 could not be extracted; hence, only TAMET is assessed in this study. As the meteorological sensor does not directly provide water vapor pressure but instead provides relative humidity, the uncertainty of water vapor pressure is calculated through error propagation during the conversion of relative humidity to water vapor pressure

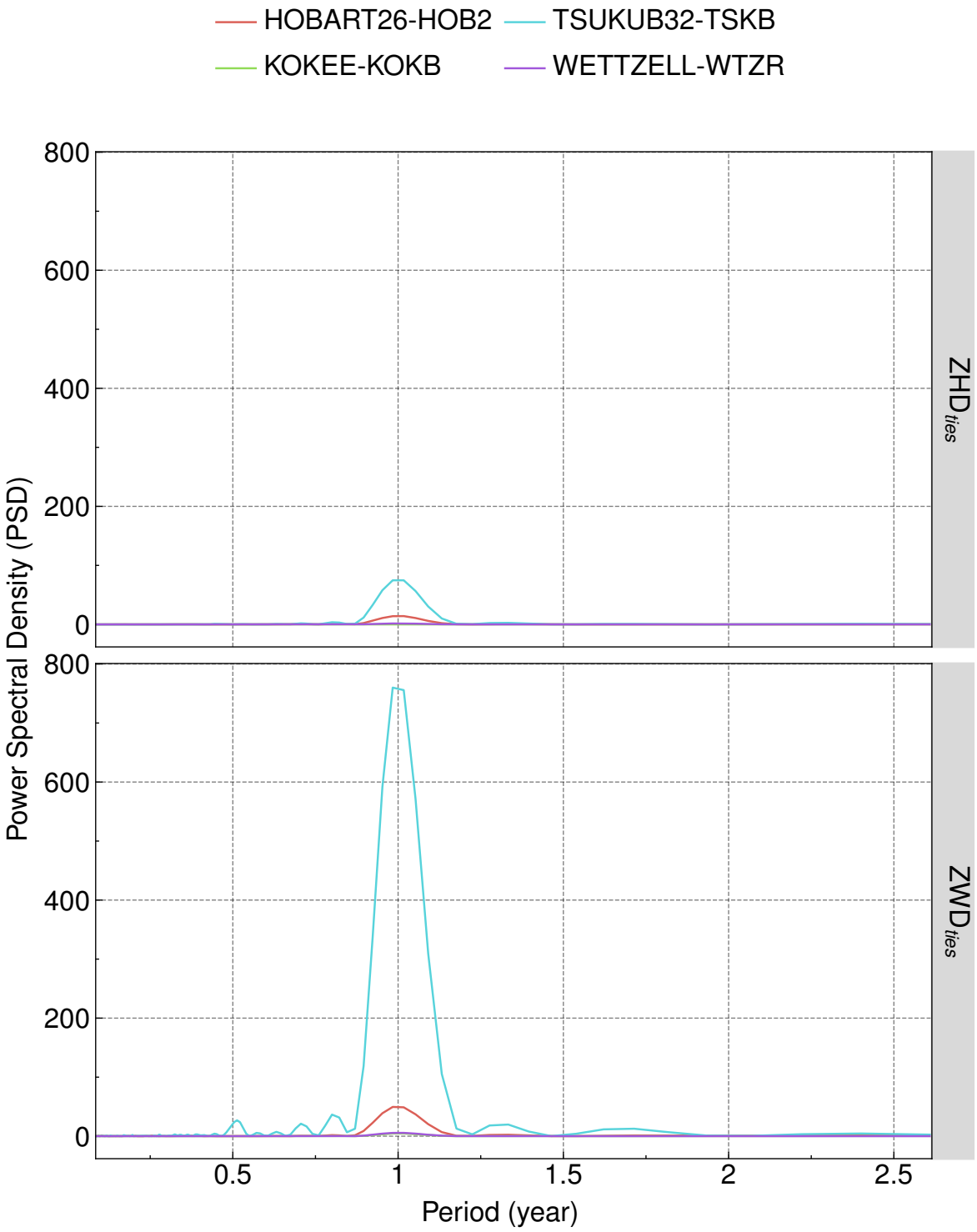

Figure 3.8: The power spectral density (PSD) of the periodic signal in the tropospheric ties was estimated from the Lomb-Scargle periodogram (Lomb, 1976; Scargle, 1982) for both ZHD (top) and ZWD (bottom) between VLBI and GNSS at four co-location sites between 2008 and 2014. These sites include Wettzell (WETTZELL-WTZR), Germany (with a height difference of 3.5 m); Hobart (HOBART26-HOB2), Australia (with a height difference of 24.5 m); Tsukuba (TSUKUB32-TSKB), Japan (with a height difference of 18.6 m); and Kokee Park (KOKEE-KOKB) (with a height difference of 9.5 m), USA. The tropospheric ties were derived from TAVM3.

using the uncertainties of temperature and relative humidity. Additionally, two scenarios with different uncertainties of the height coordinate were conducted: 5 mm and 1 cm.

Station-pair	Pressure (hPa)	Temperature (°C)	Relative Humidity (%)	Water Vapor Pressure (hPa)[a]
TSUKUB32	0.2	0.1	3	0.5
NYALES20	0.1	0.45	1	0.1
ONSALA60	0.5	1	5	0.9
WETTZELL	0.1	0.1	2.5	0.3
KOKEE[b]	0.1	0.2	2	0.4

Table 3.1: The uncertainties of meteorological parameters from the meteorological sensor at the VLBI radio telescopes.
[a]The values were calculated through an error propagation using uncertainties of relative humidity and temperature when converting relative humidity to water vapor pressure using the Magnus equation.
[b]The temperature and relative humidity uncertainties are not available in the station log file. The values obtained from the sensor datasheet.[1]

Table 3.2 presents the uncertainties of TAMET for ZHD and ZWD ties. The results show that the uncertainties are below the sub-millimeter level for all station pairs and for both ZHD and ZWD ties. However, the station pairs TSUKUB32-TSKB and ONSALA60-ONS1 exhibit larger uncertainties in ZWD ties compared to the other pairs. Additionally, the station pair ONSALA60-ONS1 has a larger uncertainty in ZHD ties compared to the other pairs. Furthermore, the uncertainties of ZHD ties in the second scenario are slightly larger than those in the first scenario, whereas the uncertainties in ZWD ties remain the same for both scenarios.

Station-pair	ZHD ties (mm)	ZWD ties (mm)
First scenario: 5 mm uncertainties of height coordinates		
TSUKUB32-TSKB	0.003	0.035
NYALES20-NYA1	0.003	0.002
ONSALA60-ONS1	0.015	0.056
WETTZELL-WTZR	0.002	0.004
KOKEE-KOKB	0.002	0.015
Second scenario: 1 cm uncertainties of height coordinates		
TSUKUB32-TSKB	0.004	0.035
NYALES20-NYA1	0.004	0.002
ONSALA60-ONS1	0.015	0.056
WETTZELL-WTZR	0.004	0.004
KOKEE-KOKB	0.004	0.015

Table 3.2: Uncertainties of tropospheric ties for two scenarios derived from the analytical equation using meteorological data from the meteorological sensors (TAMET) for ZHD and ZWD ties for various station pairs.

The uncertainty of tropospheric ties has been demonstrated to be at the sub-millimeter level, as revealed by the results obtained. The magnitude of uncertainty for each component is dependent on various meteorological quantities. For instance, the uncertainty of the ZHD ties relies on the accuracy of pressure measurements, while the uncertainty of the ZWD ties depends on the water vapor pressure. It should be noted that the uncertainty of height coordinates is not significantly affected by the uncertainty of tropospheric ties. Additionally, the ZWD ties

[1] `https://www.comm-tec.com/Docs/Manuali/Paros/MetComparison.pdf`

exhibit a greater variation than the ZHD ties, resulting in larger uncertainties in the ZWD ties than in the ZHD ties.

3.2.2 Gradient ties

In this study, the characteristics of gradient ties were investigated. Unlike tropospheric ties, gradient ties can only be derived from ray-tracing. Therefore, ray-traced gradient ties were obtained from the ray-traced horizontal gradient parameter provided in the station-wise VMF3 (Landskron et al., 2018) and their differences were examined. Five years of data from eleven selected co-location sites were used, similar to the study of tropospheric ties. The north and east components of gradient ties were investigated and referred to as TGN and TGE, respectively.

Figure 3.9 presents a comparison of ray-traced gradient ties between TSUKUB32 and TSKB stations at the Tsukuba co-location site. The results show that the mean offsets for both TGN and TGE were close to zero, with a standard deviation at the level of 0.01 mm. Moreover, the standard deviation was higher during the summer compared to the winter. Furthermore, Figure 3.10 shows a comparison of ray-traced gradient ties between WETTZELL and WTZR stations at the Wettzell co-location site. The mean offsets were also close to zero, but the standard deviation was ten times smaller compared to the TSUKUB32-TSKB pair and showed no difference between summer and winter. This study found that the mean offsets were at the sub-millimeter level despite the different horizontal differences for different co-location sites, as shown in Figure 3.11. However, the standard deviation was found to be correlated with the height differences for both TGE and TGN, as demonstrated in Figure 3.12.

The results indicate that gradient ties, similar to tropospheric ties, are time-dependent. The mean offsets are at the sub-millimeter level for all co-location sites and do not correlate with the horizontal distance between two stations in this study, unlike tropospheric ties, which do correlate with height differences. On the other hand, the variation of gradient ties increases with height differences. Moreover, the variation of gradient ties is greater during humid atmospheric conditions, such as in summer, when the height difference is high, as observed in the TSUKUB32-TSKB pair (height difference 18.6 m). However, when the height difference is small, the variation is similar under any atmospheric condition, as demonstrated in the WETTZELL-WTZR pair. Despite the varying height differences and atmospheric conditions, the magnitude of gradient ties (both mean offset and variation) remains at the sub-millimeter level for all co-location sites in this study.

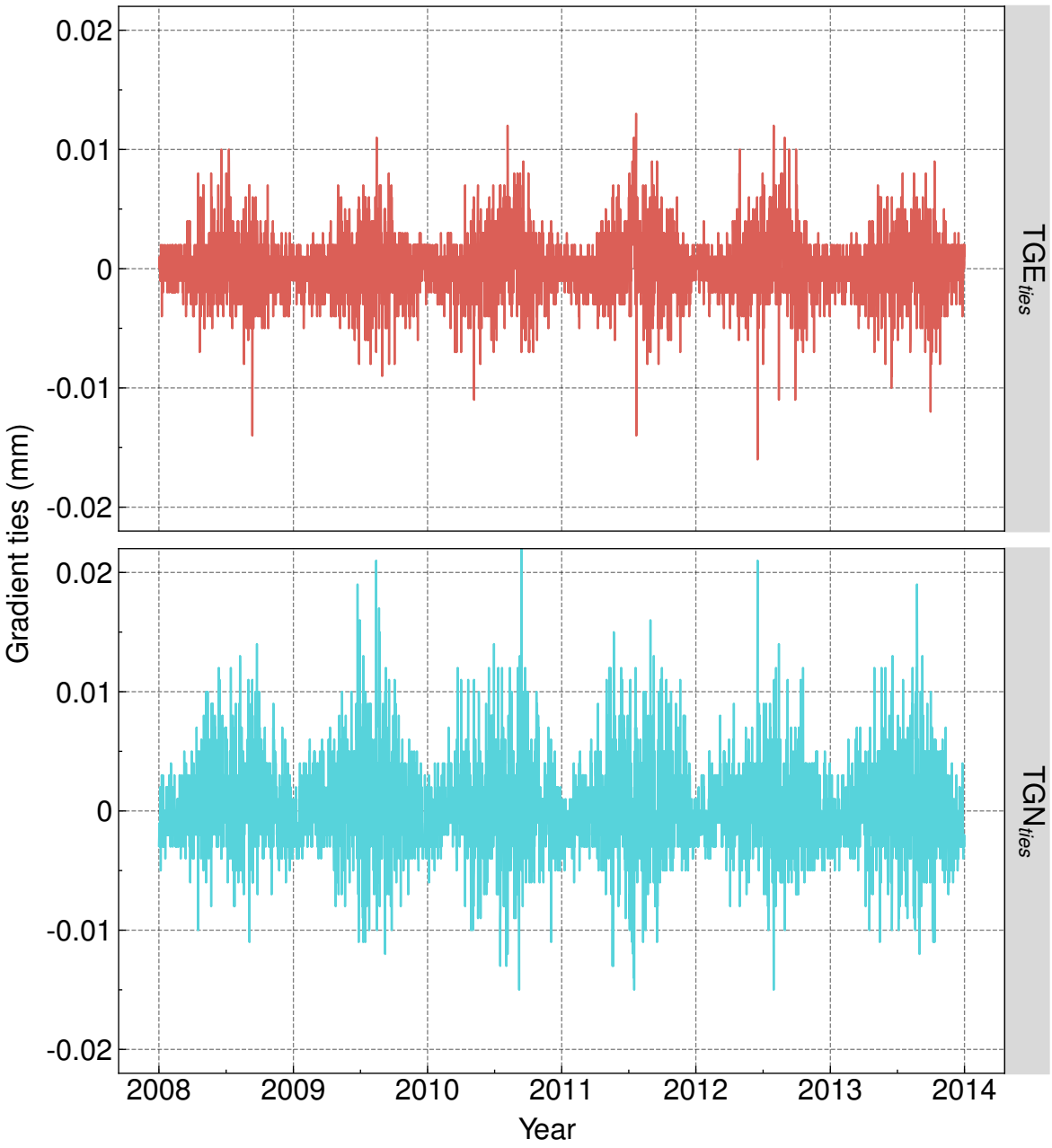

Figure 3.9: The east (top) and north (bottom) components of gradient ties between VLBI and GNSS at Tsukuba, Japan (18.6 m height difference), derived from ray-tracing from 2008 to 2014. The variation shows a higher magnitude during the summer months compared to winter. The acronyms TGE and TGN refer to east and north gradient ties, respectively.

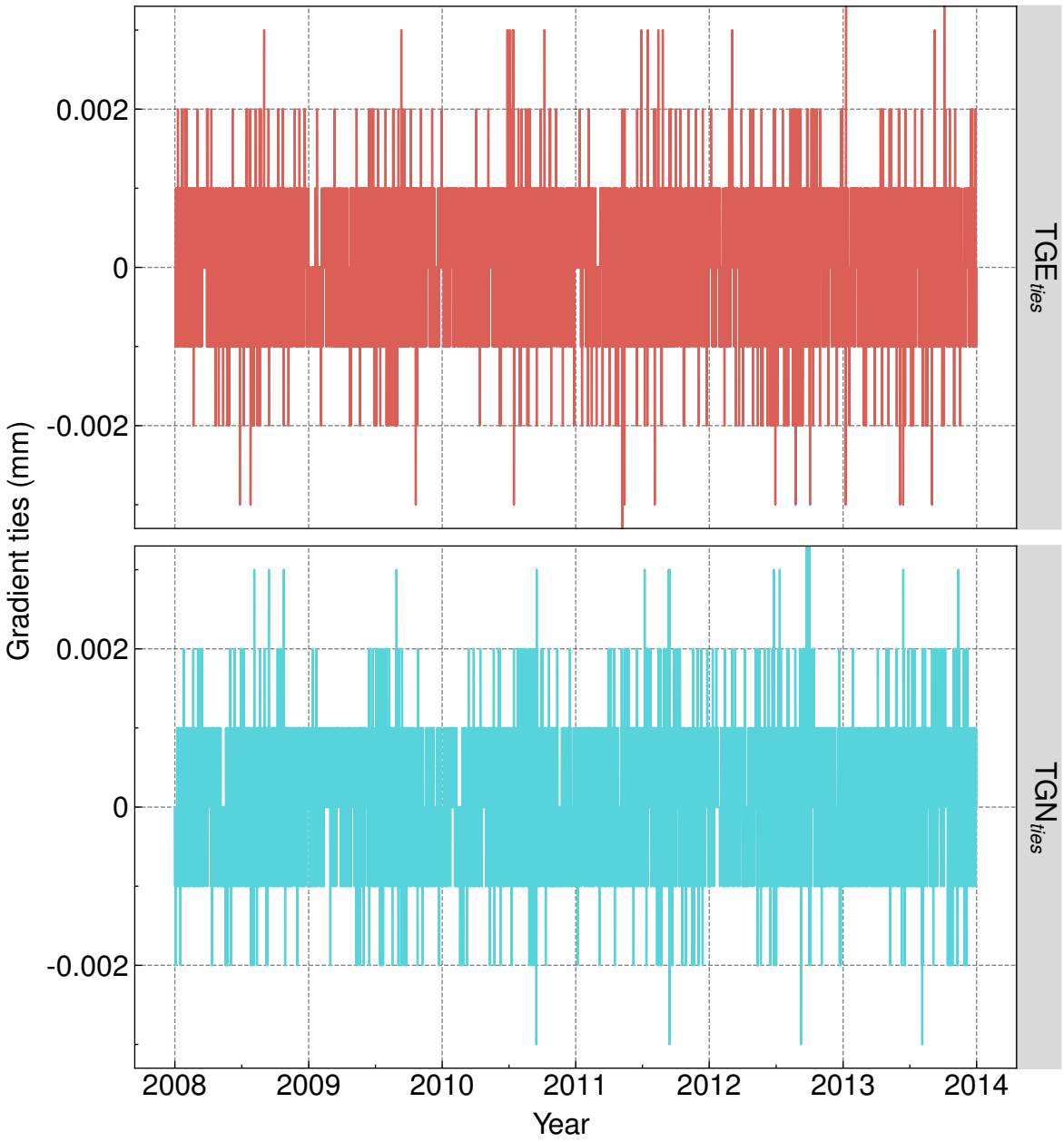

Figure 3.10: The east (top) and north (bottom) components of gradient ties between VLBI and GNSS at Wettzell, Germany (3.5 m height difference), derived from ray-tracing from 2008 to 2014. The acronyms TGE and TGN refer to east and north gradient ties, respectively.

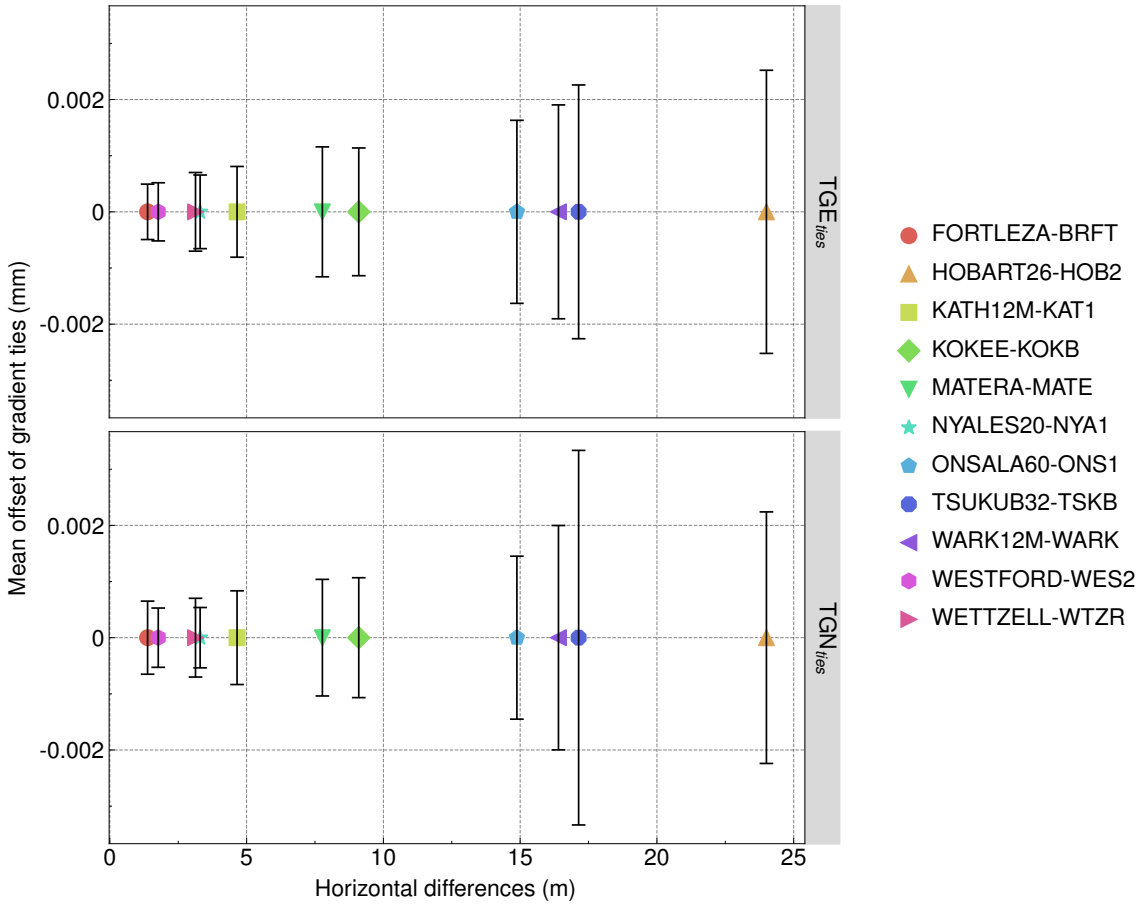

Figure 3.11: A comparison of the mean gradient ties for east (top) and north (bottom) components is presented against the horizontal differences between VLBI and GNSS reference point positions at eleven VLBI and GNSS co-location sites between 2008 and 2014. The acronyms TGE and TGN refer to east and north gradient ties, respectively.

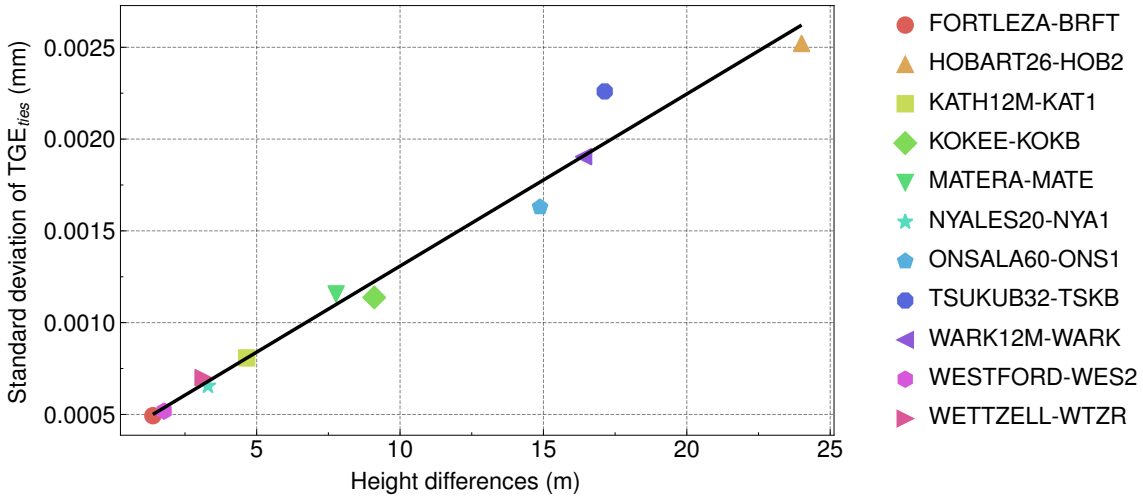

(a) East gradient ties

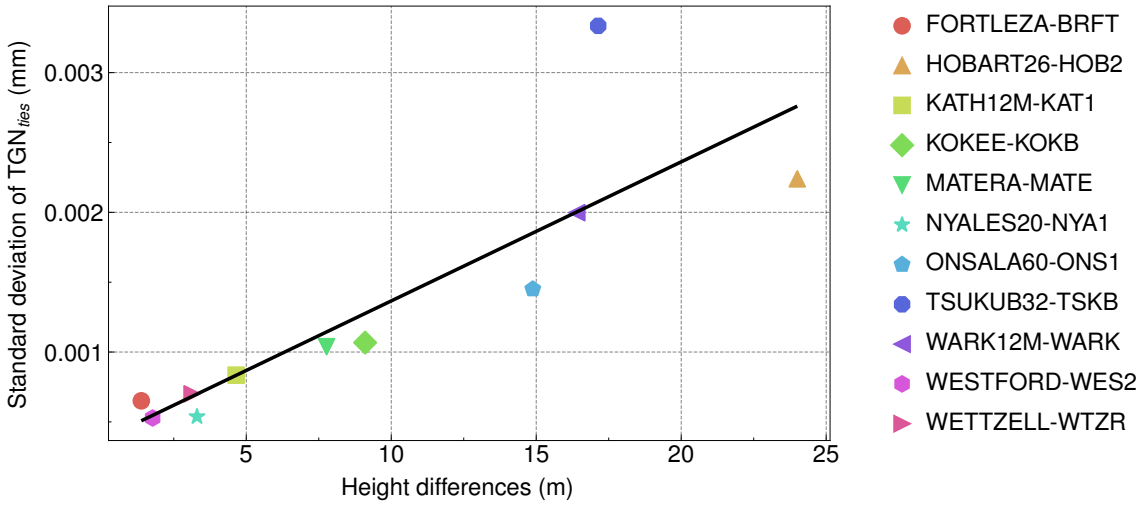

(b) North gradient ties

Figure 3.12: A comparison of the standard deviations of gradient ties is presented for the east (top) and north (bottom) components. The standard deviations are plotted against the height differences between VLBI and GNSS reference point positions at eleven co-location sites. The black line represents the linear fit.

3.3 GNSS and VLBI intra/inter-techniques comparison of tropospheric parameters

The derivation of tropospheric ties relies on several factors, including the height difference between two reference points, time, and the atmospheric conditions at the co-location site. However, this approach may not always yield accurate results, as systematic effects can lead to discrepancies between the observed tropospheric parameter differences obtained from microwave-based space geodetic techniques, such as VLBI and GNSS, and the values obtained through tropospheric ties. This section investigates the systematic effects that could cause a discrepancy between observed tropospheric parameter differences and tropospheric ties at co-location sites. To investigate this issue, this study performs an intra/inter-technique comparison of GNSS and VLBI on ZTD and horizontal gradient parameters. Although some may consider this unnecessary due to the small magnitude of these parameters (sub-millimeter level), it is still worthwhile to examine any systematic effects in horizontal gradients since a better estimation of the horizontal gradient leads to an improvement in station horizontal coordinates (Douša et al., 2020). Furthermore, for co-location sites, it is typically assumed that the horizontal gradients between adjacent space geodetic technique reference points are equal because of their proximity, as depicted in Figure 3.16. Consequently, the gradient ties are expected to be close to zero as shown in Section 3.2.2. Nevertheless, certain factors may introduce systematic effects causing a discrepancy between the observed horizontal gradient differences and the gradient ties.

3.3.1 GNSS intra-technique comparison of tropospheric parameters

To investigate the discrepancy between observed ZTD differences and tropospheric ties in GNSS, this study performs a GNSS intra-technique comparison on ZTD and horizontal gradient parameters. The tropospheric products from the repro3 product series of CODE (Selmke et al., 2020) are used in this study, which is a product from a major reprocessing campaign for the ITRF2020 (Altamimi et al., 2022). This product provides two-hour temporal resolution of ZTD parameters and daily horizontal gradients. The time-series of 12 years from 2008 to 2020 were selected from four co-location sites, namely Wettzell, Germany; Zimmerwald, Switzerland; Hartebeesthoek, South Africa; and Ny Ålesund, Norway. Moreover, two different tropospheric ties, TR and TAVM3, were selected for comparison with GNSS-observed ZTD differences. In this analysis, the weighted mean (WM) and weighted standard deviation (WSTD) are used to calculate the mean offset and variation for observed ZTD differences, TR, and TAVM3. Additionally, differences beyond 3-sigma are defined as outliers and removed from the analysis.

Figure 3.13 compares the observed ZTD differences, TAVM3, and TR, as well as the height differences between two GNSS stations, WTZA and WTZR, at the Wettzell co-location site from 2008 to 2020. The results show discrepancies between the observed ZTD differences, TAVM3, and TR. Furthermore, a significant shift in the ZTD difference time series resulted from changing antennas. Similarly, Figure 3.14 illustrates a similar comparison between two GNSS stations, ZIMM and ZIM2, in Zimmerwald, Switzerland. The results also demonstrate discrepancies between observed ZTD differences and TAVM3 and TR. Moreover, a significant worsening occurred in both the height differences and the ZTD differences at the end of 2011.

This was due to a degradation in the number of observations during the same period, as shown in Figure 3.15. According to Figure 3.15, the number of ZIMM station observations decreased gradually during the same period that differences in height and ZTD deteriorated. Brockmann et al. (2016) attributed this to a malfunctioning ZIMM antenna caused by an antenna pre-amplifier, which was also found in a previous study by Steigenberger et al. (2007).

Table 3.3 shows statistical values of observed ZTD differences, TR, and TAVM3, as well as height differences for each antenna pair at four GNSS co-located sites. The results indicate that a discrepancy between observed ZTD differences and TR and TAVM3 is typically around 1 to 3 mm when one or both antennas have different radomes or when different antenna types are used in the station pair. For example, the ZIMM-ZIM2 station pair showed a large discrepancy of -2.7 mm when ZIM2 was equipped with TRM55971.00. Similarly, the WTZA-WTZR pair had a large discrepancy of 3 mm when WTZR was equipped with LEIAR25. However, when the antenna pair is of the same type, such as the WTZR-WTZZ pair equipped with LEIAR25.R3, the discrepancy between observed ZTD differences and TR and TAVM3 is only 0.4 mm. In addition, good agreement was found between observed ZTD differences, TAVM3, and TR between HRAO and HRAB, even though they use different antenna types, and neither of them was equipped with a radome. The WSTD of observed ZTD differences was roughly 2 mm for all comparisons in this analysis, with the smallest variation (1.21 mm) found in the comparison between WTZR and WTZZ when both were equipped with the same antenna and radome (LEIAR25.R3 LEIT). Nevertheless, the difference is not significant compared to the other results. The results demonstrate that the use of different instruments, particularly antennas

Station pair	Antenna pair	ΔH (mm)	ΔZTD (mm)	TR (mm)	TAVM3 (mm)
WTZA-WTZR	ASH700936C_M SNOW-AOAD/M_T NONE	-103.45	-1.81 (2.23)	0.0 (0.0)	0.03 (0.0)
	ASH700936C_M SNOW-LEIAR25 LEIT	-92.04	-3.12 (2.26)	-0.0 (0.0)	0.03 (0.0)
	ASH700936C_M SNOW-LEIAR25.R3 LEIT	-99.30	-1.61 (2.21)	0.0 (0.0)	0.03 (0.0)
WTZA-WTZZ	ASH700936C_M SNOW-TPSCR3_GGD CONE	31.92	-1.58 (1.93)	-0.04 (0.22)	-0.01 (0.0)
	ASH700936C_M SNOW-LEIAR25.R3 LEIT	26.79	-1.13 (2.22)	-0.03 (0.21)	-0.01 (0.0)
WTZR-WTZZ	AOAD/M_T NONE-TPSCR3_GGD CONE	134.46	0.45 (1.56)	-0.03 (0.21)	-0.04 (0.0)
	LEIAR25.R3 LEIT-TPSCR3_GGD CONE	129.70	0.44 (1.27)	-0.0 (0.0)	-0.04 (0.0)
	LEIAR25.R3 LEIT-LEIAR25.R3 LEIT	126.59	0.42 (1.3)	-0.03 (0.21)	-0.04 (0.0)
ZIMM-ZIM2	TRM29659.00 NONE-TRM55971.00 NONE	-80.87	-2.72 (1.99)	0.0 (0.05)	0.02 (0.0)
	TRM29659.00 NONE-TRM59800.00 NONE	-95.95	-0.29 (2.22)	0.0 (0.07)	0.03 (0.0)
HRAO-HARB	ASH701945E_M NONE-TRM29659.00 NONE	-143931.16	40.09 (2.68)	39.46 (2.7)	38.68 (2.25)
	ASH701945E_M NONE-TRM59800.00 NONE	-143928.59	38.78 (2.82)	38.99 (2.63)	38.32 (2.22)
NYA1-NYAL	ASH701073.1 SNOW-AOAD/M_B DOME	5720.91	-0.4 (1.39)	-0.61 (0.76)	-1.76 (0.03)

Table 3.3: GNSS co-location sites were used to compare observed ZTD differences, TR, and TAVM3 of GNSS intra-technique comparisons. The results are presented in WM (WSTD) format.

and radomes, can lead to discrepancies between the observed ZTD differences and tropospheric ties in GNSS. However, there is an exceptional case when different types of antennas are used without a radome for a station pair, which does not cause a discrepancy between the observed ZTD differences and the tropospheric ties, as demonstrated by HRAO-HRAB and ZIMM-ZIM2. Nevertheless, using a different antenna design can also cause a discrepancy between the observed ZTD differences and the tropospheric ties model, as demonstrated in the case of ZIMM-ZIM2 when TRM55971.00 was used for ZIM2, despite neither station having a radome. A malfunctioning antenna significantly impacts the estimation at a certain station, thereby reducing the quality of observed ZTD and height differences.

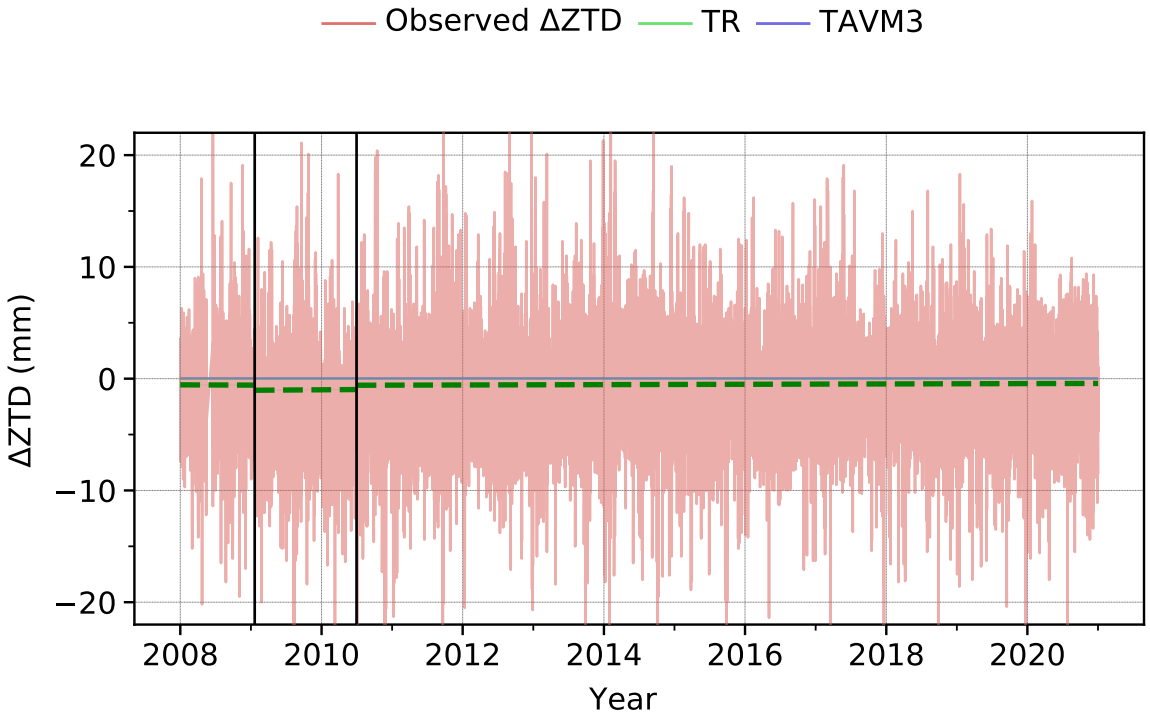

(a) ZTD differences between WTZA and WTZR. The green dashed line shows the mean offset of the time series.

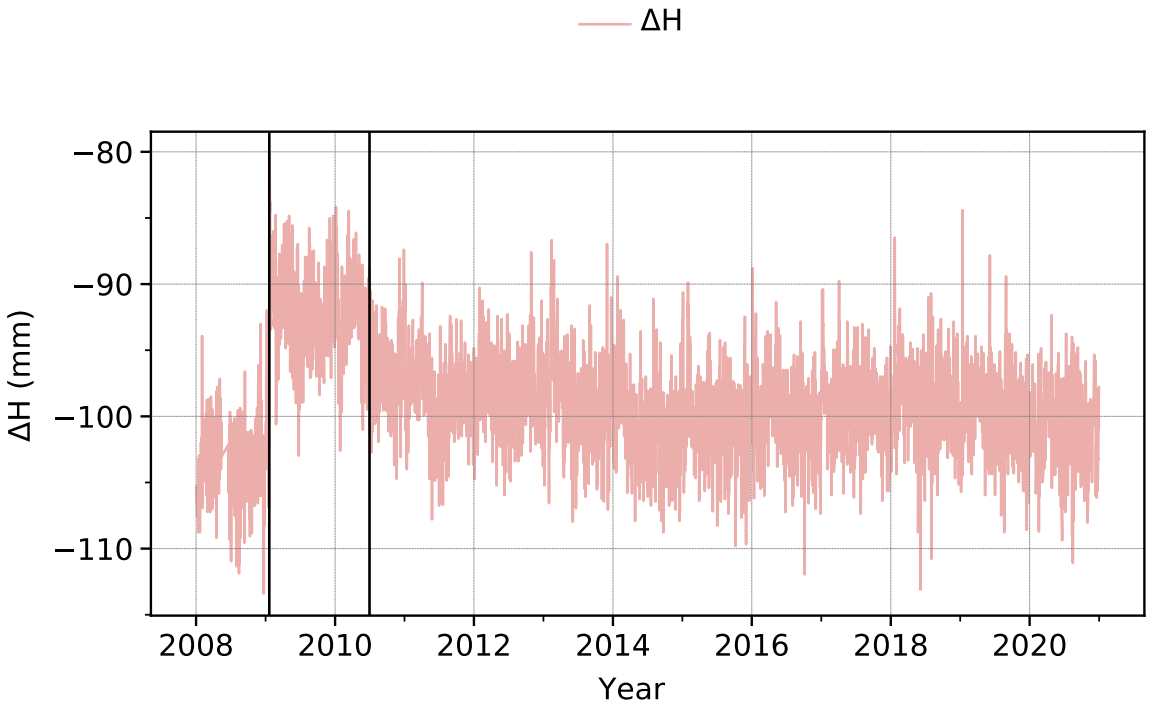

(b) Height differences between WTZA and WTZR

Figure 3.13: The comparison of differences in ZTD and height components between two GNSS stations at the Wettzell co-location site, namely WTZA, and WTZR. The height difference between the two GNSS stations is approximately 10 cm. The figure shows the comparison of observed ZTD differences, TAVM3, and TR. In addition, the antenna change events (black solid line) are also shown.

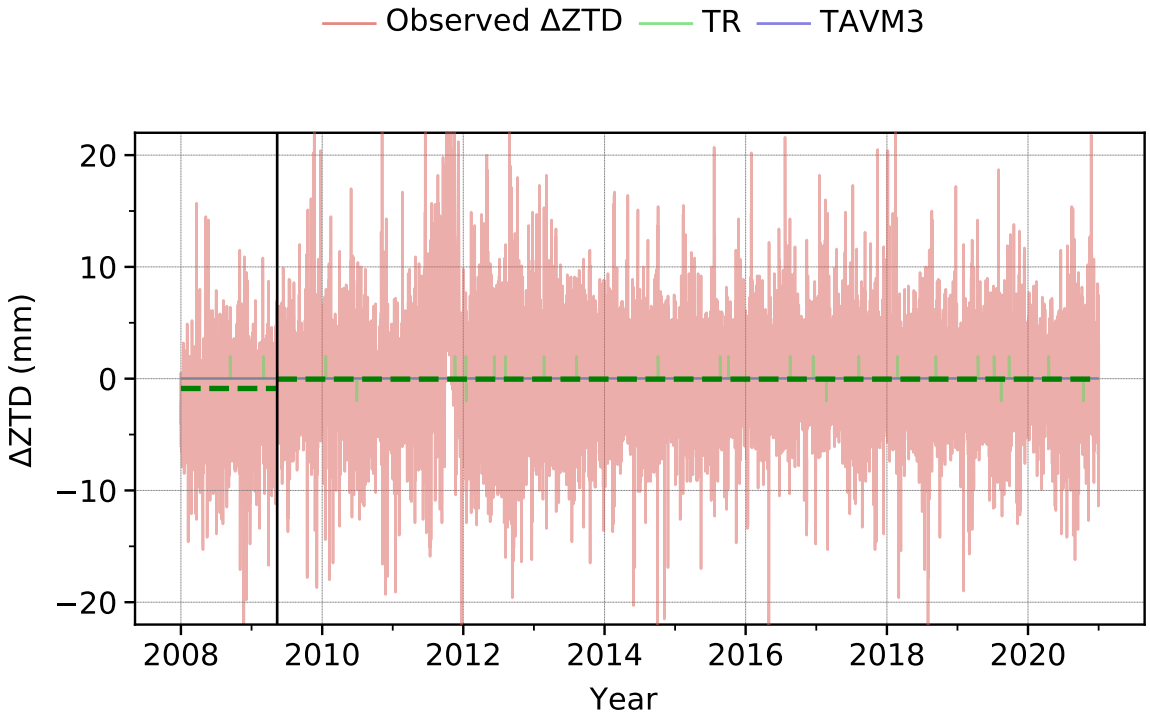

(a) ZTD differences between ZIMM and ZIM2. The green dashed line shows the mean offset of the time series.

(b) Height differences between ZIMM and ZIM2

Figure 3.14: The comparison of differences in ZTD and height components between two GNSS stations at Zimmerwald, Switzerland, namely ZIMM and ZIM2. The height difference between the two GNSS stations is approximately 10 cm. The figure shows the comparison of observed ZTD differences, TAVM3, and TR. In addition, the antenna change events (black solid line) are also shown.

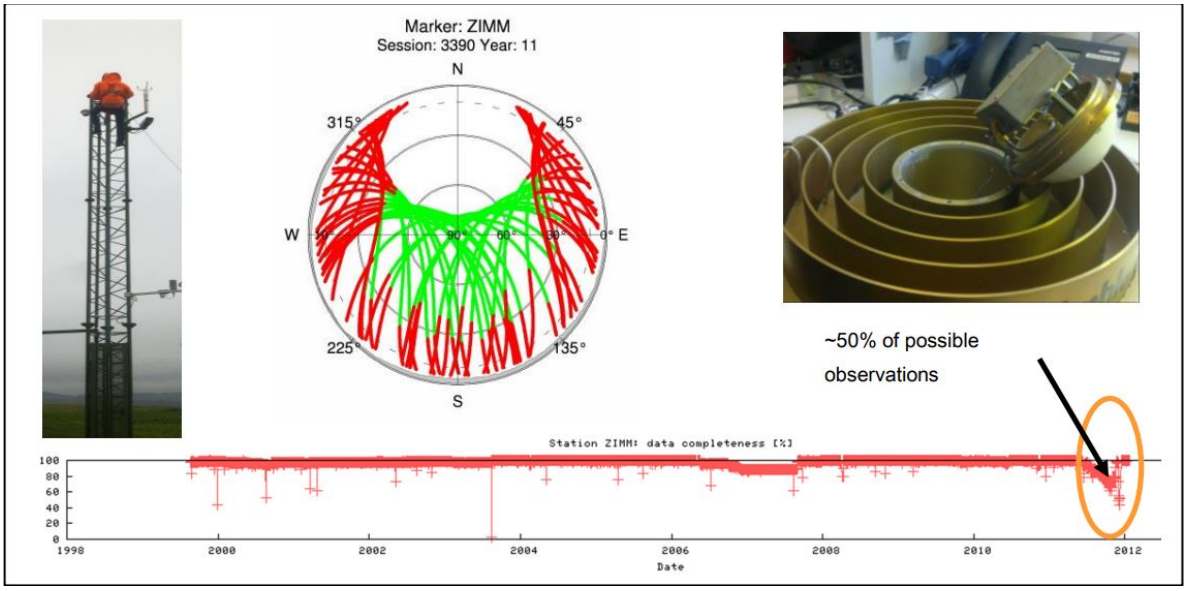

Figure 3.15: The number of observations at ZIMM stations from 2000 to 2011 (Figure from (Brockmann et al., 2016)). The actual observations were fewer than the expected observations at the end of 2011. This was due to a faulty antenna pre-amplifier. The station resumed normal operation after the antenna pre-amplifier was replaced.

The analysis of the discrepancy between the observed horizontal gradient differences and the expected horizontal gradient differences in GNSS was conducted for both the north-south (TGN) and east-west (TGE) components. A similar analysis method as that used for the ZTD parameter was applied. For co-location sites, it is typically assumed that the horizontal gradients between adjacent reference points in space geodetic techniques are equal due to their proximity. Therefore, this study used a value of zero for the expected horizontal gradient differences.

Figure 3.17 compares the estimated horizontal gradients in the east and north between WTZA and WTZR, revealing a shift in estimated horizontal gradient differences in both the north and east components caused by the change in antenna, similar to the observed ZTD differences. As shown in Figure 3.18, a malfunctioning antenna at ZIMM also degraded the bias of the horizontal gradients in both the north and east components. Table 3.4 shows the comparison of horizontal gradient differences for four GNSS co-location sites. Unlike ZTD parameters, the use of different antenna types does not show a large bias in the north and east gradients. A bias of 0.12 mm was found in the TGE at the WTZA-WTZR pair when WTZR was equipped with LEIAR25.R3. According to Figure 3.19, large residuals occurred in the low-elevation observations, which are highly sensitive to the estimation of horizontal gradients, at the WTZZ station, particularly in the east-west direction. Figure 3.16 illustrates that GNSS antennas at the Wettzell co-location site are situated close to a half-wall in the east-west part of the antenna, which can introduce multipath effects. Consequently, the substantial residuals observed in the low-elevation measurements can be attributed to multipath effects, resulting in unexpected biases in the observed horizontal gradient differences. Similarly, a bias of roughly 0.16 mm was found in the north gradient between HRAO and HARB due to the multipath effect that occurred in the north part of the low-elevation observations of HRAO station, as demonstrated in Figure 3.20. A large variation of 0.2 mm was found in the

HRAO-HARB pair. This is due to a different amount of low-elevation observations between the two stations. HRAO only observed GPS and later added GLONASS after 2014 in the data period, whereas HARB has observed GPS and GLONASS since 2008 and later added Galileo in 2012. Similar cases were found in other co-location sites in this study. However, the WTZR-WTZZ pair showed the least variation compared to others because both WTZR and WTZZ have observed GPS and GLONASS, which led to a consistent number of observations at low elevation throughout the data period.

Figure 3.16: The location of three GNSS antennas at the Wettzell co-location site that was used in the comparison (Courtesy from IGS).

Station pair	Antenna pair	ΔTGN (mm)	ΔTGE (mm)
WTZA-WTZR	ASH700936C_M SNOW-AOAD/M_T NONE	-0.02 (0.11)	-0.03 (0.14)
	ASH700936C_M SNOW-LEIAR25 LEIT	-0.07 (0.1)	0.02 (0.14)
	ASH700936C_M SNOW-LEIAR25.R3 LEIT	-0.05 (0.1)	-0.12 (0.22)
WTZA-WTZZ	ASH700936C_M SNOW-TPSCR3_GGD CONE	-0.04 (0.1)	-0.08 (0.14)
	ASH700936C_M SNOW-LEIAR25.R3 LEIT	-0.02 (0.1)	-0.11 (0.22)
WTZR-WTZZ	AOAD/M_T NONE-TPSCR3_GGD CONE	-0.01 (0.07)	-0.1 (0.07)
	LEIAR25.R3 LEIT-TPSCR3_GGD CONE	0.0 (0.01)	-0.03 (0.02)
	LEIAR25.R3 LEIT-LEIAR25.R3 LEIT	0.04 (0.05)	0.01 (0.08)
ZIMM-ZIM2	TRM29659.00 NONE-TRM55971.00 NONE	0.04 (0.14)	0.2 (0.15)
	TRM29659.00 NONE-TRM59800.00 NONE	-0.09 (0.13)	0.06 (0.16)
HRAO-HARB	ASH701945E_M NONE-TRM29659.00 NONE	-0.15 (0.22)	0.06 (0.23)
	ASH701945E_M NONE-TRM59800.00 NONE	-0.17 (0.2)	0.04 (0.21)
NYA1-NYAL	ASH701073.1 SNOW-AOAD/M_B DOME	-0.07 (0.12)	0.09 (0.15)

Table 3.4: GNSS co-location sites were used to compare observed horizontal gradient differences of GNSS intra-technique comparisons. The results are presented in WM (WSTD) format. The terms ΔTGE and ΔTGN refer to the differences in east and north gradients, respectively.

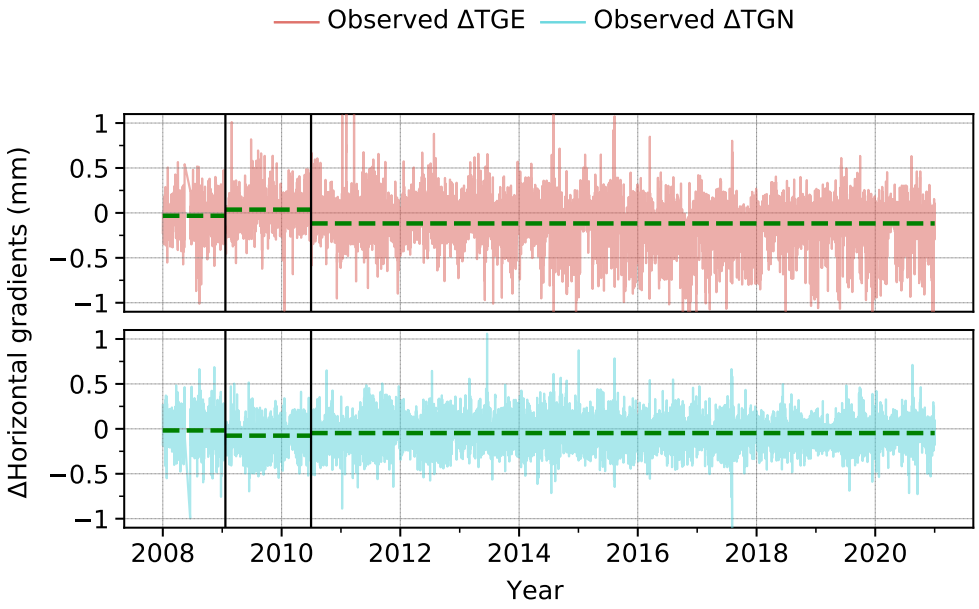

Figure 3.17: The time series depicts observed horizontal gradient differences between two GNSS stations at the Wettzell co-location site, namely WTZA and WTZR. The horizontal distance between them is approximately 1 meter. The antenna change events (black solid line) are also shown. The green dashed line shows the mean offset for each antenna. The terms ΔTGE and ΔTGN refer to the differences in east and north gradients, respectively.

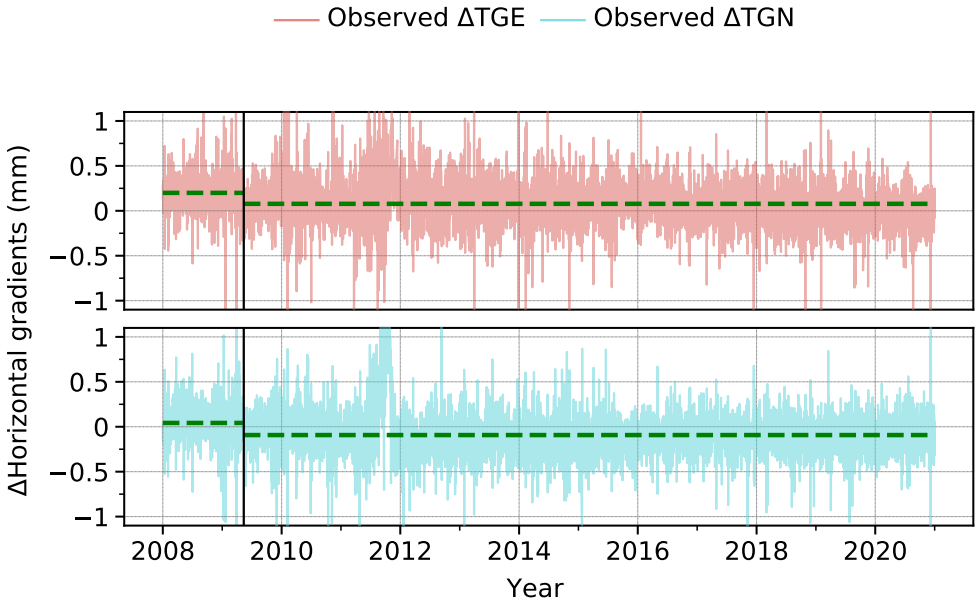

Figure 3.18: The time series depicts observed horizontal gradient differences between two GNSS stations at the Zimmerwald co-location site, namely ZIMM and ZIM2. The horizontal distance between them is approximately 2 meters. The antenna change events (black solid line) are also shown. The green dashed line shows the mean offset for each antenna. The terms ΔTGE and ΔTGN refer to the differences in east and north gradients, respectively.

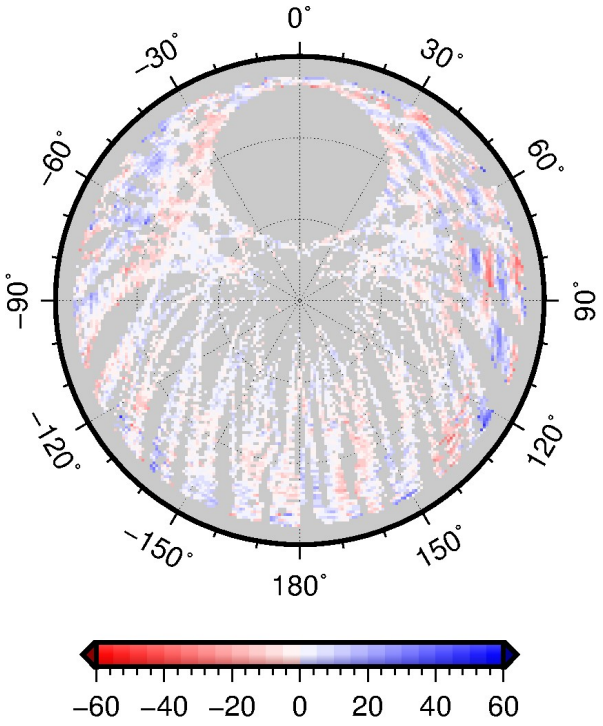

(a) Residual plot of WTZR station

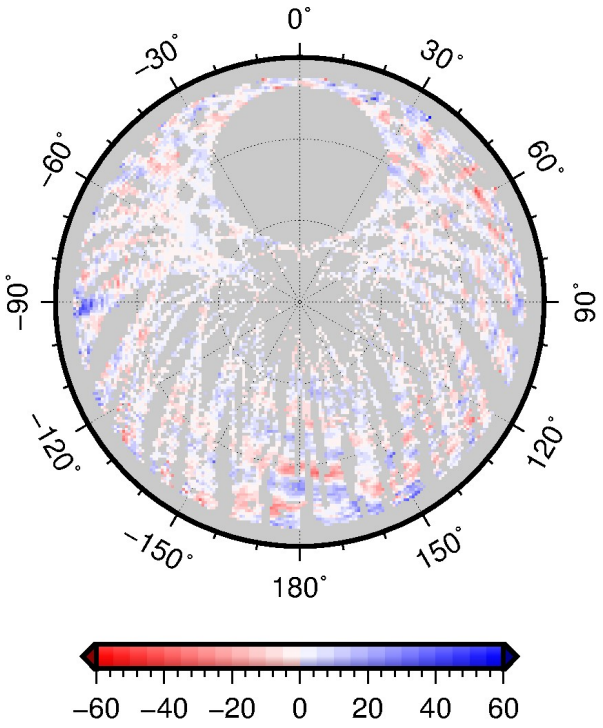

(b) Residual plot of WTZZ station

Figure 3.19: A snapshot of one-month residuals of ionosphere-free phase observations of WTZR and WTZZ in January 2013 (1^{st} January to 30^{th} January). The residuals are given in millimeters. The sky plots reveal that WTZZ has slightly larger residuals than WTZR for observations at low elevations.

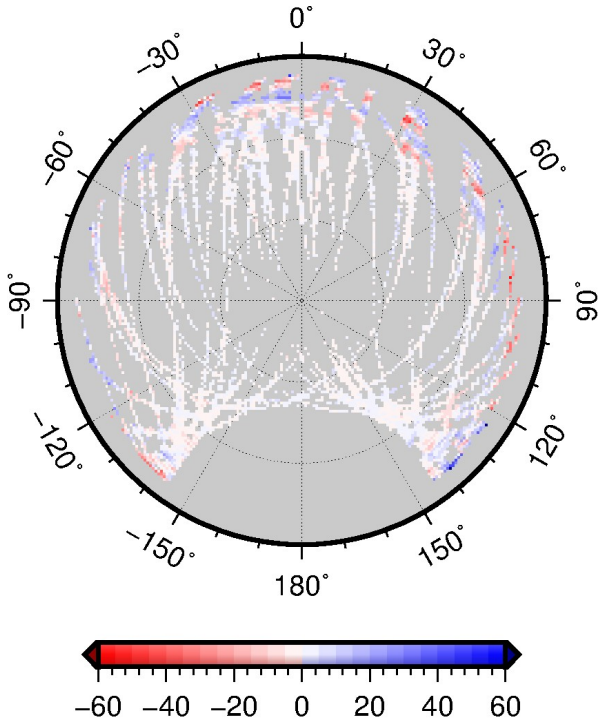

(a) Residual plot of HRAO station

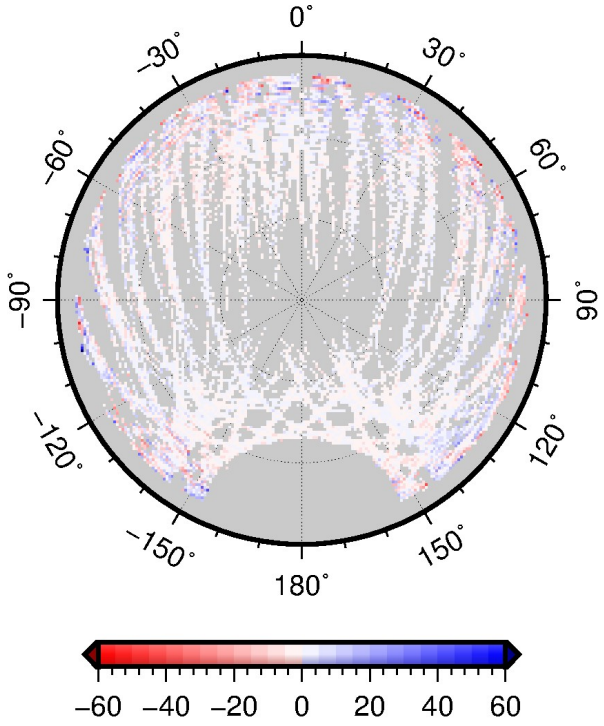

(b) Residual plot of HARB station

Figure 3.20: A snapshot of two-week residuals of ionosphere-free phase observations of HRAO and HRAB in May 2014 (5^{st} May to 20^{th} January). The residuals are given in millimeters. The sky plots reveal that HRAO has slightly larger residuals than HARB for observations at low elevations.

The results demonstrate that the main contribution to the bias is the multipath effect at low-elevation observations for each station, regardless of whether different instruments are used. The different numbers of observations at low elevation in station pairs lead to a high variation in observed horizontal gradient differences. Furthermore, a malfunctioning antenna significantly impacts the observed horizontal gradients at a certain station, thereby affecting the observed horizontal gradient differences similar to observed ZTD differences.

3.3.2 VLBI intra-technique comparison of tropospheric parameters

In this section, the VLBI intra-technique comparisons of tropospheric parameter differences are demonstrated. As previously stated, VLBI has a lengthy history of observations, but there is only one VLBI radio telescope at each site, making it impossible to perform intra-technique VLBI comparisons despite the abundant historical data. Since the establishment of the VLBI Global Geodetic Observing System (VGOS) (Petrachenko et al., 2009), it has become possible to perform VLBI intra-technique comparisons by installing additional VLBI radio telescopes at the same site, such as Wettzell, Germany. In this study, the reprocessed tropospheric parameters obtained from the Potsdam Open-source Radio interferometry Tool (PORT) (Schuh et al., 2021) using the configuration from the GFZ ITRF2020 reprocessing campaign. The VLBI-derived tropospheric parameters of twelve years of data from 2008 to 2020 were selected. TAVM3 and TR were used as tropospheric ties to compare with observed ZTD differences, while a zero value was employed for expected horizontal gradient differences.

The comparison between the observed ZTD differences and TAVM3 obtained from the WETTZELL and WETTZ13N radio telescopes from 2015 to 2021 is presented in Figure 3.21. The results show good agreement between the observed ZTD differences, TAVM3, and TR, with the observed ZTD differences having a mean offset of 0.75 mm, and the mean offsets of TAVM3 and TR being approximately 1.00 mm, which is reasonable given the height differences of roughly 3.42 m. The standard deviation of observed ZTD differences is 2.45 mm, similar to the GNSS intra-technique comparison. Moreover, the time series shows no significant change, as expected since the VLBI radio telescope does not change over time compared to GNSS equipment.

Figure 3.22 shows that the mean offset of the observed north and east horizontal gradient differences was -0.00 and 0.03 mm, respectively, with variations of approximately 0.26 and 0.23 mm, respectively. Additionally, the observed horizontal gradient differences are not subject to significant changes. These results suggest that there is no instrumental bias in observed VLBI tropospheric ties in this analysis.

It is important to note that this long-term comparison was conducted only at the Wettzell co-location site, which is the only location where long-term observations were possible for two telescopes in this study. Therefore, it is difficult to generalize the observed tropospheric parameter differences and tropospheric ties to other locations. Nevertheless, the VLBI intra-technique comparison reveals a better agreement between the observed ZTD differences and tropospheric ties, as well as a smaller bias in horizontal gradient differences, compared to the GNSS intra-technique comparison. Additionally, VLBI is not affected by multipath effects due to surrounding obstacles and no changes in equipment occur at the VLBI radio telescope, resulting in more stable tropospheric parameters.

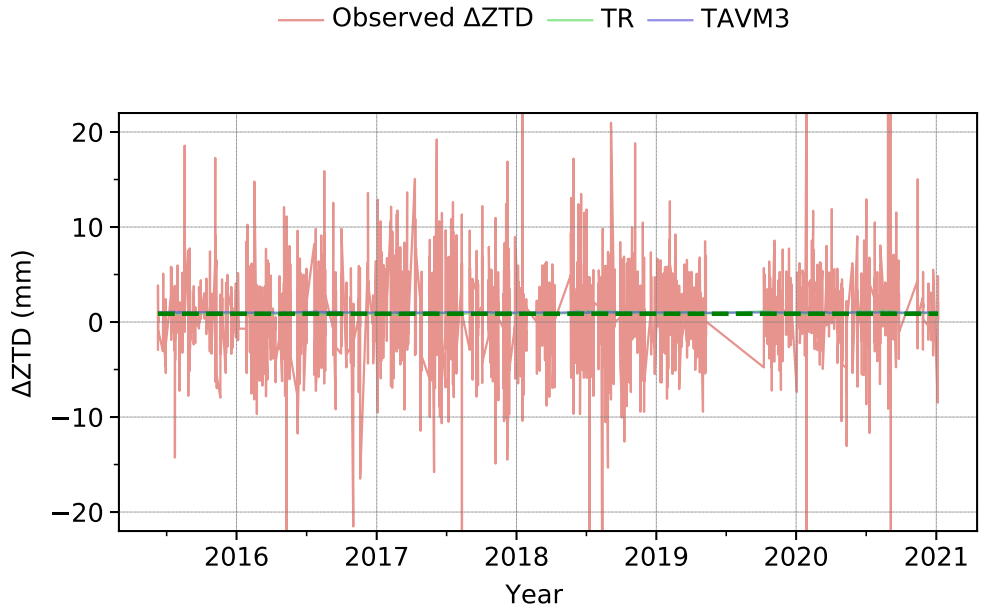

(a) ZTD differences between WETTZELL and WETTZ13N. The green dashed line shows the mean offset of the time series.

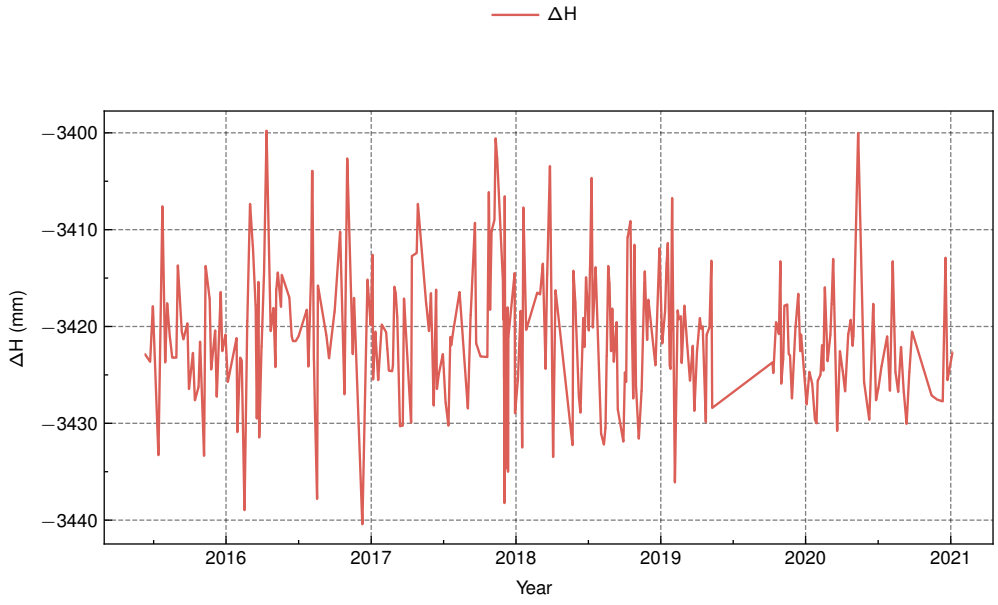

(b) Height differences

Figure 3.21: The comparison of ZTD and height components between two VLBI radio telescopes at Wettzell co-location site, namely WETTZELL, and WETTZ13N. The height difference is approximately 3.4 m. The figure shows the comparison of observed ZTD differences, TAVM3, and TR.

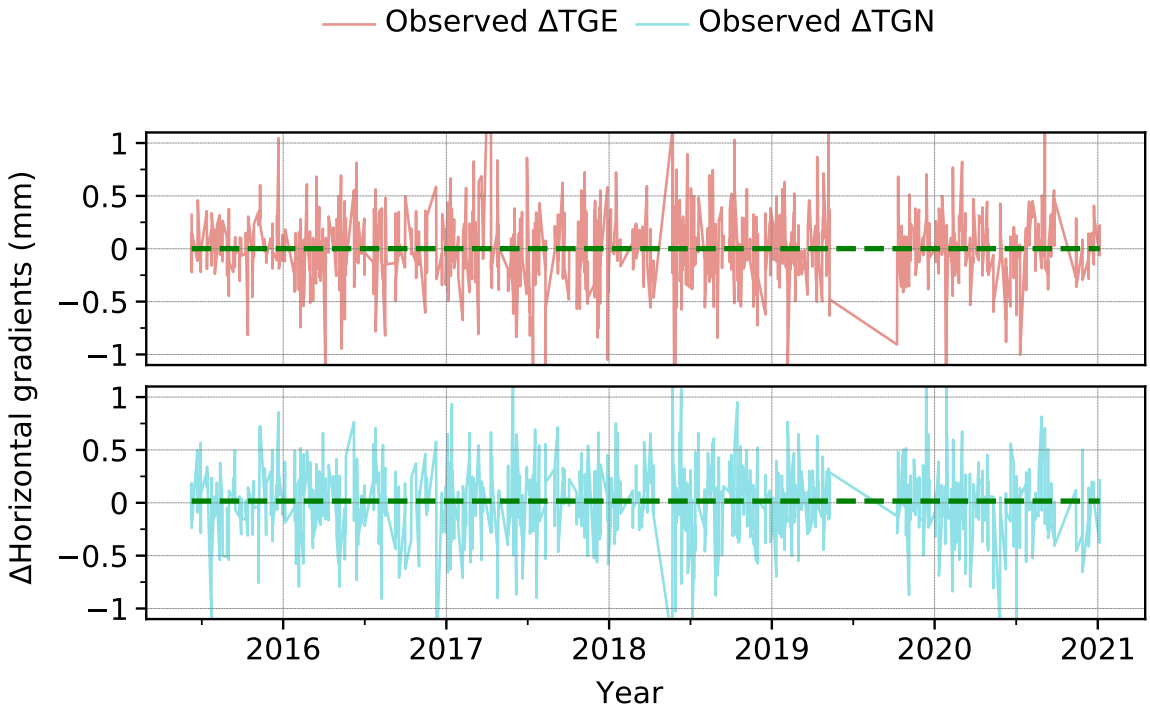

Figure 3.22: This figure presents observed horizontal gradient differences between two VLBI radio telescopes located at the Wettzell co-location site: WETTZELL and WETTZ13N. The green dashed line represents the mean offset of the time series. The terms ΔTGE and ΔTGN refer to the differences in east and north gradients, respectively.

3.3.3 VLBI and GNSS inter-technique comparison of tropospheric parameters

In this section, a discrepancy between observed tropospheric parameters and tropospheric ties between VLBI and GNSS is evaluated. For this analysis, six GNSS and VLBI co-location sites are selected for investigation. In this analysis, VLBI and GNSS-derived tropospheric parameters of twelve years (2008-2020) from sections 3.3.1 and 3.3.2 are used. TR and TAVM3 are also employed to compare observed ZTD differences and tropospheric ties. Regarding a comparison of horizontal gradient differences, a zero value is employed for expected horizontal gradient differences. A similar analysis method as the two previous sections is also carried out in this study.

The statistical values for the comparison of observed ZTD differences and tropospheric ties are presented in Table 3.5. When the GNSS antenna was not equipped with a radome, the observed ZTD differences and tropospheric ties were in good agreement. For example, when comparing HOBART26 and HOB2, the mean offset of observed ZTD differences, TAVM3, and TR agreed at the level of 0.1 mm. A similar case was also found for the YARRA12M-YARR pair. Furthermore, despite the presence of a radome, a good agreement was found for GNSS antennas equipped with the LEIAR25.R3 LEIT. The observed ZTD differences, TAVM3, and TR also demonstrated good agreement at the level of 0.1 mm in the comparison between WETTZELL and WTZR. However, when comparing WETTZELL and WTZZ, where WTZZ was equipped with the LEIAR25.R3 LEIT, a discrepancy of 0.5 mm between observed

ZTD differences and tropospheric ties was observed. Large residuals were found in WTZZ observations due to multipath effects, as shown in Figure 3.19. Additionally, despite using the same antenna, the comparison between ONSALA60 and ONSA revealed a discrepancy in observed ZTD differences caused by the replacement of microwave-absorbing material, as shown in Figure 3.24. The remaining comparisons with GNSS antennas equipped with radomes revealed a 1-2 mm difference between observed ZTD differences and tropospheric ties, depending on the type of antenna. As in the comparison in Section 3.3.1, changing antennas in GNSS techniques caused a shift in the time series. The standard deviation of observed ZTD differences ranged from 1 to 2 mm, which agreed with the results in VLBI and GNSS intra-technique comparisons.

Station pair	Antenna pair	ΔH (mm)	ΔZTD (mm)	TR (mm)	TAVM3 (mm)
WETTZELL-WTZA	VLBI-ASH700936C_M SNOW	3123.90	0.92 (1.79)	-0.93 (0.86)	-0.93 (0.03)
WETTZELL-WTZR	VLBI-AOAD/M_T NONE	3123.41	0.27 (1.85)	-0.91 (0.85)	-0.93 (0.02)
	VLBI-LEIAR25 LEIT	3125.24	-1.68 (1.81)	-0.93 (0.86)	-0.92 (0.03)
	VLBI-LEIAR25.R3 LEIT	3123.78	-0.87 (1.78)	-0.93 (0.86)	-0.93 (0.03)
WETTZELL-WTZS	VLBI-ASH701945G_M SNOW	5624.45	-0.75 (1.87)	-2.0 (0.0)	-1.67 (0.05)
	VLBI-LEIAR25.R3 NONE	5624.82	-1.75 (1.75)	-1.95 (0.15)	-1.65 (0.05)
	VLBI-LEIAR25.R3 LEIT	5623.66	-1.52 (1.83)	-2.0 (0.0)	-1.67 (0.05)
WETTZELL-WTZ3	VLBI-LEIAR25.R3 LEIT	5623.41	-1.33 (1.89)	-2.0 (0.0)	-1.67 (0.05)
WETTZELL-WTZZ	VLBI-TPSCR3_GGD CONE	3124.76	0.16 (1.84)	-0.96 (0.86)	-0.93 (0.03)
	VLBI-LEIAR25.R3 LEIT	3123.78	-0.44 (1.82)	-0.96 (0.86)	-0.93 (0.03)
HOBART26-HOB2	VLBI-AOAD/M_T NONE	24032.24	-7.72 (1.62)	-7.95 (0.15)	-7.55 (0.16)
KOKEE-KOKB	VLBI-ASH701945G_M NONE	9596.80	-1.77 (2.14)	-2.71 (0.83)	-2.82 (0.06)
KOKEE-KOKV	VLBI-ASH701945G_M NONE	9596.68	-1.83 (2.2)	-2.73 (0.83)	-2.82 (0.06)
YARRA12M-YARR	VLBI-LEIAT504 NONE	6864.33	-1.84 (1.81)	-2.0 (0.0)	-2.09 (0.09)
NYALES20-NYA1	VLBI-ASH701073.1 SNOW	3090.81	1.91 (2.05)	-1.04 (0.86)	-0.95 (0.02)
NYALES20-NYA2	VLBI-JAV_RINGANT_G3T NONE	5955.57	2.61 (2.0)	-2.0 (0.0)	-1.83 (0.03)
	VLBI-JAVRINGANT_G5T NONE	5968.88	-0.31 (1.64)	-2.0 (0.0)	-1.83 (0.03)
NYALES20-NYAL	VLBI-AOAD/M_B DOME	8808.56	1.64 (2.06)	-1.95 (0.15)	-2.7 (0.04)
MATERA-MAT1	VLBI-ASH701941.B NONE	8866.76	-2.68 (1.74)	-2.66 (0.81)	-2.65 (0.07)
	VLBI-TRM29659.00 NONE	8867.92	-0.34 (1.71)	-2.73 (0.86)	-2.68 (0.08)
	VLBI-LEIAR20 NONE	8872.38	-1.57 (1.98)	-2.74 (0.83)	-2.69 (0.08)
MATERA-MATE	VLBI-TRM29659.00 NONE	7851.56	3.59 (2.12)	-2.0 (0.0)	-2.29 (0.12)
	VLBI-LEIAT504GG NONE	7868.77	-0.8 (1.76)	-2.04 (0.14)	-2.37 (0.07)
	VLBI-LEIAR20 NONE	7872.38	-1.34 (2.11)	-2.23 (0.48)	-2.39 (0.07)
HART15M-HRAO	VLBI-ASH701945E_M NONE	-4585.69	2.76 (1.63)	1.32 (0.69)	1.23 (0.07)
HART15M-HRAG	VLBI-LEIAR25.R3 LEIT	2413.82	0.24 (1.66)	-0.57 (0.69)	-0.65 (0.04)
TSUKUB32-TSKB	VLBI-AOAD/M_T DOME	17484.29	-3.12 (2.12)	-5.96 (0.16)	-5.66 (0.3)
	VLBI-AOAD/M_T NONE	17474.72	-4.65 (2.66)	-6.0 (0.0)	-6.17 (0.13)
	VLBI-AOAD/M_T DOME	17479.05	-4.31 (2.05)	-5.54 (0.77)	-5.61 (0.32)
ONSALA60-ONSA	VLBI-AOAD/M_B OSOD	13710.68	-2.2 (1.82)	-4.09 (0.25)	-4.36 (0.12)
	VLBI-AOAD/M_B NONE	13726.98	-4.51 (1.93)	-4.22 (0.46)	-4.48 (0.16)
	VLBI-AOAD/M_B OSOD	13695.65	-1.86 (2.31)	-4.23 (0.48)	-4.35 (0.12)
ONSALA60-ONS1	VLBI-LEIAR25.R3 LEIT	14808.47	-3.59 (2.09)	-4.75 (0.83)	-4.69 (0.14)

Table 3.5: The comparison of observed ZTD differences, TR, and TAVM3, for VLBI and GNSS techniques at six co-location sites over a twelve-year period. The WM and WSTD are presented as a statistic value for each GNSS antenna usage period with WM (WSTD) format.

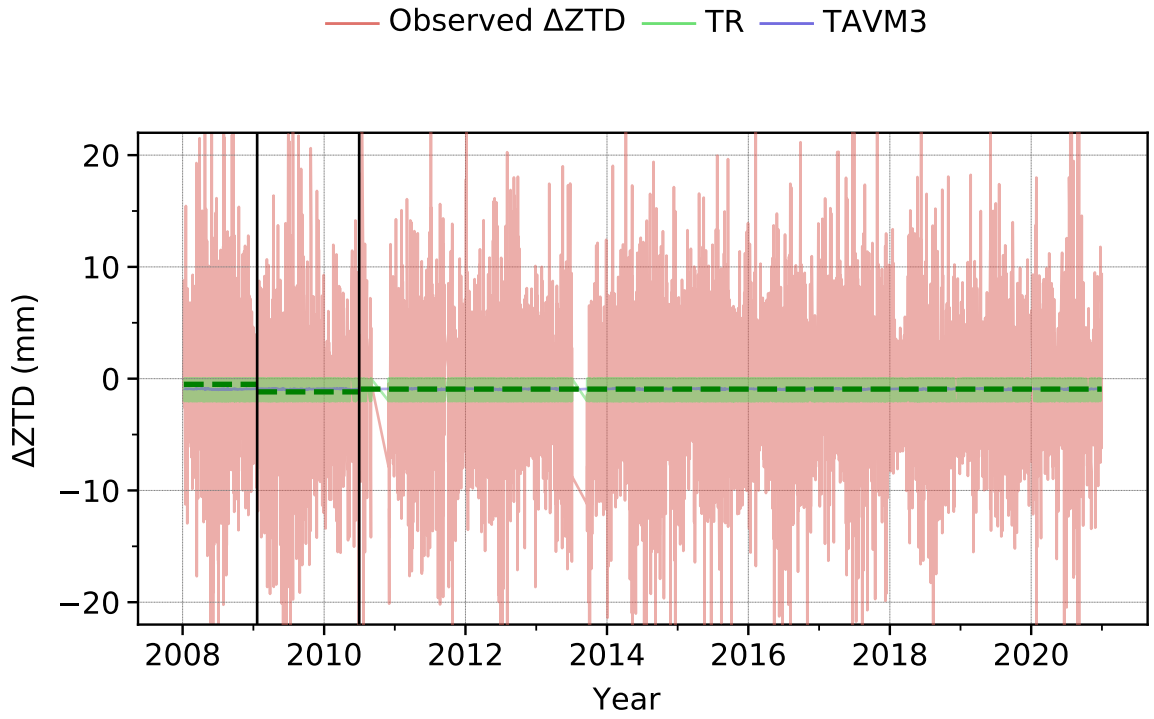

(a) ZTD differences between WETTZELL and WTZR. The green dashed line shows the mean offset of the time series.

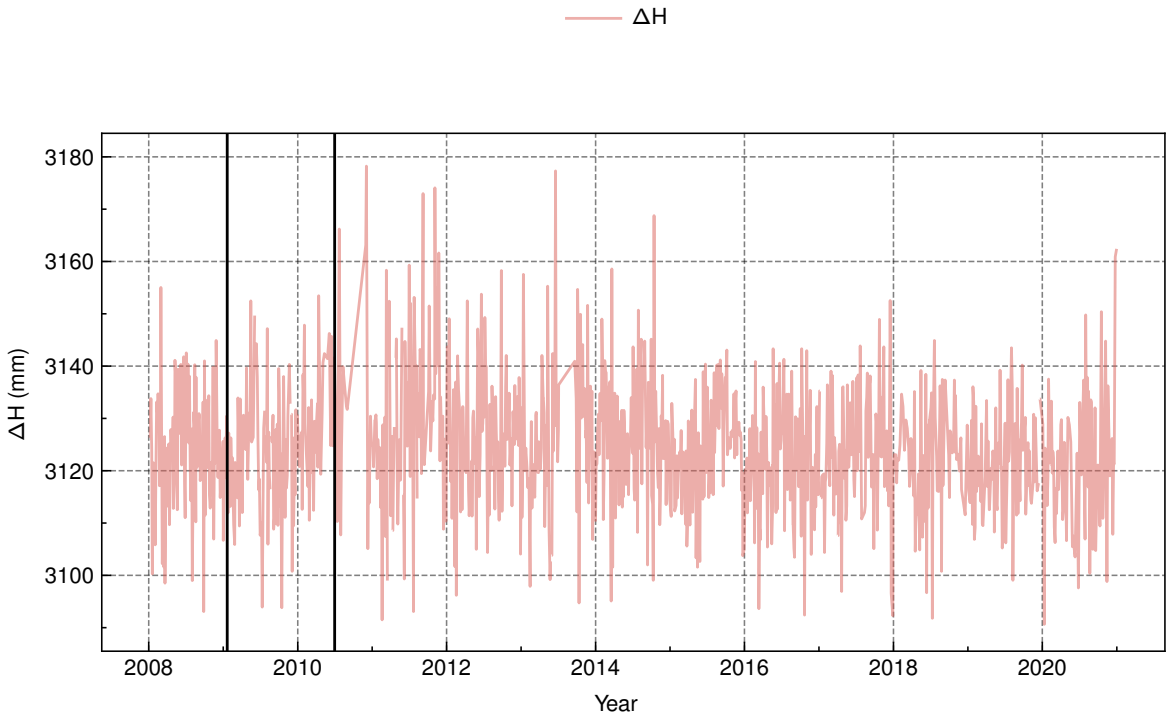

(b) Height differences between WETTZELL and WTZR

Figure 3.23: The time series depicts ZTD and height differences between VLBI radio telescope and GNSS station at Wettzell co-location site, namely WETTZELL and WTZR. The height difference is approximately 3.1 m. The figure shows the comparison of observed ZTD differences, TR, and TAVM3. In addition, the antenna change events (solid black line) are also shown.

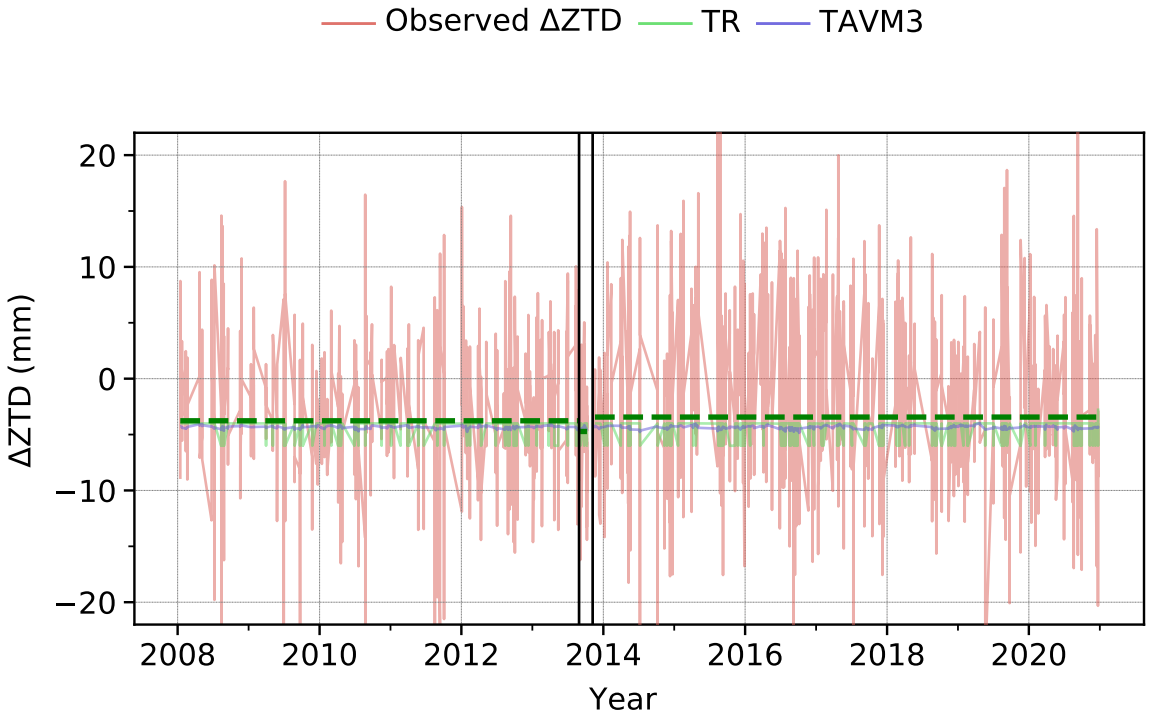

(a) ZTD differences between ONSALA60 and ONSA. The green dashed line shows the mean offset of the time series.

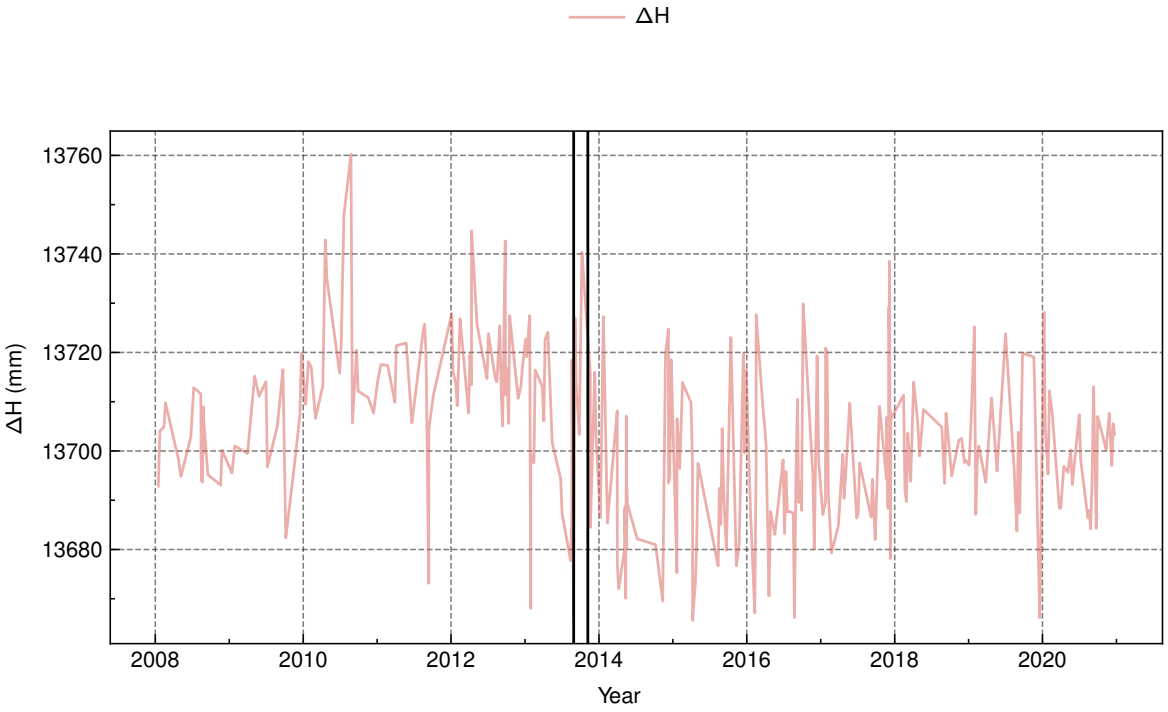

(b) Height differences between ONSALA60 and ONSA

Figure 3.24: The comparison of ZTD and height components between VLBI radio telescope and GNSS station at Onsala co-location site, namely ONSALA60 and ONSA. The height difference is approximately 3.1 m. The figure shows the comparison of observed ZTD differences, TR, and TAVM3. In addition, the renewal of the microwave absorbing shield event (solid black line) is also shown.

In this analysis, a comparison is made between the horizontal gradients of VLBI and GNSS. Table 3.6 displays the statistical values for the observed east and north gradient differences. The results indicate that most of the comparisons do not show significant biases for observed north and east gradient differences. Figure 3.25 demonstrates that changing the antenna in the GNSS technique also causes a shift in time series, which is similar to the ZTD comparison results. However, the magnitude of the horizontal gradients is at the sub-millimeter level, which makes it less obvious. The standard deviation is also higher than in the VLBI and GNSS intra-technique comparisons. Furthermore, even though the GNSS station is not equipped with a radome, a significant standard deviation of 0.7 mm was found between HOBART26 and HOB2, as shown in Figure 3.26. This was likely due to the strong multipath effect observed at low elevations. On the other hand, when comparing TSUKUB32 and TSKB, where TSKB was not equipped with a radome, the large magnitude of mean offset and variation was due to only 26 common epochs being found in this analysis.

The comparison between the horizontal gradients of VLBI and GNSS shows insignificant biases for observed north and east gradient differences. However, changing the antenna in the GNSS technique causes a shift in the time series, similar to the ZTD comparison result. The standard deviation is higher in this comparison due to different estimation intervals for horizontal gradient parameters and various software packages. This finding is also consistent with the study by Puente (2021), which compared tropospheric parameters from GNSS and VLBI from various products during CONT17 and found a similar variation of observed horizontal gradient differences when comparing VLBI and GNSS-derived horizontal gradients. Additionally, the presence or absence of a radome affects the standard deviation, with a significant standard deviation found in HOBART26 and HOB2, likely due to the strong multipath effect at low elevations. Finally, the large magnitude of mean offsets and variations in TSUKUB32 and TSKB is due to the limited number of common epochs found in this analysis.

Station pair	Antenna pair	ΔTGN (mm)	ΔTGE (mm)
WETTZELL-WTZA	VLBI-ASH700936C_M SNOW	0.03 (0.42)	0.08 (0.43)
WETTZELL-WTZR	VLBI-AOAD/M_T NONE	-0.02 (0.39)	0.08 (0.34)
	VLBI-LEIAR25 LEIT	-0.05 (0.39)	0.04 (0.4)
	VLBI-LEIAR25.R3 LEIT	-0.01 (0.42)	-0.04 (0.4)
WETTZELL-WTZS	VLBI-ASH701945G_M SNOW	0.03 (0.4)	0.07 (0.38)
	VLBI-LEIAR25.R3 NONE	-0.03 (0.37)	-0.08 (0.37)
	VLBI-LEIAR25.R3 LEIT	0.02 (0.42)	-0.01 (0.4)
WETTZELL-WTZ3	VLBI-LEIAR25.R3 LEIT	0.03 (0.42)	-0.04 (0.41)
WETTZELL-WTZ2	VLBI-LEIAR25.R3 LEIT	0.03 (0.43)	-0.01 (0.42)
WETTZELL-WTZZ	VLBI-TPSCR3_GGD CONE	-0.03 (0.39)	-0.03 (0.36)
	VLBI-LEIAR25.R3 LEIT	0.02 (0.42)	-0.04 (0.41)
WETTZ13N-WTZA	VLBI-ASH700936C_M SNOW	0.04 (0.41)	0.1 (0.45)
WETTZ13N-WTZ3	VLBI-LEIAR25.R3 LEIT	0.02 (0.41)	-0.04 (0.4)
WETTZ13N-WTZ2	VLBI-LEIAR25.R3 LEIT	0.01 (0.41)	-0.02 (0.4)
HOBART26-HOB2	VLBI-AOAD/M_T NONE	0.05 (0.72)	0.0 (0.66)
YARRA12M-YARR	VLBI-LEIAT504 NONE	-0.09 (0.52)	-0.01 (0.51)
NYALES20-NYA1	VLBI-ASH701073.1 SNOW	0.04 (0.4)	-0.04 (0.39)
NYALES20-NYA2	VLBI-JAV_RINGANT_G3T NONE	-0.16 (0.45)	-0.14 (0.47)
	VLBI-JAVRINGANT_G5T NONE	-0.19 (0.38)	0.16 (0.37)
NYALES20-NYAL	VLBI-AOAD/M_B DOME	-0.02 (0.42)	0.05 (0.4)
TSUKUB32-TSKB	VLBI-AOAD/M_T DOME	0.07 (0.62)	-0.06 (0.55)
	VLBI-AOAD/M_T NONE	0.34 (0.82)	-0.15 (0.75)
	VLBI-AOAD/M_T DOME	-0.1 (0.53)	-0.22 (0.52)
ONSALA60-ONSA	VLBI-AOAD/M_B OSOD	0.01 (0.35)	-0.01 (0.39)
	VLBI-AOAD/M_B NONE	-0.27 (0.48)	-0.35 (0.55)
	VLBI-AOAD/M_B OSOD	0.04 (0.4)	-0.01 (0.4)
ONSALA60-ONS1	VLBI-LEIAR25.R3 LEIT	-0.01 (0.4)	-0.06 (0.39)

Table 3.6: A comparison of the observed tropospheric horizontal gradient between VLBI and GNSS techniques at six co-location sites over a twelve-year period. The WM and WSTD are presented as a statistic value for each GNSS antenna usage period with WM (WSTD) format. The terms ΔTGE and ΔTGN refer to the differences in east and north gradients, respectively.

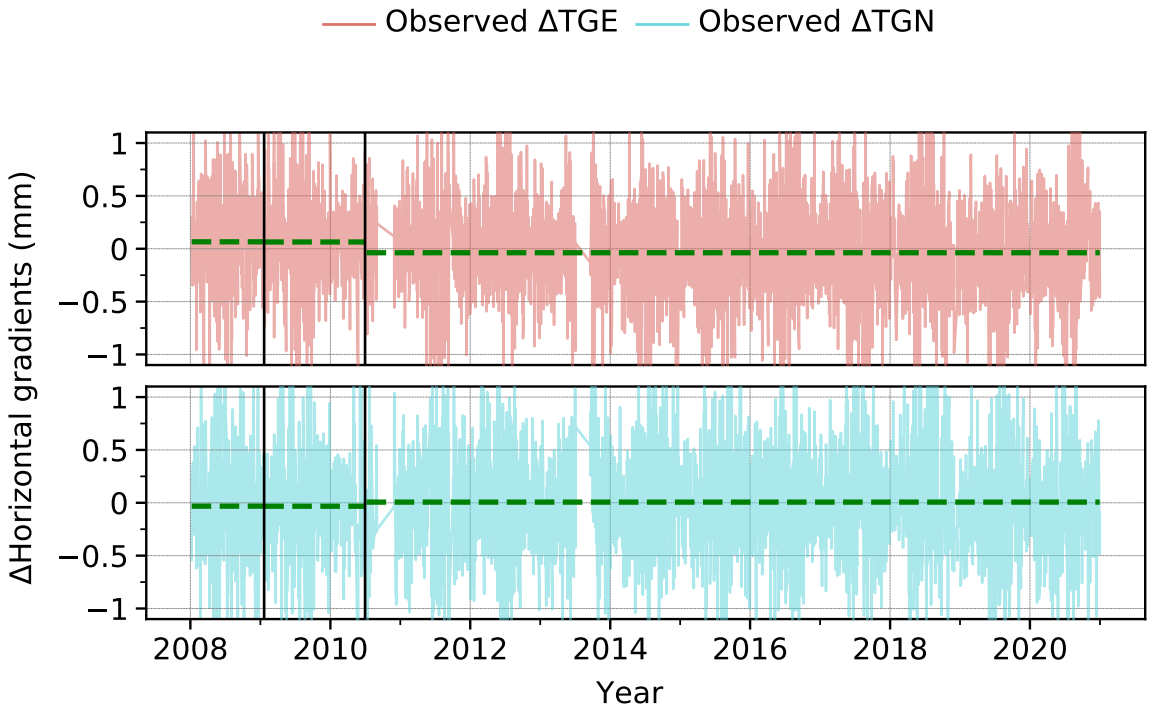

Figure 3.25: The time series presents observed horizontal gradient differences between VLBI radio telescope and the GNSS station at the Wettzell co-location site, namely WETTZELL and WTZR. The figure shows the comparison of horizontal gradients. In addition, the antenna change events (solid black line) are also shown. The terms ΔTGE and ΔTGN refer to the differences in east and north gradients, respectively.

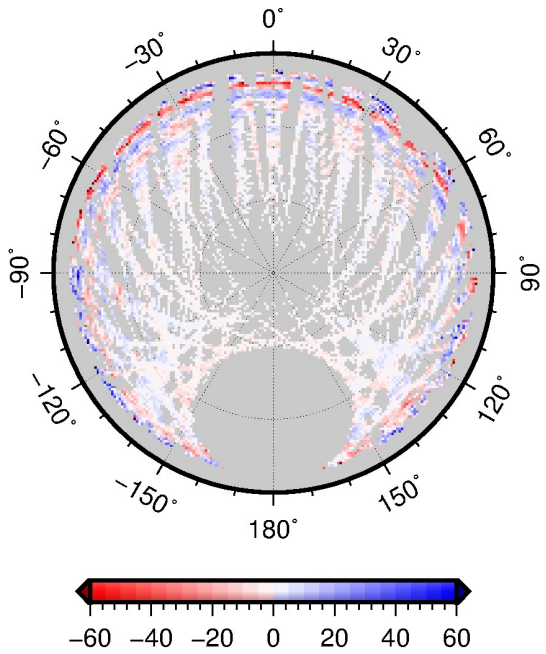

Figure 3.26: A snapshot of one-month residuals of ionosphere-free phase observations of HOB2 in January 2013 (1^{st} January to 30^{th} January). The residuals are given in millimeters. The sky plot demonstrates that HOB2 has large residuals at low-elevation observations, resulting in a significant standard deviation in observed ZTD and horizontal gradient differences.

Overall, the comparison studies in sections 3.3.1, 3.3.2, and 3.3.3 indicate that GNSS is the primary contributor to the discrepancy between observed tropospheric parameters and tropospheric ties. Although demonstrating an insignificant difference between observed tropospheric parameters and tropospheric ties, there is inconclusive evidence that VLBI is free from instrumental effects, as only one site was compared in this study. Nevertheless, VLBI shows more promise than GNSS, as it exhibits better agreement between observed tropospheric parameter differences and tropospheric ties. Regarding the comparison of horizontal gradients, no clear evidence of systematic effects in the estimated horizontal gradients is found. However, the primary contributors to the discrepancy in GNSS-derived horizontal gradients are the number of observations at low elevations and the multipath effect. In contrast, VLBI is typically observed at low elevations, with no obstructions surrounding the VLBI radio telescope, and is therefore unlikely to experience these effects in VLBI-derived horizontal gradients. Moreover, the increasing observed variation in horizontal gradient differences between VLBI and GNSS is due to a different interval estimation of horizontal gradients. These results demonstrate that the main cause of the discrepancy between observed ZTD differences and tropospheric ties arises from GNSS. The impact of using different instruments on the observed tropospheric parameter differences varies depending on the instrument used. Additionally, a malfunctioning antenna significantly impacts observed tropospheric parameters and therefore affects the observed tropospheric parameter differences. However, no significant evidence of an instrument effect on observed tropospheric gradient differences is found, as the mean bias is small compared to its variation. In this thesis, the discrepancy between observed tropospheric parameters, especially the ZTD parameter, and tropospheric ties due to the instrument is referred to as "instrumental bias." To prove this hypothesis, the author conducted a GNSS co-location site experiment, which is described in section 4.1.

4

Combination of VLBI and GNSS atmospheric parameters

The following chapter describes two unique GNSS co-location experiments, which were conducted to validate the assumption of instrumental bias identified in the preceding section. Chapter 4.1 describes the effects detected in the previous chapter's GNSS and VLBI tropospheric parameters through a unique experiment. Additionally, this chapter outlines the modeling of these effects based on a unique GNSS co-location experiment. The strategies for combining VLBI and GNSS, as well as the methodology for investigating the capability of tropospheric ties, are described in detail in Chapter 4.2.

4.1 An GNSS co-location experiment at GFZ Potsdam

4.1.1 A20 experiment

According to the findings presented in Section 3.3, the instrumental bias is a major contributor to the discrepancies between the tropospheric ties and the observed tropospheric parameter differences. To support this assertion, the author conducted a GNSS co-location experiment on the roof of the A20 building located at the Telegrafernberg campus of GFZ Potsdam, Potsdam, Germany. The experiment involved four GNSS stations placed at different heights and in close horizontal proximity to one another (within 2 m). The four stations were named A201, A202, A203, and A204, with A201 and A202 being positioned four and two meters higher than A203 and A204, respectively, as shown in Figure 4.1. A201, A202, and A203 employed the same antenna and receiver, whereas A204 was equipped with a radome. Additionally, four different tropospheric tie models were evaluated in this experiment. This setup facilitated the assessment of whether the use of different instruments causes a discrepancy between the tropospheric ties and the observed tropospheric parameter differences. Furthermore, the experiment investigated the performance of tropospheric tie models.

This experiment demonstrates the application of four different tropospheric ties in the comparison of GNSS-derived ZTD parameters. Five types of comparisons were conducted

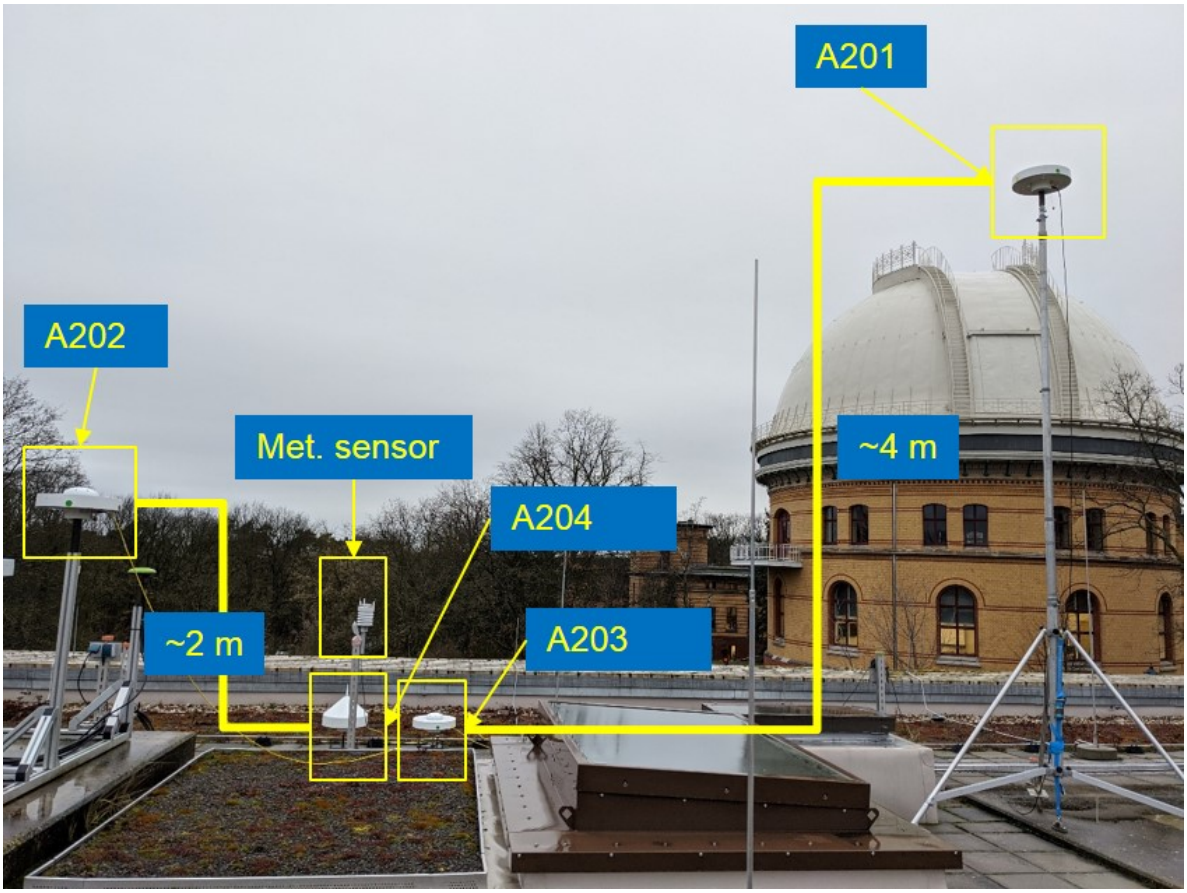

Figure 4.1: The GNSS co-location experiment set-up on the rooftop of A20 building (Telegrafenberg, Potsdam Germany). All stations used the same antenna and receiver but A204 was equipped with a radome. The antenna names, height differences, and meteorological sensor are shown (from Kitpracha et al. (submitted)).

as shown in Table 4.1. Firstly, a comparison of ZTD parameters was conducted without applying tropospheric ties (T0). Secondly, a comparison of ZTD parameters was conducted with the application of tropospheric ties from the analytical model with meteorological data from GPT3 (TAGPT3) and NWM (TANWM). Finally, a comparison of ZTD parameters was conducted with the application of ray-traced tropospheric ties (TR). For more information on the experiment's detailed data analysis, please refer to Kitpracha et al. (submitted).

Table 4.2 presents the comparison results of observed ZTD differences between station

Case	Tropospheric ties method	Meteorological data
T0	not applying ties	x
TAGPT3	analytical equation	GPT3
TANWM	analytical equation	NWM
TAMET	analytical equation	Meteorological sensor
TR	ray-tracing	NWM

Table 4.1: Description of ZTD comparison cases along with the tropospheric ties information used in the A20 experiment comparison (modified from Kitpracha et al. (submitted)).

pairs for all cases in the A20 experiment. According to the results, the mean offset for the A201 and A203 comparison was −1.5 mm with a standard deviation of 1.7 mm for T0. When applying tropospheric ties for comparison, the mean offset was significantly reduced by 1.3 mm,

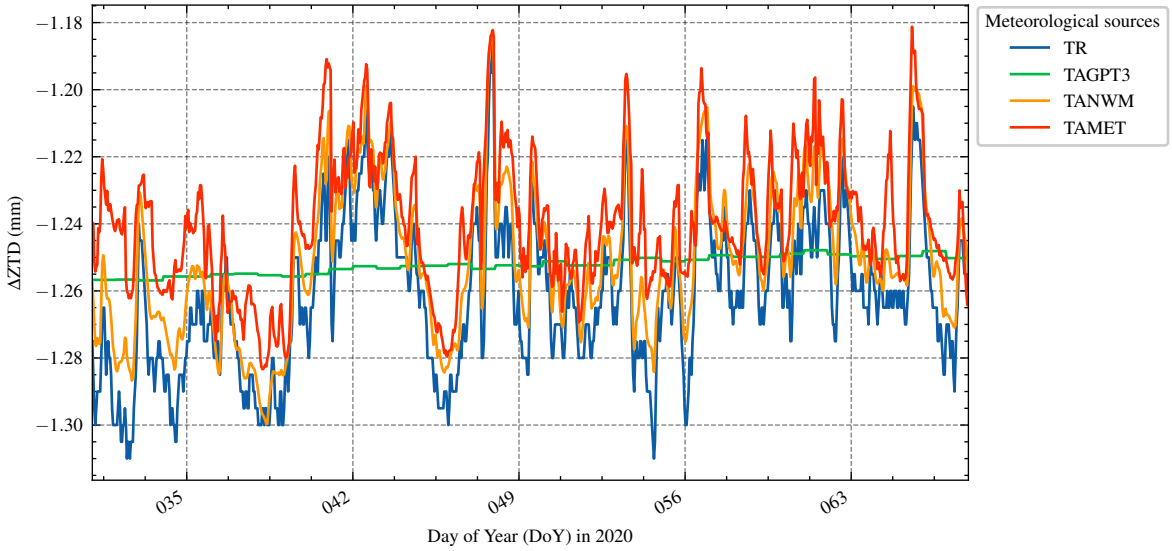

Figure 4.2: Tropospheric ties during the experiment between A201 and A203 stations (4 m height difference) from individual methods modified from Kitpracha et al. (submitted)).

as demonstrated by TAGPT3, TANWM, TAMET, and TR cases. However, there was no improvement in the standard deviation, as the variation of tropospheric ties was less than 0.1 mm in this experiment, as shown in Figure 4.2. A similar result was also observed in the comparison of A201-A202 and A202-A203 station pairs. These results underscore a strong agreement between observed ZTD differences and tropospheric ties when utilizing the same GNSS instrument across two stations. In contrast, an unexpected mean offset of 0.26 mm was observed in T0 between A201 and A204, despite a height difference of four meters, which would typically result in a 1 mm mean offset as seen in the A201-A203 pair. Therefore, when applying tropospheric ties, the mean offsets were notably increased by 1.3 mm for TAGPT3, TANWM, TAMET, and TR cases. However, no significant impact on the standard deviation was observed. Similar findings were also noted in A202-A204 and A203-A204 station pairs. These results illustrate that employing different instruments between GNSS stations leads to an unexpected discrepancy between observed ZTD differences and tropospheric ties.

Furthermore, the experiment also involved a comparison of GNSS-derived horizontal gradients. Statistical values of the comparison of horizontal gradients, both north and east gradients, for all station pairs in this experiment are presented in Table 4.3.

The observed horizontal gradient differences in the A201-A202 comparison revealed the least mean offset of 0.018 mm for observed east gradient differences. This result aligns with expectations, as both stations were located in close horizontal proximity. In contrast, a mean offset of −0.14 mm was observed for the A201-A203 pairs in east gradient differences, approximately ten times larger than that for the A201-A202 pair. This outcome was unexpected, considering the similarity in horizontal distance between the two stations and the fact that the A201-A203 pair employed the same GNSS instrument as the A201-A202 pair. Similar findings were also observed for the remaining station pairs. Furthermore, the best agreement of north gradients was found in the A201-A202 pair, with a mean offset of 0.008 mm. However, for the remaining station pairs, significant mean offsets were observed at the 0.1 mm level. This situation mirrored the findings in the east gradients. Additionally, the WRMS of the observed

north gradient differences were consistently smaller than those of the observed east gradient differences in this experiment.

The comparison of horizontal gradients in this experiment suggests that factors other than the GNSS instrument contributed to the degradation of observed horizontal gradients at the A203 and A204 stations. As depicted in Figure 4.1, obstacles were present in the vicinity of the A203 and A204 stations, and the antennas were installed close to the ground surface. These conditions could introduce multipath effects at the A203 and A204 stations. This is corroborated by the presence of large post-fit residuals in low-elevation observations, which are sensitive to horizontal gradient estimation, at A203 and A204 stations (see Figure 4.3). Moreover, there were fewer observations in the northern part due to the inclination of GNSS orbits, leading to greater variation in observed north gradient differences compared to observed east gradient differences, as indicated by the WRMS values. Overall, the results

Station-pair	T0	TAGPT3	TANWM	TAMET	TR
A201-A202	-1.10±1.03 (1.51)	-0.34±1.03 (1.09)	-0.34±1.02 (1.09)	-0.35±1.02 (1.09)	-0.33±1.02 (1.09)
A201-A203	-1.45±1.67 (2.22)	-0.20±1.67 (1.69)	-0.20±1.65 (1.67)	-0.22±1.63 (1.66)	-0.18±1.67 (1.68)
A201-A204	0.26±1.99 (2.10)	1.51±1.99 (2.50)	1.50±1.97 (2.48)	1.47±1.95 (2.44)	1.52±1.99 (2.50)
A202-A203	-0.35±1.69 (1.73)	0.14±1.69 (1.69)	0.14±1.68 (1.68)	0.15±1.67 (1.66)	0.13±1.69 (1.68)
A202-A204	1.37±2.02 (2.44)	1.85±2.02 (2.74)	1.84±2.01 (2.72)	1.82±2.00 (2.70)	1.85±2.02 (2.74)
A203-A204	1.70±2.25 (2.82)	1.70±1.25 (2.82)	1.70±1.23 (2.80)	1.69±1.21 (2.78)	1.70±1.25 (2.82)

Table 4.2: Mean offsets, standard deviations, and WRMS of the observed ZTD differences during the experiment for all cases. All values are in millimeters. The results are presented in weighted mean±weighted standard deviation (weighted root mean square) format (modified from Kitpracha et al. (submitted)).

Comparison cases	Differences of mean values (mm)		WRMS (mm)	
	East gradient	North gradient	East gradient	North gradient
A201-A202	0.018	0.008	0.221	0.299
A201-A203	-0.140	0.054	0.460	0.559
A201-A204	0.093	0.135	0.424	0.551
A202-A203	-0.158	0.052	0.449	0.553
A202-A204	0.076	0.132	0.413	0.572
A203-A204	0.229	0.082	0.532	0.561

Table 4.3: Mean biases and WRMS of the tropospheric gradient differences from the experiment for all station pairs (from Kitpracha et al. (submitted)).

of this experiment demonstrate the effectiveness of the tropospheric ties when two GNSS stations use the same instrument. The observed ZTD differences are solely biased by height differences in this case. These findings are in agreement with the results presented in Section 3.3.1, which compared two GNSS stations with the same antenna. The study shows that using different instruments, especially antennas, introduces instrumental bias, resulting in a discrepancy between the observed ZTD differences and the tropospheric ties. Additionally, the experiment indicates that tropospheric ties can be derived either through ray-tracing or analytical equations using different meteorological sources. Therefore, one can choose between the two methods depending on their requirements. While the analytical equation offers better temporal resolution, it is based on certain assumptions about atmospheric conditions and may not be accurate for all locations. Conversely, ray-traced ties are derived directly from

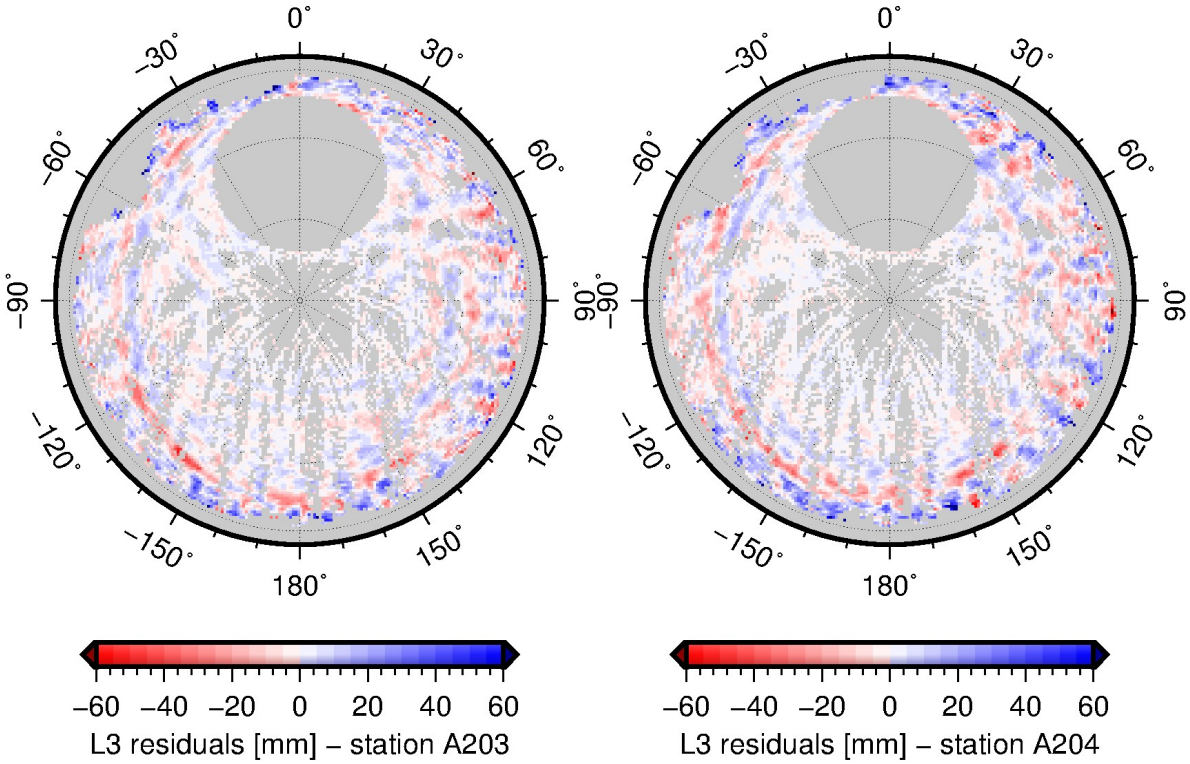

(a) Residual plot of A203 antenna.

(b) Residual plot of A204 antenna.

Figure 4.3: Residulas of ionospheric-free phase observations of A203 and A204 stations for the entire experiment (modified from Kitpracha et al. (submitted)). The units are given in millimeters. As demonstrated in Figure 4.1, there are obstacles in the vicinity of the antennas in the low-elevation antenna's line of sight. These likely caused the multipath effects in the low-elevation observations.

the NWM, accounting for the atmosphere condition at a specific location, but their temporal resolution depends solely on the NWM. The observed horizontal gradient differences are relatively unaffected by the instrumental bias but are primarily influenced by multipathing observed in low-elevation observations.

In reality, it is challenging to find GNSS co-location sites where the same instrument is used. Therefore, addressing instrumental bias is critical in reducing discrepancies between tropospheric ties and observed tropospheric parameter differences. As a result, the author carried out a second experiment to investigate an instrumental bias in GNSS tropospheric parameters.

4.1.2 A17 experiment

The goal of this experiment was to address instrumental bias in observed differences in tropospheric parameters in GNSS. The deployment of a vertical steering pole at the experimental station is a unique feature of this experiment. This device allows for the adjustment of the reference vertical positions of various GNSS antenna types to ensure millimeter-level alignment, eliminating station height-dependent tropospheric effects and providing consistent multipath effects to all experiment antennas. As a result, any differences observed are attributed to the instrumental bias of each antenna.

The experiment included two permanent stations, POTS and POTM, which are connected to the international GNSS service (IGS) and GFZ networks, as well as one experimental station.

The GNSS observations at the experimental station were retrieved simultaneously using two different receivers, and the experimental stations were designated as A17F and A17G. To address the instrumental bias in this experiment, four different antenna types were used at the experimental station (see Table 4.4). The experiment took place on the rooftop of the A17 building at GFZ Potsdam in Potsdam, Germany, from November 1^{st}, 2021, to January 10^{th}, 2022. The installation of a vertical steering pole, which allows the reference point position to be vertically changed within 10 cm (see Figure 4.4), is a unique feature of this experiment.

The experiment comprised two phases. In the first phase, the height difference between

Figure 4.4: The GNSS co-location experiment set-up on the rooftop of A17 building (Telegrafenberg, Potsdam Germany). Two permanent GNSS stations, namely POTS and POTM, were placed on a similar level and continuously operated. The experimental station A17F/G was attached to a vertical steering pole that allows the mitigation of height shift when changing the antenna during the experiment. The picture was taken from Kitpracha et al. (submitted)).

station A17F/G and POTS/M was obtained, and the height difference due to changes in the antenna was measured. Average height differences were determined for each experimental station antenna, and the shift in the reference point position of the test antennas was calculated

by comparing the mean difference with respect to the first antenna. In the second phase, three GNSS stations were re-observed, and the experimental station was vertically adjusted according to the shift obtained from the first phase when changing antennas. The assumption is that the height shift did not significantly affect the tropospheric parameters, especially ZHD parameters, because the antenna reference point position was considered to be the same for each experimental antenna. Therefore, only ZWD parameters between the reference stations and the experimental station were compared in this stage, and mean differences were calculated. To determine the instrumental bias in GNSS-derived tropospheric parameters, it was necessary to eliminate the impact due to the reference station. Therefore, double-differencing was conducted using the JG5 antenna of the experimental station as a reference to quantify the bias. This approach ensures the elimination of the reference station's impact and attributes the remaining bias to the instrumental bias. For more information on the experiment's detailed data analysis, please refer to Kitpracha et al. (submitted).

Figure 4.5 demonstrates a comparison between two reference stations, namely POTS and POTM, in this experiment. The comparison revealed a mean offset and standard deviation of -0.5 mm and 1.45 mm, respectively. This outcome was expected, as the two reference stations utilized different antenna types. This result aligns with the findings in Section 3.3.1, where station pairs with different antenna types were compared, revealing a height difference at the order of 10 cm. Figure 4.6 displays the mean height differences of the experimental stations (A17F/A17G) with respect to the reference station, POTS. The results indicate that the mean height difference of each experimental antenna agreed at approximately the 2 mm level. This illustrates the precision in steering the vertical reference point positions within a relatively short period. However, the J3T antenna was excluded due to its inability to achieve agreement within two millimeters with the other antennas. The agreement of height difference with respect to POTS between A17F and A17G was at a sub-millimeter level. This suggests that the impact of using different GNSS receivers is not significant compared to the effect of using different GNSS antennas. Figure 4.7 illustrates the comparison of observed ZWD parameters and height differences of the experimental antennas with respect to the two reference stations. The results demonstrate no significant shift in the height difference time series; however, shifts in observed ZWD difference time series were observed during the antenna change event. This implies that the shift in the ZWD differences time series was not caused by a geometrical shift of the reference position, but rather likely due to the use of different GNSS antenna types. Additionally, a rainstorm event occurred during the observing period of the SEP antenna, as evidenced by a rapid change in water vapor and atmospheric pressure in Figure 4.8. This weather event significantly influenced the biases in observed ZWD differences. Moreover, the mean offsets of the JG5 antennas in two different periods exhibited a slight difference. This discrepancy was likely attributed to differences in observation quality between the two periods.

Furthermore, the experiment conducted a comparison of horizontal gradients. Table 4.5 illustrates the observed horizontal gradient comparison between A17F and two reference stations, namely POTS and POTM. The results indicate that the discrepancies in east gradient values exceeded those in north gradient values. Notably, high residuals were observed in the western part of the observations due to multipath effects stemming from a half wall situated on the station's western side. These findings align with those of the A20 experiment, detailed

in Section 4.1.1, which also identified biases in observed horizontal gradient differences due to multipath effects.

Since the primary objective of this experiment was to discern instrumental bias, a double-differencing approach was employed. Table 4.6 presents the instrumental biases extracted for the ZWD parameter in each experimental antenna. The potential biases originating from the reference stations were effectively eliminated during the double-differencing process. Consequently, the remaining biases primarily represent instrumental bias within GNSS-derived tropospheric parameters. However, a minor bias was observed in the JG5 antenna, which was unexpected given that instrumental bias should theoretically be uniform. As mentioned previously, this discrepancy is likely attributed to differences in observation quality between the two observation periods.

Based on the results obtained from the experiment, it was found that the mean height differences of each experimental antenna were in close agreement at the millimeter level. Therefore, it can be concluded that the height-dependent effects on the observed ZWD differences can be disregarded since the experimental antennas are presumed to be in the same position. However, the observed ZWD differences revealed a different mean bias for each experimental antenna, which can be attributed to instrumental bias. Additionally, a severe rainstorm occurred during the observation period when the experimental station was equipped with the SEP antenna, resulting in a significant shift in the observed ZWD differences, as shown in Figure 4.7. This experiment successfully obtained the instrumental bias for each experiment antenna, which can be used to correct the tropospheric ties to reduce the discrepancy between observed tropospheric parameters and tropospheric ties. The instrumental bias obtained using the approach in this experiment will later be demonstrated in the combination of VLBI and GNSS with tropospheric ties in section 4.2.4.

Station	antenna	radome	Abbreviation
POTM	LEIAR25.R4	LEIT	LR4
POTS	JAVRINGANT_G5T	NONE	JG5
A17F/G	JAVRINGANT_G5T	NONE	JG5
	LEIAR10	NONE	L10
	LEIAR20	NONE	L20
	JAV_GRANT-G3T	NONE	J3T
	SEPCHOKE_B3E6	NONE	SEP

Table 4.4: List of antennas in the A17 rooftop experiment. The designation of the antenna follows the IGS standard name (from Kitpracha et al. (submitted)).

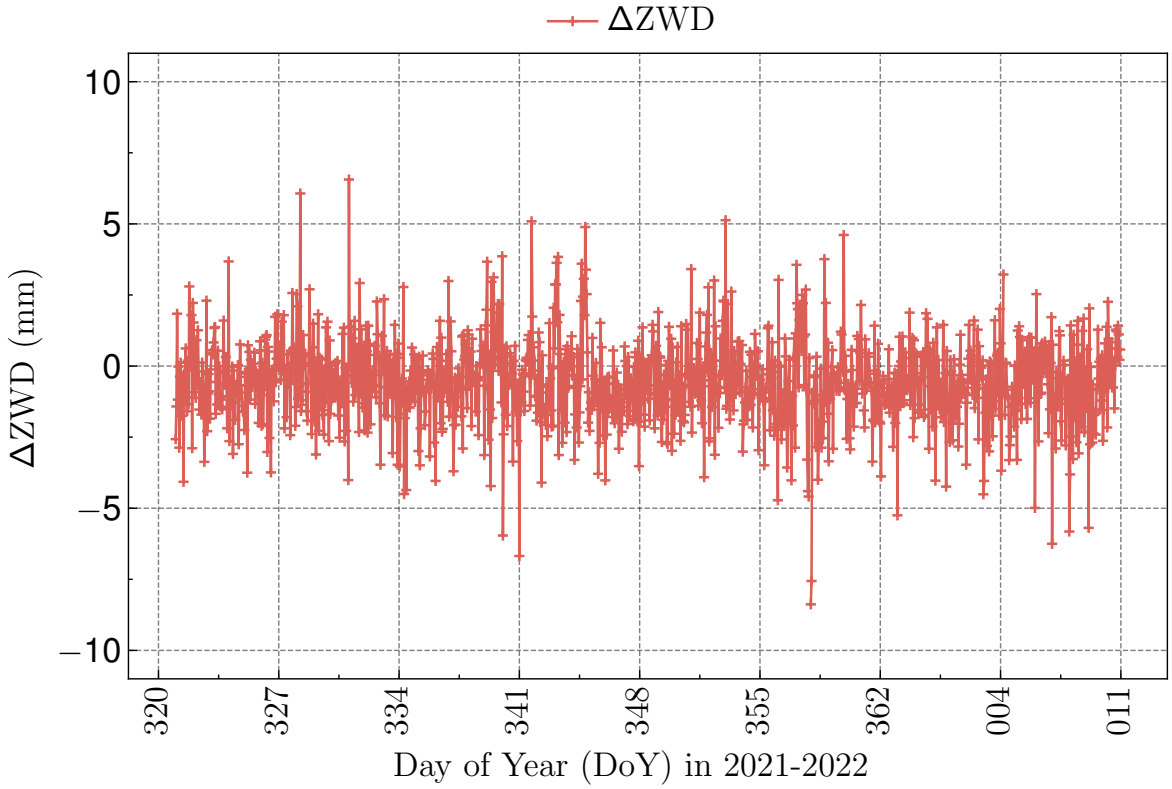

(a) A time series of observed ZWD differences between two reference stations: POTS and POTM, in the A17 experiment.

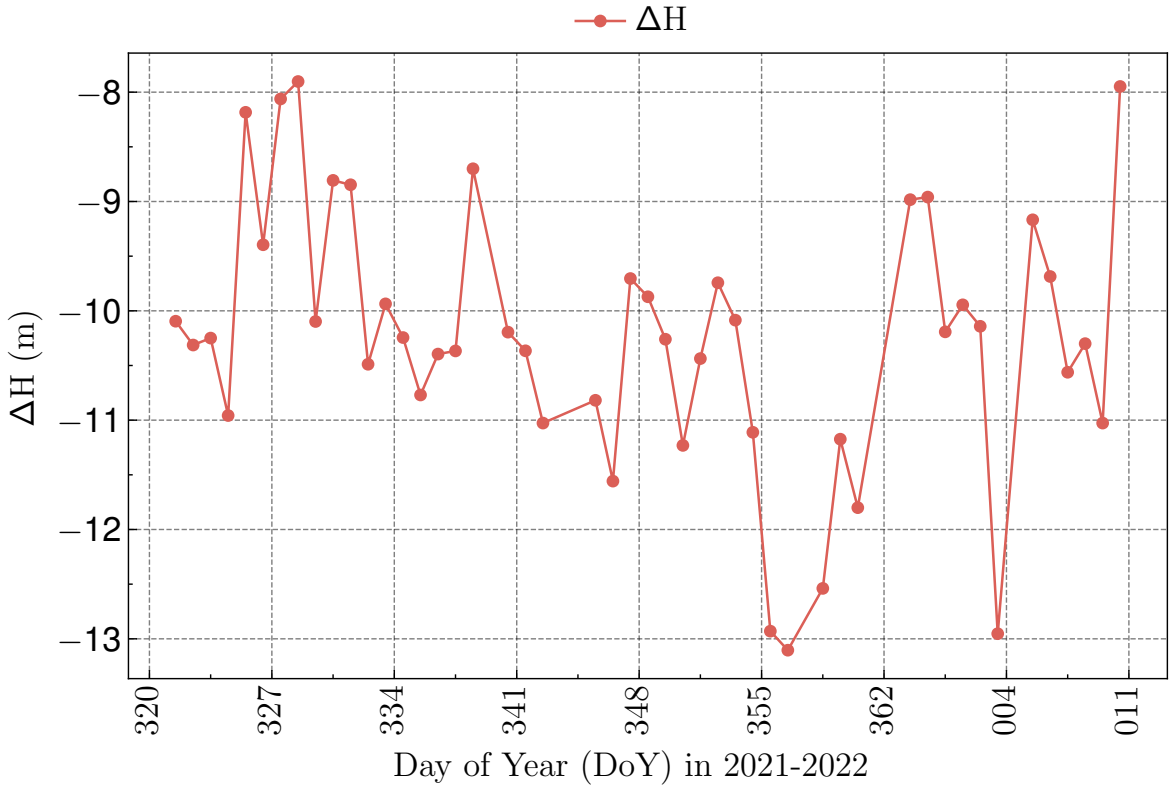

(b) A time series of height differences between two reference stations: POTS and POTM, in the A17 experiment.

Figure 4.5: The comparison of ZWD parameters and height coordinates between the POTS and POTM in the A17 experiment (modified from Kitpracha et al. (submitted)).

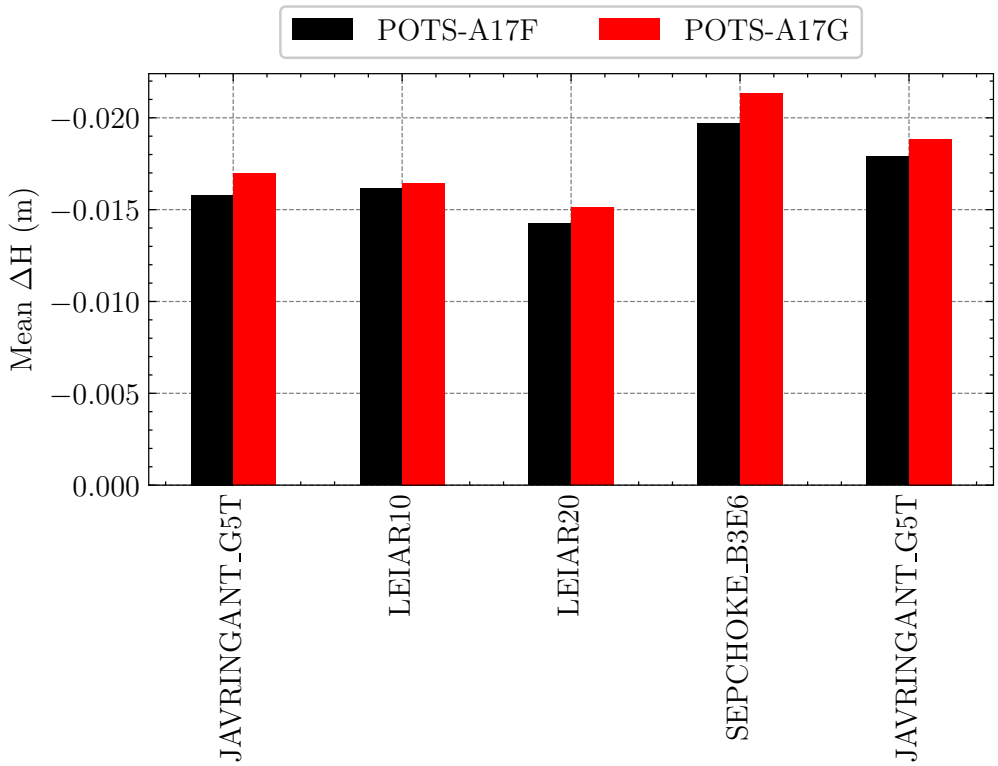

Figure 4.6: The mean height differences between A17F/A17G stations and reference station (POTS) for each experimental antenna (modified from Kitpracha et al. (submitted)).

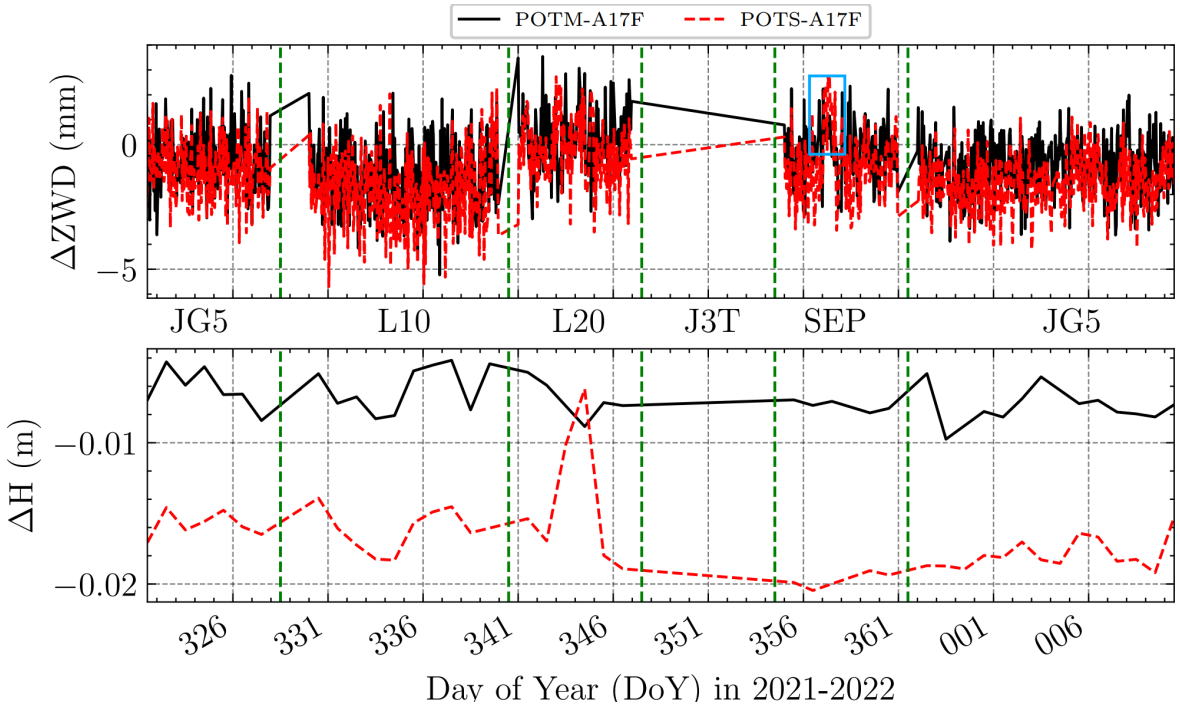

Figure 4.7: A comparison of ZWD w.r.t. reference station for the A17 rooftop experiment, as well as the height differences. Abbreviations of the test antenna types are given between the plots. The J3T antenna was skipped due to the unsuccessful steering reference point position. Green dashed lines indicate an antenna change. Light blue rectangle indicates the severe weather event. The figure is taken from Kitpracha et al. (submitted).

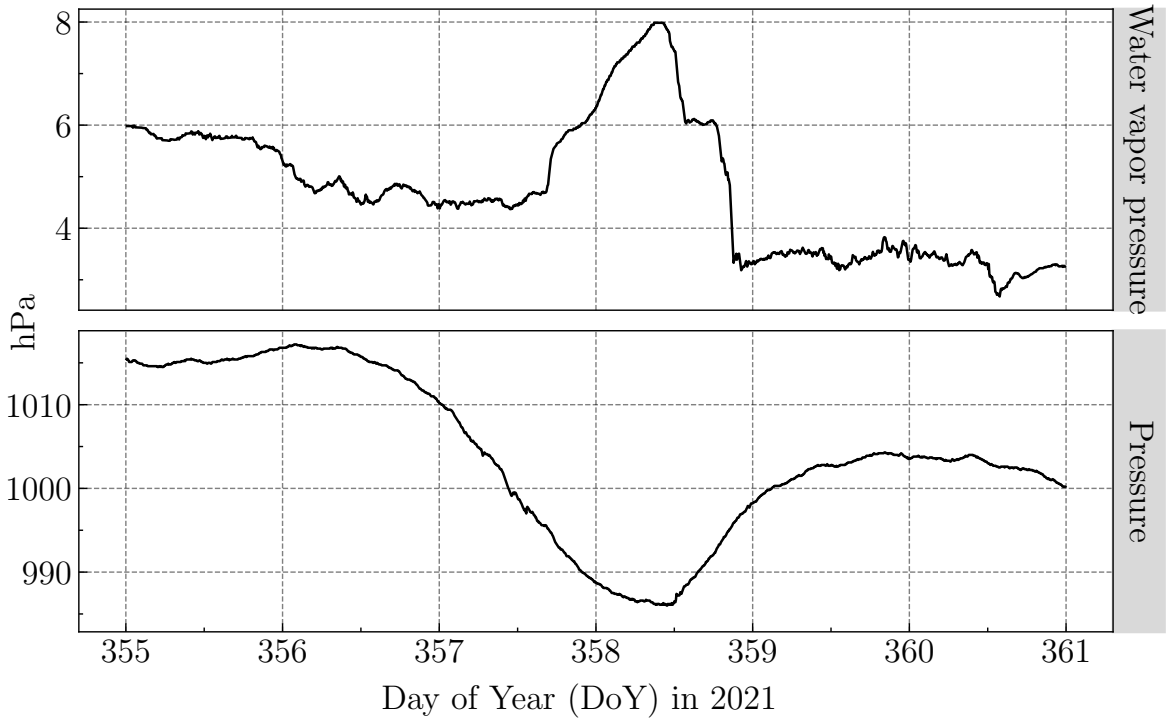

Figure 4.8: A snapshot of in situ atmospheric pressure (bottom) and water vapor pressure (top) during the A17 experiment when the experimental station utilized the SEP antenna. The units are given in hPa. Significant peaks and drops in water vapor and atmospheric pressure, respectively, suggest the occurrence of a rainstorm during the observation of the SEP antenna. Please note that the scales of the two subfigures are different.

Antenna	North gradients		East gradients	
	POTM-A17F	POTS-A17F	POTM-A17F	POTS-A17F
JAVRINGANT_G5T	0.069 (0.269)	0.072 (0.248)	0.147 (0.260)	0.090 (0.253)
LEIAR10	-0.007 (0.285)	-0.041 (0.312)	0.129 (0.291)	0.116 (0.328)
LEIAR20	-0.061 (0.273)	-0.055 (0.287)	0.119 (0.261)	0.097 (0.271)
SEPCHOKE_B3E6	-0.039 (0.255)	0.011 (0.284)	0.032 (0.234)	0.022 (0.253)
JAVRINGANT_G5T	0.052 (0.260)	0.079 (0.228)	0.128 (0.241)	0.087 (0.241)

Table 4.5: The statistics of tropospheric horizontal gradient differences between the A17F station and the two reference stations (POTM/POTS) for the individual antennas. All values are given in millimeters. The results are presented as weighted mean (WRMS). The table is taken from Kitpracha et al. (submitted).

Antenna types	POTM-A17F	POTM-A17G	POTS-A17F	POTS-A17G
LEIAR10	-0.79	-0.53	-0.92	-0.66
LEIAR20	0.89	1.12	0.69	0.84
SEPCHOKE_B3E6	0.38	0.55	0.14	0.29
JAVRINGANT_G5T	-0.29	-0.17	-0.52	-0.35

Table 4.6: The antenna-dependent biases of ZWD extracted from the double-differencing approach for A17F/A17G w.r.t. two reference stations (POTS/POTM). The units are given in millimeters.

4.2 VLBI and GNSS combination based on tropospheric ties

The thesis aims to investigate the practical application of tropospheric ties in the combination of VLBI and GNSS. This study aims to address several significant inquiries, including:

- Impact of combining tropospheric parameters using tropospheric ties on geodetic parameters.
- What the minimum condition is for utilizing tropospheric ties, such as the minimum number of local ties.
- Whether they can act as supplement ties if local ties encounter issues.
- What is the appropriate temporal resolution for utilizing tropospheric ties.
- Whether instrumental bias correction can enhance the accuracy of results achieved through the use of tropospheric ties.
- What the appropriate weighting is for tropospheric ties.

By answering these inquiries, this research will contribute to an improved comprehension of the potential and limitations of tropospheric ties in the combination of VLBI and GNSS.

To address the research questions, this thesis investigated the impact of combining tropospheric parameters using a combination of Very Long Baseline Interferometry (VLBI) and Global Navigation Satellite System (GNSS) at the NEQ level. The author selected the continuous VLBI observation campaign 2014 (CONT14) (May 6–20, 2014), which was a special VLBI session held in 2014. Unlike typical VLBI sessions, which occur once or twice per week at irregular times, This special VLBI session begins at 00:00 UTC, consistent with other space geodetic techniques. Moreover, it observes continuously for two weeks. This enables VLBI to demonstrate its full capability for deriving geodetic parameters and allows for comparisons with other techniques or their precise combination. When combined with GNSS, the irregular start times of regular VLBI sessions, typically between 17:00 and 18:30 UTC, could result in suboptimal performance (Thaller, 2008).

To ensure consistency and avoid degrading the combination of VLBI and GNSS, it is necessary to harmonize the apriori model and parameterization of each technique's single analysis. Therefore, GNSS and VLBI observations were reprocessed in this study.

4.2.1 GNSS and VLBI analyses

In this study, the Bernese GNSS software version 5.2 (Dach et al., 2015) was utilized to process 258 stations from the IGS global network, including co-located stations with the VLBI radio telescopes. To analyze the data, an ionosphere-free linear combination of dual-frequency GPS and GLONASS observations was employed. The CODE repro3 campaign (Selmke et al., 2020) was used as a reference for the analysis configuration, which is a major reprocessing campaign that is being conducted to prepare for the Internation Terrestrial Reference Frame 2020 (ITRF2020).

However, several parameters, including GNSS orbits, clock parameters, geocenter coordinates, GNSS satellite phase center offsets, and sub-daily ERP estimation, were revised

in this thesis to reduce matrix size and calculation time. These parameters were deemed irrelevant to the investigation of the effect of combining tropospheric parameters, which was the main objective of this study. As such, satellite orbit parameters were estimated using apriori information from CODE orbits from the IGS repro3 campaign, while satellite clock parameters were fixed using CODE clocks products from the same campaign.

Station coordinates were estimated with daily temporal resolution as a correction with respect to ITRF2020 (Altamimi et al., 2022), while the ERP was estimated as a Piecewise Linear Function (PWLF) with daily temporal resolution based on IERS C04 (Bizouard et al., 2019). For tropospheric parameters, the ECMWF-based ZHD from VMF1 was utilized as an apriori, while the ZWD was established as a parameter and estimated with hourly temporal resolution. The zenith delays, both ZHD and ZWD, were mapped into the slant direction using the mapping functions provided by VMF1. Horizontal gradients were estimated using a zero-apriori value with a temporal resolution of 6 hours using Chen and Herring's mapping function (Chen and Herring, 1997).

Satellite/station antenna phase center offsets and variations were retrieved from the igsR3 ANTEX[1], and a cutoff elevation angle of three degrees was applied. Furthermore, an elevation-dependent down-weighting of observations based on $1/cos(z)^2$, where z is the zenith angle, was also applied. No-Net translation (NNT) and No-Net Rotation (NNR) conditions were used for datum definition to obtain individual solutions. Additionally, the constraint-free NEQ was prepared for the combination in Bernese internal format. Information on the apriori model and its parameterization can be found in Table 4.7 and Table 4.8, respectively.

The author presents an analysis of Very Long Baseline Interferometry (VLBI) observations using the Potsdam Open source Radio Interferometry Tools (PORT) (Schuh et al., 2021). In order to ensure consistency with the GNSS solution, the author implemented the ITRF2020 reprocessing configuration similar to the GNSS analysis. The author modeled the station coordinates and Zenith Wet Delay (ZWD) using the same apriori and estimation interval as in the GNSS analysis. However, the horizontal gradients were estimated with respect to the apriori empirical DAO model (MacMillan and Ma, 1997), while maintaining the same temporal resolution as the GNSS analysis.

VLBI is capable of estimating a complete set of EOP, including polar motion, UT1-UTC, and Celestial Pole Offset, which we estimated using PWLF with daily temporal resolution relative to the International Earth Rotation and Reference Systems Service (IERS) C04 series. This study estimated the source coordinates using the No-Net Rotation (NNR) conditions with respect to the International Celestial Reference Frame 3 (ICRF3) catalog (Charlot et al., 2020).

To obtain individual solutions, the No-Net Translation (NNT) and NNR constraints were applied for the datum definition. However, for the combination process, the author produced constraint-free Normal Equation (NEQ) in SINEX [2]. When creating the SINEX file, the author translated the EOP into offsets and drifts, following the requirement of the SINEX format. Tables 4.7 and 4.8 provide details on the apriori model and parameterization of VLBI data processing, respectively.

[1] `http://ftp.aiub.unibe.ch/users/villiger/igsR3_2077.atx`
[2] `https://files.igs.org/pub/data/format/sinex_v210_proposal.pdf`

	GNSS	VLBI
Station coordinates		
Apriori information	ITRF2020 (Altamimi et al., 2022)	ITRF2020 (Altamimi et al., 2022)
Solid Earth Tides	IERS Convention 2010 (Petit and Luzum, 2010)	IERS Convention 2010 (Petit and Luzum, 2010)
Solid Earth Pole Tides	IERS Convention 2010 (Petit and Luzum, 2010)	IERS Convention 2010 (Petit and Luzum, 2010)
Ocean Loading	FES2014b	FES2004
Atmospheric tidal loading	Goddard Space Flight Center (GSFC) (Petrov and Boy, 2004)	IERS Convention 2010 (Petit and Luzum, 2010)
Atmospheric non-tidal loading	Not applied	Not applied
Troposphere modelling		
Apriori values	ZHD computed from 6 hourly VMF1 grids	ZHD computed from 6 hourly VMF1 grids
Mapping function	VMF1	VMF1
Horizontal gradients	Using zero apriori values	Using apriori from DAO model (MacMillan and Ma, 1997)
Horizontal gradients mapping function	Chen and Herring (Chen and Herring, 1997)	Chen and Herring (Chen and Herring, 1997)
Earth Orientation Parameters		
Polar motion	Apriori values from IERS C04	Apriori values from IERS C04
UT1-UTC	Apriori values from IERS C04	Apriori values from IERS C04
Celestial Pole Offsets	Apriori values from IERS C04 with IAU2000R06 model	Apriori values from IERS C04 with IAU2006 model
High-Frequency EOP model	Apriori values from Desai and Sibois (2016)	Apriori values from Desai and Sibois (2016)
Technique specific corrections		
Antenna phase center offsets and variations	IGSR3.ATX	
Satellite orbits and clocks	Apriori from CODE IGS repro3	
Thermal expansion		Applied values from Nothnagel (2009)
Gravitational deformation		Applied values from IVS[3]
Source coordinates		Apriori values from ICRF3 catalogue (Charlot et al., 2020)

Table 4.7: Apriori information of VLBI and GNSS analysis in this study.

	GNSS	VLBI
Station coordinates	Daily offsets	Daily offsets
Troposphere modelling		
Zenith Wet Delays	Estimated with hourly resolution at full UTC hours	Estimated with hourly resolution at full UTC hours
Horizontal gradients	Estimated with daily intervals (00:00-24:00 UTC)	Estimated with daily intervals (00:00-24:00 UTC)
Earth Orientation Parameters		
UT1-UTC	Estimated as PWLF with daily intervals (00:00-24:00 UTC), with a tight constraint applied to the first value	Estimated as PWLF with daily intervals (00:00-24:00 UTC)
Celestial Pole Offsets	Fixed to apriori values	Estimated as PWLF with daily intervals (00:00-24:00 UTC)
Technique specific parameters		
Satellite orbits and clocks	Orbital parameters were estimated, but clock parameters were fixed to apriori values	-
Source coordinates	-	Fixed to the ICRF3 catalogue

Table 4.8: Parameterization of VLBI and GNSS analysis in this thesis.

4.2.2 Combination strategy

As stated earlier, the author combined VLBI and GNSS at the NEQ level. The method of combination for each parameter is described, as each parameter possesses unique characteristics. Global parameters, such as Earth Orientation Parameters (EOP), can be directly combined without the need for external data. However, station coordinates and tropospheric parameters cannot be directly combined. Their relationship, including local and tropospheric ties, is introduced as a pseudo-observation. Furthermore, some parameters must be transformed to achieve consistency during the combination process. For instance, the reference epoch of station coordinates must be the same for all NEQ during the combination process. Additionally, during the combination process, the EOP from VLBI is retrieved from the SINEX file. These are typically presented as offsets and drifts and are converted to PWLF. To save computation time, some parameters, such as satellite orbital parameters and tropospheric delay of non-colocated sites, which are not the primary focus of the study, are reduced. The mathematical

foundations and methods for reducing, manipulating, transforming, and combining NEQ are widely available in reputable literature, such as Rothacher (2002); Thaller (2008).

The author obtained the 15 daily NEQ from GNSS and VLBI during CONT14, as mentioned above, using the analytical approach described in section 4.2.1. The combining processes were performed using the ADDNEQ2 program, which is a part of the Bernese GNSS software package.

This study involved performing single-technique solutions and inter-technique combinations. Single-technique solutions (SING) were individually computed for VLBI and GNSS by stacking 15 daily VLBI and GNSS NEQs. These solutions served as the basis for investigation in this thesis. The datum definition for single-technique solutions varied depending on the technique. For VLBI, NNT and NNR were applied to all VLBI radio telescopes, whereas for GNSS, NNR was only applied to IGS core stations for single-technique solutions. The inter-technique combination was achieved by combining 15 daily NEQs from both VLBI and GNSS. The datum definition for the combined network was applied to GNSS with NNR conditions at IGS core stations. Local ties were used to combine station coordinate parameters at co-location sites to transfer datum information from GNSS to VLBI. The local tie vectors with an epoch close to the CONT14 period were selected, resulting in eight VLBI and GNSS co-location sites (see Table 4.9). During the combination process, the local ties were introduced as a pseudo-observation. In some cases, the variance and covariance information of local ties is not available (Rothacher et al., 2011). To ensure consistency of local ties weighting in the combination, a standard deviation of 1 mm was applied to all local ties. For combining tropospheric parameters, this thesis used TR as the tropospheric tie information to combine ZWD parameters. In addition, zero was used as the gradient tie information for combining gradient parameters. Similar to local ties, tropospheric ties and gradient ties were introduced as pseudo-observations in the combination process. The weighting of tropospheric ties will be investigated in various scenarios later in section 4.2.3.

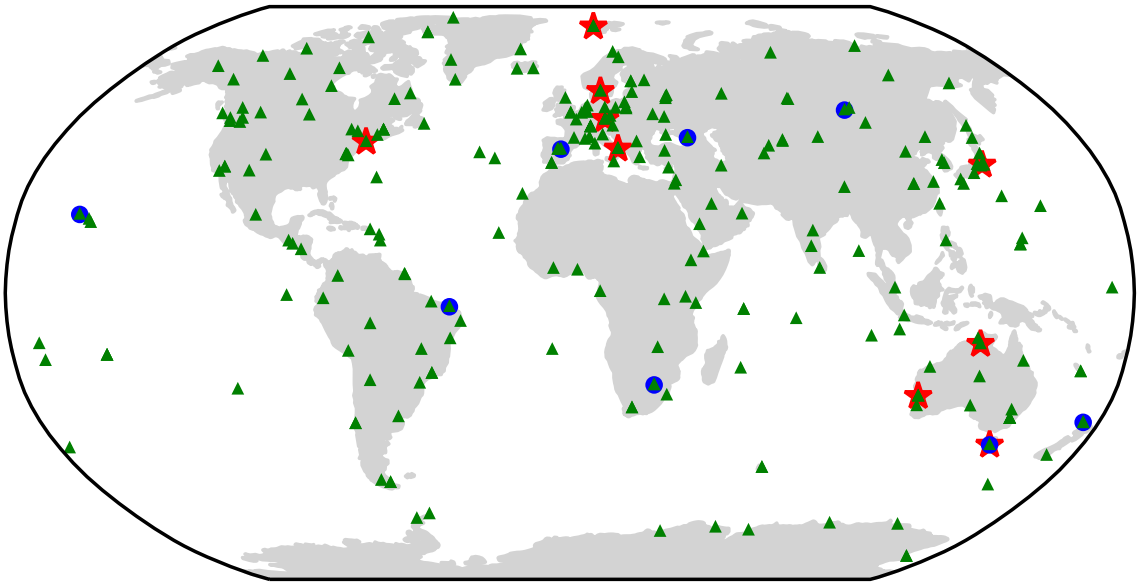

Figure 4.9: The global distribution of VLBI-GNSS stations used in the combination. The green triangles and blue dots represent GNSS stations and VLBI telescopes, respectively. The red stars are indicated VLBI-GNSS co-location sites, according to Table 4.9.

Site	Local ties			VLBI stations	GNSS stations
	ΔX (m)	ΔY (m)	ΔZ (m)		
Ny-Ålesund	28.7970	102.1670	-6.4640	NYALES20 (7331)	NYA1
Yaragadee	130.1486	32.9987	-60.9451	YARRA12M (7376)	YAR2
	147.2997	36.4823	-66.1146	YARRA12M (7376)	YAR3
	129.1133	34.5131	-57.5209	YARRA12M (7376)	YARR
Hobart	-165.3732	-67.6277	75.8214	HOBART26 (7242)	HOB2
	81.2024	5.9025	-70.3342	HOBART12 (7374)	HOB2
Katherine	58.9258	79.6989	56.2657	KATH12M (7375)	KAT1
Tsukuba	-209.5587	29.7305	-216.8834	TSUKUB32 (7345)	TSKB
Matera	40.4304	-2.8013	-55.3195	MATERA (7243)	MATE
Onsala	-52.6318	40.4620	43.8663	ONSALA60 (7213)	ONSA
Wettzell	-38.6112	-117.3950	59.4239	WETTZELL (7224)	WTZA
	-40.8011	-118.3969	61.3155	WETTZELL (7224)	WTZR
	-39.6784	-117.7101	60.4098	WETTZELL (7224)	WTZZ
Westford	-26.7960	-41.0220	-30.4760	WESTFORD (7209)	WES2
Katherine	58.9258	79.6989	56.2657	KATH12M (7375)	KAT1

Table 4.9: Local ties information for the co-location sites used in the combination study. The local ties information was obtained from ITRF2020 local ties in the SINEX format.

4.2.3 Methodology for analyzing the potential and limitations of tropospheric ties in VLBI and GNSS combination

This section details the investigation into the capabilities and limitations of tropospheric ties as outlined in the earlier research questions. To address these research questions, various investigation scenarios have been considered. As this study examines the effects of combining tropospheric parameters on geodetic parameters, the combination study will focus on two parameters: station coordinates and tropospheric parameters, including zenith delays and horizontal gradients. Furthermore, this section describes the method used to quantify the impact on two geodetic parameters of interest.

4.2.3.1 Impact quantifying method on geodetic parameters

To evaluate the efficiency of applying tropospheric ties in the station coordinates derived from the combination of VLBI and GNSS, this study employs station coordinate repeatability as an indicator of enhancement. In this context, repeatability refers to the extent to which the TRF can be replicated using observations from a different day with the same datum definition. To determine station coordinate repeatability, the study calculates the seven-parameter Helmert transformation between daily combined station coordinates with respect to the 15-day combined solution station coordinates. The resulting coordinate residuals, denoted as r, from the transformations provide the station coordinate repeatability.

$$R_{ista} = \sqrt{\frac{\sum_{n=1}^{nsol} r_n^2}{nsol - 1}} \tag{4.1}$$

where $nsol$ is the number of solutions in which the station $ista$ is included. In this study, $nsol$ is 15, according to the CONT14 period. It must be noted that all residuals R_{ista} are

separated into three components in a topocentric system. Therefore, the station coordinates repeatabilities are computed into East R^E_{ista}, North R^N_{ista}, and Up R^U_{ista} components. Based on the repeatability, it demonstrates how well the station fits into the datum definition.

This study also assesses the improvement in troposphere parameters derived from a combination of VLBI and GNSS utilizing tropospheric ties, particularly ZTD and horizontal gradients. The ZTD parameters and horizontal gradients derived from the ERA5 reanalysis NWM (Hersbach et al., 2020) using the ray-tracing technique with GFZ in-house ray-tracing software developed by Zus et al. (2012) are used as an external validation for the combined troposphere parameters. The weighted mean (WM) and Weighted Root Mean Square (WRMS) are used as statistical indicators.

4.2.3.2 Combination experiment setup

To address the research questions mentioned earlier, five combination experiments were designed. The first scenario involved testing the combination of tropospheric parameters for two VLBI radio telescopes at the Hobart co-location site. The second scenario investigated whether tropospheric ties could completely replace local ties by combining VLBI parallel networks during CONT17 (28 November - 12 December 2017), which was another special VLBI session held in 2017 similar to CONT14. The third scenario aimed to determine the efficiency of tropospheric ties in scenarios where one of the components of local ties is either absent or exhibits a significant discrepancy. The fourth scenario determined the optimal temporal resolution for combining tropospheric parameters of VLBI and GNSS. Finally, the fifth scenario examined the improvement of applying instrumental bias correction for tropospheric ties in the combination of VLBI and GNSS. In each scenario, the impact of tropospheric ties weighting was also explored using different standard deviations. The methodology for each scenario is explained in detail in subsequent paragraphs. A combination process based on the strategy mentioned in section 4.2.2 was performed for all scenarios. Table 4.10 provides an overview of the experiment setup, including the selected co-location sites, and the weighting scenarios for tropospheric and gradient ties in each experiment setup.

In the first scenario, the combination of the tropospheric parameters for the two VLBI radio telescopes at the Hobart co-location site was tested. Two VLBI radio telescopes at the Hobart co-location site were observed simultaneously during CONT14. For this investigation, these two VLBI radio telescopes were excluded from the datum definition. TR was used as the tropospheric ties to combine ZWD parameters. The impact of tropospheric ties weighting was also investigated, and four different standard deviations were applied for tropospheric ties: 1 mm (ZW1M), 3 mm (ZW3M), 5 mm (ZW5M), and 1 cm (ZW1C).

The second scenario addresses the question of whether tropospheric ties can completely transfer the datum information during the combination as local ties. It is essential to clarify that the purpose of employing local ties is to transfer datum information from one network to another, aiming to resolve the rank deficiency resulting from the absence of datum definition in the NEQ of space geodetic techniques. Thus, this dissertation expands on prior research by Kitpracha et al. (2022), by combining VLBI parallel networks during CONT17. The unique feature of CONT17 was that three independent networks with different network geometry were observed in parallel: two legacy networks and one VGOS network. As there was only

Scenario	Methodology	Co-location sites	Tropospheric ties applying/weighting scenario
1	Combined tropospheric parameters of two VLBI radio telescopes at the Hobart co-location site during CONT14.	Hobart	Tropospheric ties: - 1 mm (ZW1M) - 3 mm (ZW3M) - 5 mm (ZW5M) - 1 cm (ZW1C)
2	Two different combination scenarios of two VLBI parallel networks during CONT17 were created, one utilizing only local ties, and the other using tropospheric ties but without the height component of local ties.	Wettzell	Tropospheric ties: - 1 mm (ZW1M) - 3 mm (ZW3M) - 5 mm (ZW5M) - 1 cm (ZW1C)
3	Station-wise excluding the height/horizontal components of local ties and using only tropospheric/gradient ties	Seven co-location sites, where a discrepancy of local ties was greater than 1 cm, according to Table 4.11, including Wettzell and Yarragadee	Tropospheric ties: - 1 mm (ZW1M) - 3 mm (ZW3M) - 5 mm (ZW5M) - 1 cm (ZW1C) Gradient ties: - 1 mm (GW1M) - 0.1 mm (GW01) - direct stacking (GTGS)
4	Station-wise applying tropospheric ties with different temporal resolutions	Wettzell, Matera, Tsukuba, and Katherine	- Applying estimation epoch (ALL) - Applying single values (ONE) - Excluding problematic epoch (SEGEX) - Applying problematic epoch with 1 cm standard deviation (SEG1C)
5	Station-wise applying instrumental bias correction for tropospheric ties	Wettzell, Matera, and Tsukuba	Tropospheric ties: - 1 mm (ZW1M) - 3 mm (ZW3M) - 5 mm (ZW5M) - 1 cm (ZW1C)

Table 4.10: Description of combination experiment setup, including selected co-location sites, and weighting scenarios for tropospheric and gradient ties in each experiment setup.

one co-location site available (the Wettzell co-location site) between these VLBI parallel networks during CONT17, this presented an excellent opportunity to examine the efficiency of tropospheric ties in the datum transfer during the combination process. Two different scenarios were created, one utilizing only local ties, and the other using tropospheric ties but

without including the height component of local ties. Additionally, the impact of weighting on tropospheric ties was explored, with four different standard deviations (1 mm (ZW1M), 3 mm (ZW3M), 5 mm (ZW5M), and 1 cm (ZW1C)) employed as a weight for tropospheric ties.

In the third scenario, the study addresses the research question of whether the utilization of tropospheric ties can improve geodetic solutions in scenarios where one of the components of local ties is either absent or exhibits a significant discrepancy. Seven co-location sites were selected based on the height component of local ties, which exhibited a discrepancy greater than 1 cm, as shown in Table 4.11. The reference solution (LTR), which only used local ties, was used as a basis for this study's methodology. Subsequently, a station-wise combination was conducted to test the efficiency of the combining ZWD parameter. Therefore, seven solutions were computed, with each solution utilizing combined ZWD parameters and excluding the height component of local ties at each co-location site investigated. Furthermore, the study selected Wettzell and Yarragadee co-location sites to determine whether the use of solely tropospheric ties, in the absence of local ties' height component, can improve results in scenarios where local ties and single technique solutions already exhibit a good agreement. In addition, the study examined the impact of tropospheric ties weighting for each solution using four different standard deviations: 1 mm (ZW1M), 3 mm (ZW3M), 5 mm (ZW5M), and 1 cm (ZW1M) (ZW1C). Furthermore, using the same methodology as for combining ZWD parameters, this study investigated the effect of applying gradient ties when combining horizontal gradient parameters. However, for gradient ties, two different standard deviation weightings were chosen: 1 mm (GW1M), 0.1 mm (GW01), as well as direct stacking (equating the parameters) of horizontal gradient parameters (GTGS).

The fourth scenario aims to determine the optimal temporal resolution for combining tropospheric parameters of VLBI and GNSS in this thesis. To address this research question, three co-location sites (Wettzell, Matera, Tsukuba, and Katherine) were investigated and four combination cases were established. Local ties were applied similarly to the reference solution (LTR). The combination of ZWD parameters was also performed station-wise in this investigation. A standard deviation of one millimeter was applied to all scenarios in this scenario as a weight for tropospheric ties. The first case applies tropospheric ties to every estimation epoch (ALL). The second case applies a single value throughout the entire data period (ONE). The third case employs the interquartile range (IQR) rule to identify problematic epochs from single-technique solutions. A time series of observed ZWD differences determined by a single technique at the Wettzell co-location site between WETTZELL and WTZR is displayed in Figure 4.10, including the identification of a problematic epoch. As shown in Figure 4.10, problematic epochs from the third scenario (SEGEX) were excluded from the combination process. In the final case, these problematic epochs were not excluded from the combination process, but instead, tropospheric ties with a standard deviation of 1 cm were utilized (SEG1C).

Finally, the improvement of applying instrumental bias correction for tropospheric ties in the combination of VLBI and GNSS was examined. In addition, four different weights were evaluated for a combination of tropospheric ties employing instrumental bias correction. Three co-location sites with a discrepancy between observed ZTD differences and tropospheric ties larger than 1 mm, according to Table 4.12, were chosen to demonstrate the improvement of

tropospheric ties with instrumental bias correction. The modeling approach for instrumental bias will be discussed in Section 4.2.4. In addition, in order to assess an improvement when applying instrumental bias correction to tropospheric ties, tropospheric ties without instrumental bias correction were utilized with a 1 mm standard deviation weight in order to evaluate an improvement. The investigation approach was carried out in the same way as above.

Station-pair	Technique solutions - Local ties			ITRF2020 - Local ties		
	East (mm)	North (mm)	Up (mm)	East (mm)	North (mm)	Up (mm)
ONSALA60-ONSA	-5.14	9.25	0.29	-2.53	1.07	-5.49
WETTZELL-WTZA	6.57	13.97	-2.85	5.88	4.61	8.50
WETTZELL-WTZR	2.70	13.89	-3.23	2.10	4.27	-6.00
WETTZELL-WTZZ	3.89	14.16	0.88	3.08	3.97	-0.51
HOBART26-HOB2	16.98	3.83	5.87	-2.49	-1.39	-0.27
MATERA-MATE	0.40	20.91	-20.41	0.68	3.69	-0.66
HOBART12-HOB2	12.18	-2.20	26.22	-6.96	-4.85	11.97
WARK12M-WARK	20.46	3.94	19.32	3.87	1.67	2.24
KAT1-KATH12M	-31.22	1.71	11.37	-7.39	4.08	14.18
NYA1-NYALES20	16.70	-15.70	-7.79	0.59	-3.02	4.45
TSKB-TSUKUB32	-33.15	-6.92	15.68	1.20	4.41	4.93
WES2-WESTFORD	-3.65	15.07	10.15	-11.92	-0.58	15.87
YAR2-YARRA12M	-23.17	-6.71	9.66	-2.51	-0.41	-3.76
YAR3-YARRA12M	-21.70	-9.42	-3.55	-1.14	-1.97	-15.70
YARR-YARRA12M	-18.58	-8.01	11.19	0.23	-1.82	-6.75

Table 4.11: Comparison of the local ties values from Table 4.9 with the estimated coordinate differences determined by the single-technique solutions and ITRF2020 coordinates.

Station-pair	Tropospheric ties (mm)	Observed differences (mm)	Discrepancies (mm)
WETTZELL-WTZA	0.10	-1.54	1.64
WETTZELL-WTZR	0.10	-2.61	2.71
WETTZELL-WTZZ	0.15	-3.20	3.35
NYA1-NYALES20	-0.10	7.78	-7.88
TSKB-TSUKUB32	-1.00	0.48	-1.48
YAR2-YARRA12M	-0.40	-0.89	0.48
YARR-YARRA12M	-0.40	-1.14	0.74
YAR3-YARRA12M	-0.30	0.57	-0.88
HOBART26-HOB2	1.10	-1.78	2.88
HOBART12-HOB2	0.00	-6.89	6.89
WARK12M-WARK	1.00	-2.79	3.79
KAT1-KATH12M	-0.30	0.97	-1.27
ONSALA60-ONSA	0.70	-2.22	2.92
WES2-WESTFORD	-0.10	-4.09	3.99
MATERA-MATE	0.30	0.37	-0.06

Table 4.12: Comparison of the TAVM3 to the estimated ZWD differences derived from single-technique solutions.

4.2.4 Modeling the instrumental effects of tropospheric ties

This section presents the methodology used for correcting instrumental bias in tropospheric ties. To this end, the authors employed the approach utilized in the second co-location GNSS experiment, as described in section 4.1. To identify appropriate co-location sites for this

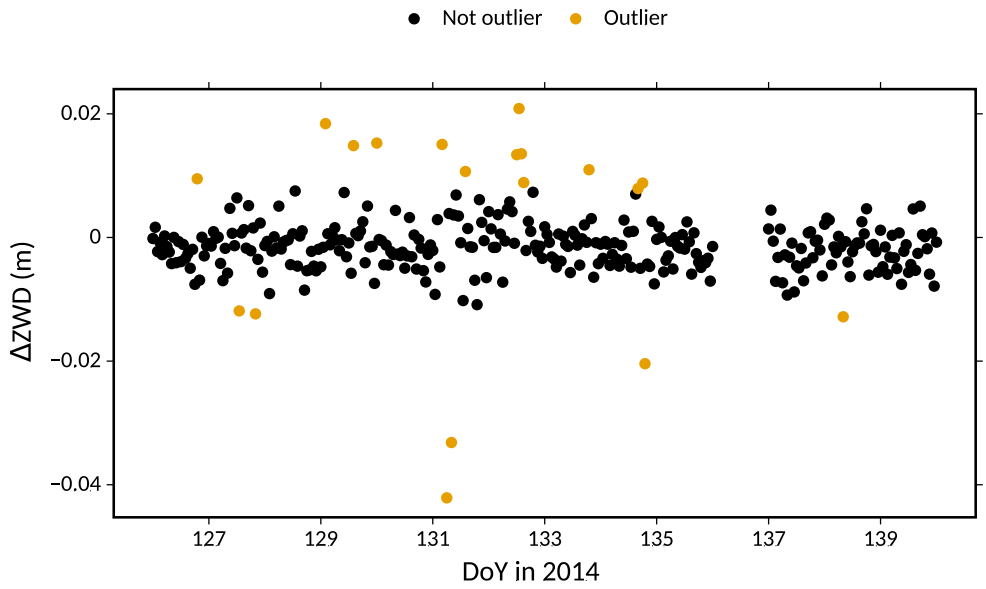

Figure 4.10: Time series of the ZWD differences between WETTZELL and WTZR, where outliers were identified using the IQR method during CONT14.

investigation, four locations were selected where the observed ZTD differences differed by more than 1 mm from the TR during CONT14, as shown in Table 3.5. The instrument bias was then calculated based on the data in Table 3.5. In contrast to the GNSS experiment, this study relied on TR to reduce the height-dependent influence in the observed ZTD differences. The assumption made was that there was no instrumental bias in VLBI, and therefore, a single-difference analysis was conducted. Table 4.13 shows the instrumental bias of tropospheric ties for the selected co-location sites, which were subsequently used as an additional correction to TR during the combination process. The test was carried out by applying TR with instrumental bias correction on top of local ties station by station, as shown in Table 4.13.

Station-pair	GNSS antenna	Mean observed ZTD differences (mm)	Mean TR (mm)	Instrumental bias (mm)
WETTZELL-WTZA	ASH700936C_M SNOW	0.92	-0.93	-1.1
MATERA-MATE	LEIAT504GG NONE	-0.8	-2.04	-1.24
NYALES20-NYA1	ASH701073.1 SNOW	1.91	-1.04	-2.95
TSUKUB32-TSKB	AOAD/M_T DOME	-4.31	-5.54	-1.2

Table 4.13: Instrumental biases of four chosen co-location sites. The co-location sites were selected from Table 3.5 where observed ZTD differences differed by more than 1 mm from TR during CONT14.

5

Analyses results

This chapter describes the results of the combined solutions derived from VLBI and GNSS techniques, which were explained in the prior chapters. This chapter focuses mainly on two fundamental geodetic parameters: station coordinates and troposphere parameters, as well as their interaction with the combined solutions. The chapter discusses the advantages and disadvantages of using tropospheric ties and the efficiency of correcting instrumental bias in tropospheric ties in the combination of space geodetic techniques.

5.1 Impact on station coordinates

This section presents the impact of utilizing tropospheric ties in the combination of VLBI and GNSS on station coordinates. To quantify the impact of using tropospheric ties, the repeatability of station coordinates is calculated using the approach described in section 4.2.3.1. This repeatability serves as an indicator of the effect of tropospheric ties on the coordinates. The results from the five experimental scenarios described in section 4.2.3.2 are presented.

In the first scenario, the combination of VLBI with tropospheric ties was demonstrated during CONT14. This was achieved by using co-located VLBI radio telescopes located in Hobart, Australia, namely HOBART12 and HOBART26. Figure 5.1 illustrates the repeatability of station coordinates for the two Hobart telescopes in each solution. The results indicate that the application of tropospheric ties leads to an improvement in the station coordinate repeatability of the HOBART12 telescope. Specifically, the ZW1M solution exhibits the most significant improvement compared to other solutions, with a 0.8 mm improvement in the upward component with respect to SING solutions. However, the HOBART26 telescope shows only marginal improvement when tropospheric ties are applied. This finding is consistent with a previous study conducted by Nilsson et al. (2015), which combined the two VLBI radio telescopes at the Hobart co-location site during CONT14 and demonstrated an improvement in station coordinate repeatabilities from combining tropospheric parameters using tropospheric ties.

The application of tropospheric ties improves the VLBI intra-technique combination with respect to the SING solution during CONT14. The results show that the HOBART12 telescope

benefits from the application of tropospheric ties with a standard deviation of 1 mm as a weighting. Another weighting scenario also demonstrated an improvement, albeit less than the ZW1M scenario. On the other hand, the HOBART26 telescope shows a lesser improvement from the application of tropospheric ties since it is part of the datum definition of the combination in this study. This suggests that a strong weight for tropospheric ties can maximize the benefit of applying tropospheric ties in the VLBI intra-technique combination.

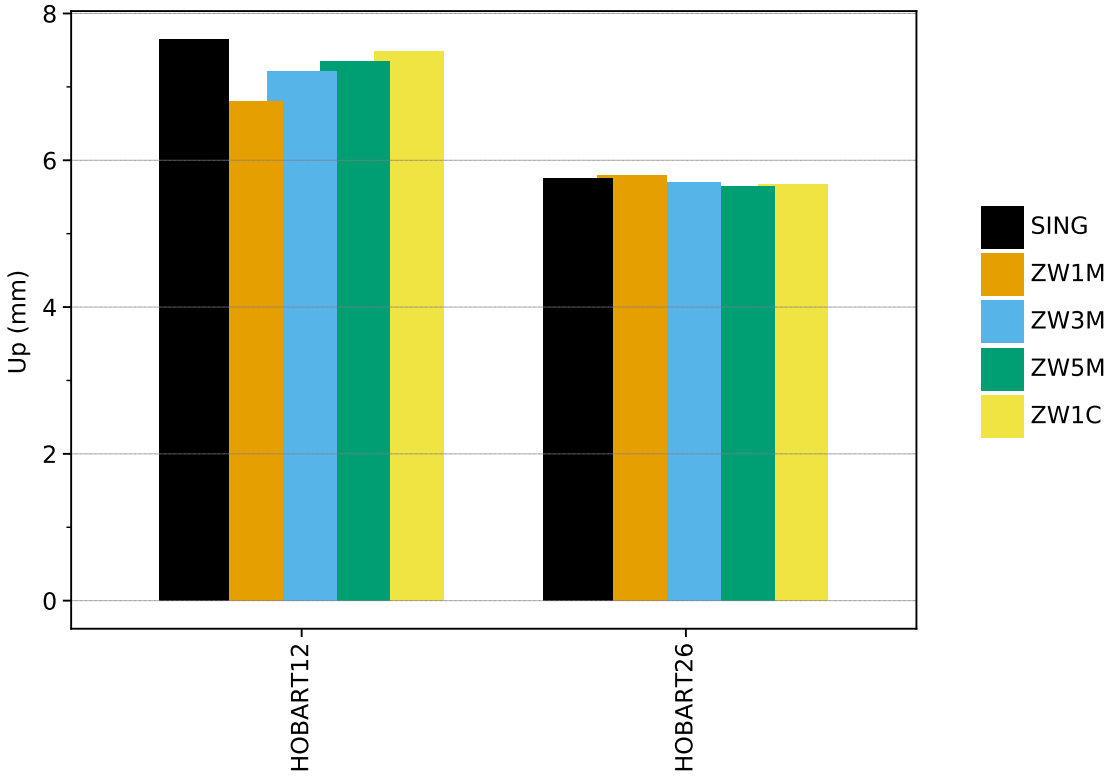

Figure 5.1: The height repeatabilities of two Hobart telescopes due to applying tropospheric ties with four different weights compared to a single technique solution.

The second scenario investigates the extended study conducted by Kitpracha et al. (2022), which combines the parallel VLBI networks during CONT17 using tropospheric ties. The results indicate that the use of tropospheric ties improves datum transfer between the parallel networks. The main improvement is demonstrated in the north and up components of non-datum station coordinates. However, this study finds that the utilization of tropospheric ties does not improve the repeatability of baseline lengths.

The results of this study suggest that tropospheric ties are effective in improving datum transfer between VLBI networks during CONT17. However, as there was only one co-location site across two VLBI parallel networks during CONT17, the repeatability of baseline lengths could not be improved. More details of the results and discussions can be found in Kitpracha et al. (2022).

Furthermore, this scenario addresses the potential of tropospheric ties to replace local ties in the datum transfer in the combination of space geodetic techniques. To investigate this, an extended study based on the approach in section 4.2.3.2 was conducted. Unfortunately, when the up component of local ties was excluded and replaced with tropospheric ties, numerical problems occurred during the inversion of NEQ. The same situation arose when the horizontal

components of local ties were excluded and gradient ties were applied. These findings indicated that tropospheric ties cannot transfer the datum information to solve the rank deficiency in the datum-free NEQ of space geodetic techniques as local ties. As demonstrated by the removal of some components of local ties and their replacement with tropospheric ties, the combined NEQ cannot be inverted during the combination of the VLBI parallel networks during CONT17. Thus, this confirms that one local tie is necessary to use tropospheric ties in combination.

The third scenario investigates the potential of tropospheric ties in improving the station coordinates when the local ties in the up component are of poor quality. To achieve this, the study omitted the height component of local ties with significant discrepancies and applied tropospheric ties with four different weighting solutions. The analysis was carried out station by station. Figure 5.2 presents the station coordinate repeatability in the up component of select stations derived from five solutions, using the methodology described in section 4.2.3. The results showed a significant improvement in the repeatability of the HOBART12 radio telescope when tropospheric ties were used instead of local ties, reducing the repeatability from 13 mm to 7 mm for the ZW1M scenario compared to the LTR solution. In contrast, only a minor improvement was observed for the GNSS station (HOB2) at the Hobart co-location site. The ZW1M solution demonstrated the most significant improvement compared to the other solutions when tropospheric ties were applied. The WARK12M and ONSALA60 telescopes showed similar improvements to the HOBART12 telescope. However, for their co-located GNSS stations, only marginal improvements were observed when applying tropospheric ties. In contrast, the repeatability of MATERA, NYALES20, TSUKUB32, WESTFORD, and YARRA12M telescopes deteriorated when tropospheric ties were used instead of local ties in the up component. However, their GNSS co-located stations demonstrated an improvement with tropospheric ties. The Wettzell co-location site, where local ties were of good quality in the up component in this study, showed only a marginal improvement with tropospheric ties instead of local ties.

In this scenario, the horizontal components of local ties, which have a large discrepancy, were also tested by excluding the horizontal components of local ties and combining horizontal gradient parameters with three different weighting scenarios. The repeatability of horizontal station coordinates for both VLBI and GNSS stations, where local ties showed a large discrepancy, is depicted in Figure 5.4 and 5.3. The results indicate that excluding horizontal components of local ties and combining horizontal gradient parameters does not improve the station coordinate repeatability for most stations. However, a few stations demonstrate marginal improvement, such as YARRA12M in the east component and MATERA in the north component. In contrast to the scenario of applying gradient ties, stacking horizontal gradient parameters demonstrated the most significant improvement compared to other scenarios.

Tropospheric ties demonstrate the capability as alternative ties when local ties have a problem, especially the up component. The study showed that replacing the problematic up component of local ties with tropospheric ties significantly improved the repeatability of station coordinates in the up component, especially for non-datum stations. The most significant improvement was observed when applying strong weight for tropospheric ties. However, if local ties already have good quality, replacing them with tropospheric ties does not improve station coordinate repeatability, as demonstrated by the station pair between WETTZELL

and WTZR. Using tropospheric ties with a bias instead of local ties can also worsen the up component of station coordinate repeatability, as shown by the station pair of NYALES20 and NYA1, because tropospheric ties can also be biased due to instrumental bias or mis-modeling in apriori values. Even when using loose weight to account for the bias in tropospheric ties, the results show a significant improvement in co-located GNSS station coordinates' up component but a dramatic deterioration in VLBI co-located telescopes.

Moreover, applying gradient ties instead of the horizontal component of local ties did not improve the horizontal coordinates because of the multipath effect, which introduces bias in the observed horizontal gradient differences, particularly at low-elevation observations of co-located GNSS stations during CONT14 as demonstrated in Figure 5.5. This effect deteriorates the combination solution when applying gradient ties or stacking gradient parameters.

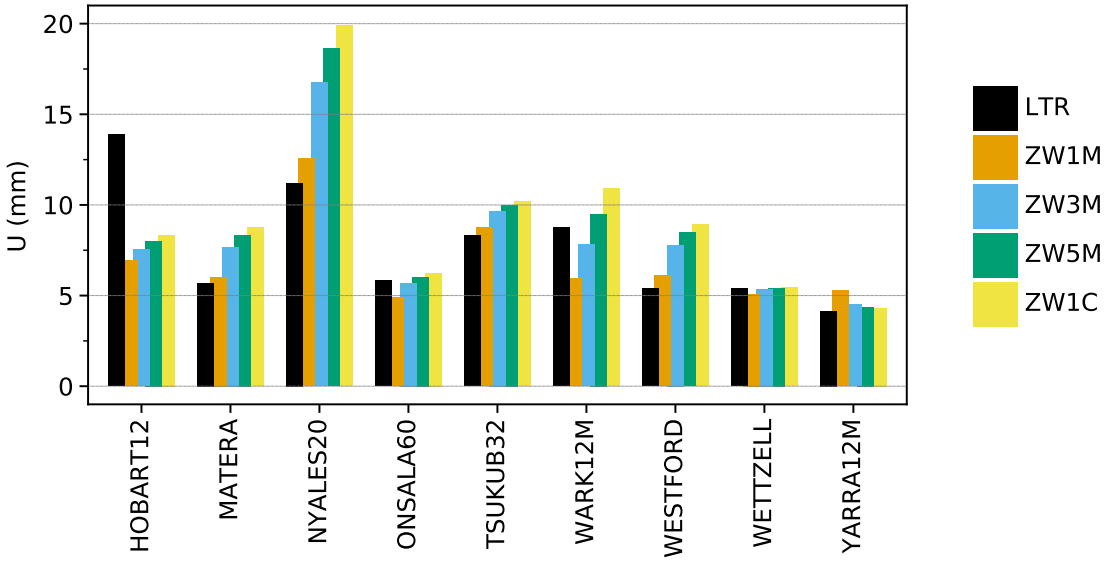

(a) The up coordinate repeatabilities of VLBI telescopes.

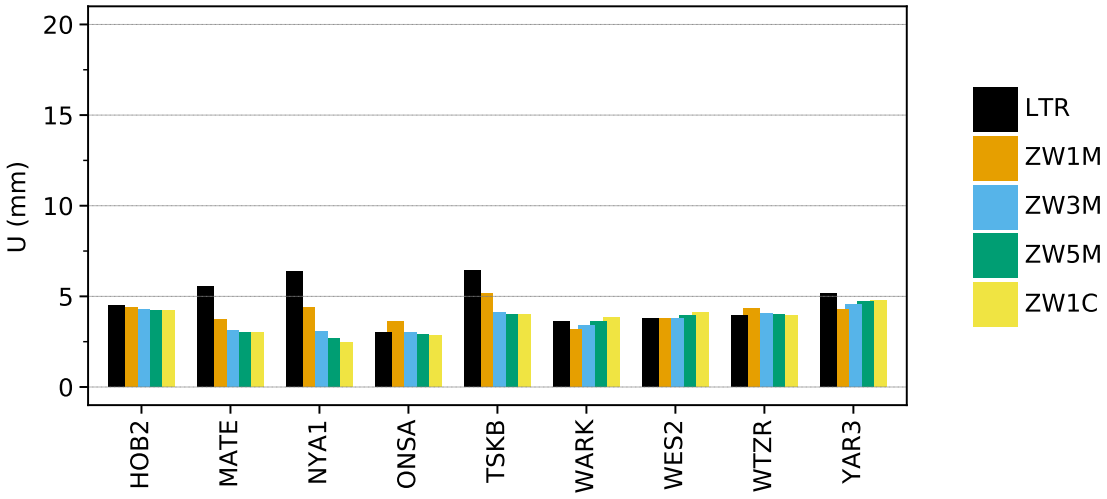

(b) The up coordinate repeatabilities of GNSS stations.

Figure 5.2: Up coordinate repeatabilities of co-location sites where the up component of local ties is questionable, as well as two co-location sites (Wettzell and Yarragade) where the up component of local ties is of good quality, derived from a station-wise combination utilizing tropospheric ties with four different weightings with respect to the reference solution (LTR).

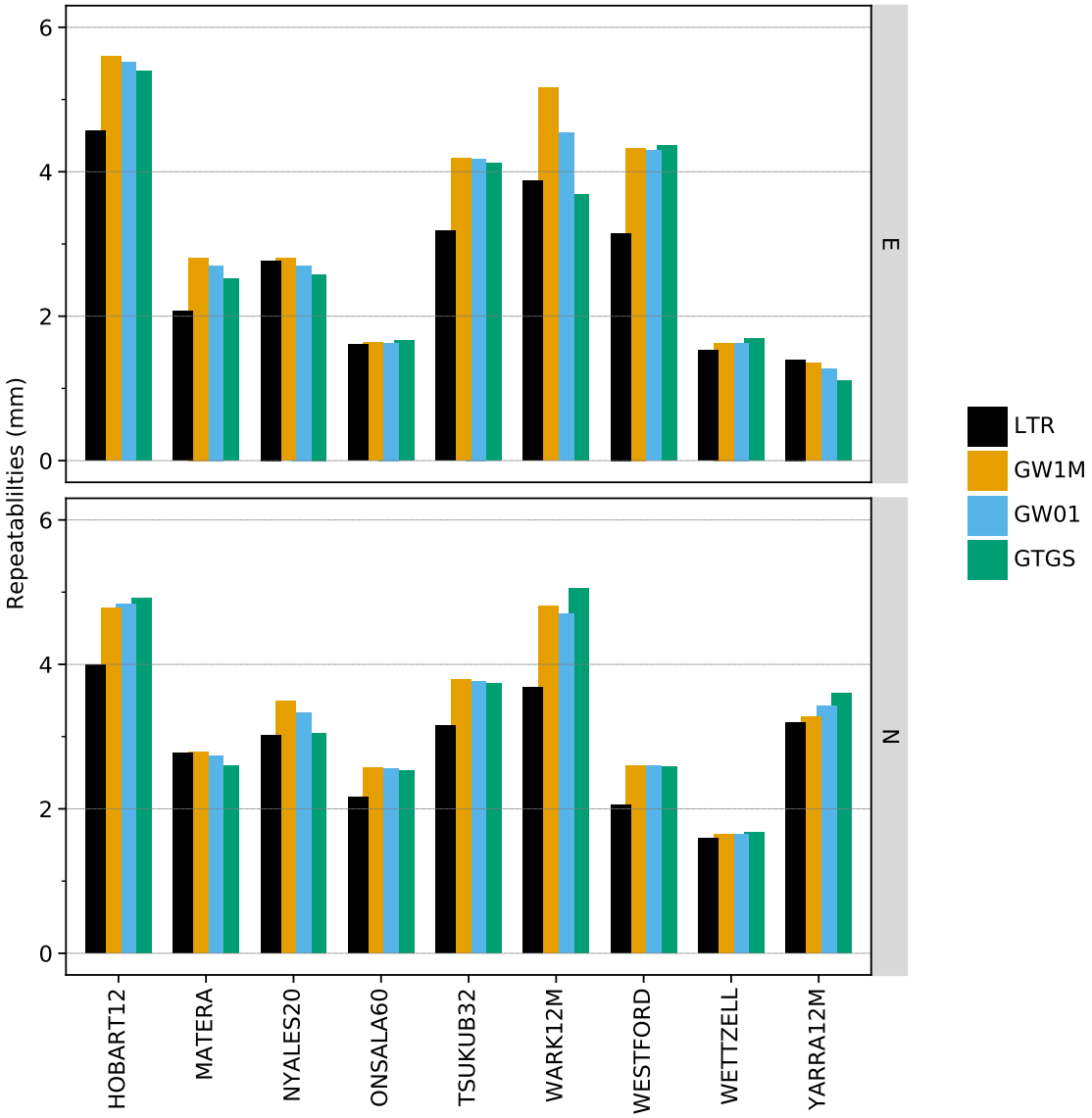

Figure 5.3: VLBI horizontal coordinate repeatabilities of co-location sites where the horizontal component of local ties is questionable, as well as two co-location sites (Wettzell and Yarragade) where the horizontal component of local ties is of good quality, derived from a station-wise combination utilizing gradient ties with three different weightings with respect to the reference solution (LTR).

In the fourth scenario, the appropriate temporal resolution for applying tropospheric ties is investigated in this study due to the time-dependent nature of troposphere parameters. Four different solutions are considered, and the up-component repeatability of VLBI and GNSS stations for each solution is shown in Figure 5.6. The results indicate that most of the selected stations demonstrate similar repeatability across all four solutions, with only WTZR, MATE, and MATERA showing a slight improvement for ONE, SEGEX, and SEG1C when compared to the ALL scenario.

This study demonstrates that applying tropospheric ties with different temporal resolutions yields similar results. This is due to the short duration of CONT14, which was only 15 days, and the fact that the seasonal effects on tropospheric ties, as described in section 3.1, do not have a significant impact in this study. Additionally, sub-daily variations in tropospheric ties

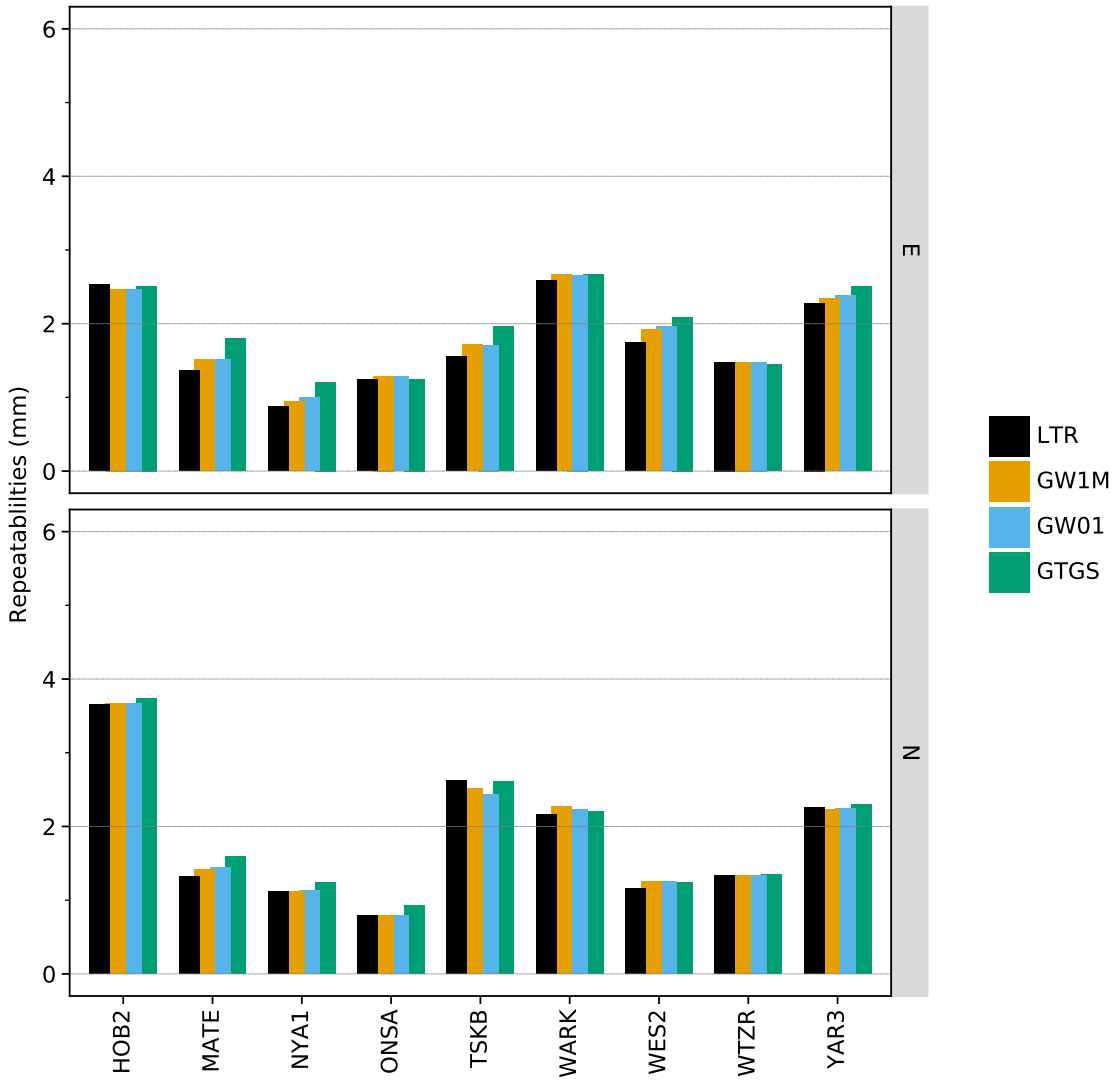

Figure 5.4: GNSS horizontal coordinate repeatabilities of co-location sites where the horizontal component of local ties is questionable, as well as two co-location sites (Wettzell and Yarragade) where the horizontal component of local ties is of good quality, derived from a station-wise combination utilizing gradient ties with three different weightings with respect to the reference solution (LTR).

are generally less than 1 mm. Excluding problematic epochs of troposphere parameters or applying loose weight when applying tropospheric ties also results in similar outcomes. This is because only 2% of all estimation epochs in this study were problematic, and thus, excluding or applying loose weight to those epochs does not significantly impact the combination in this study.

As demonstrated in Chapter 3, the comparison revealed that the instrumental bias causes a discrepancy between observed ZTD differences and tropospheric ties. Therefore, the use of instrumental bias correction in tropospheric ties is investigated in the fifth scenario. Consequently, four co-location sites were selected where the discrepancy between observed ZTD differences and tropospheric ties model was larger than 1 mm during CONT14. The benefit of instrumental bias correction was investigated in the combination process, as presented in Section 4.2.4. Figure 5.7 illustrates the station coordinate repeatabilities in the up component from six different scenarios. The results showed that applying instrumental bias correction

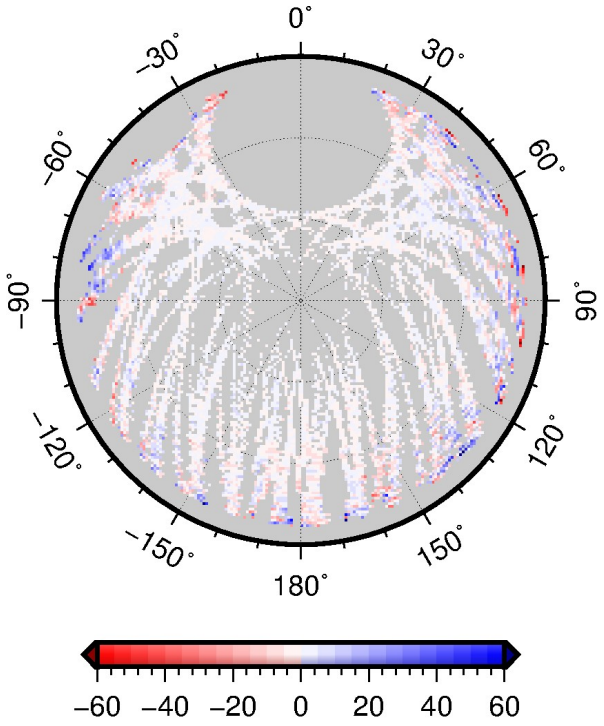

Figure 5.5: A snapshot of one-week residuals of ionosphere-free phase observations of MATE in May 2014 (6^{st} May to 13^{th} May). All measurements are given in millimeters. The sky plot reveals that MATE has large residuals that occurred in the low-elevation observations.

significantly improved the station coordinate repeatability, especially in the up component of VLBI radio telescopes compared to LTR and ZW1M scenarios. For instance, applying instrumental bias correction reduced the up-coordinate repeatability of MATERA in the ZW1MIB solution by approximately 2 mm compared to LTR solution. Similarly, its co-located GNSS station (MATE) showed an improvement of 1 mm when applying instrumental bias correction for the ZW1MIB solution compared to the LTR solution. Additionally, applying instrumental bias correction to tropospheric ties improved the deterioration by approximately 2 mm of the up component repeatability when applying tropospheric ties without instrumental bias correction at TSUKUB32 and TSKB stations. The results also showed that using a strong weight (ZW1M) demonstrated the best improvement compared to other different weighting scenarios.

Furthermore, the investigation revealed that applying instrumental bias correction significantly reduced the discrepancies between local ties and combined station coordinate differences, especially in the up component, as shown in Figure 5.8. For instance, the discrepancy of the up component at the Wettzell co-location site (between WETTZELL and WTZA) was dramatically reduced from 2 mm in the LTR solution to 0.5 mm in the ZW1MIB solution. Similarly, applying instrumental bias correction also improved the deterioration when applying only tropospheric ties, as demonstrated at Matera (between MATERA and MATE) and Tsukuba (between TSUKUB32 and TSKB) co-location sites.

The results demonstrated that applying tropospheric ties with instrumental bias correction significantly improved the station coordinates of combined solutions, especially in the up component. Moreover, the ZW1MIB scenario showed the most improvement in this study, indicating that the precision of tropospheric ties is improved by applying instrumental bias

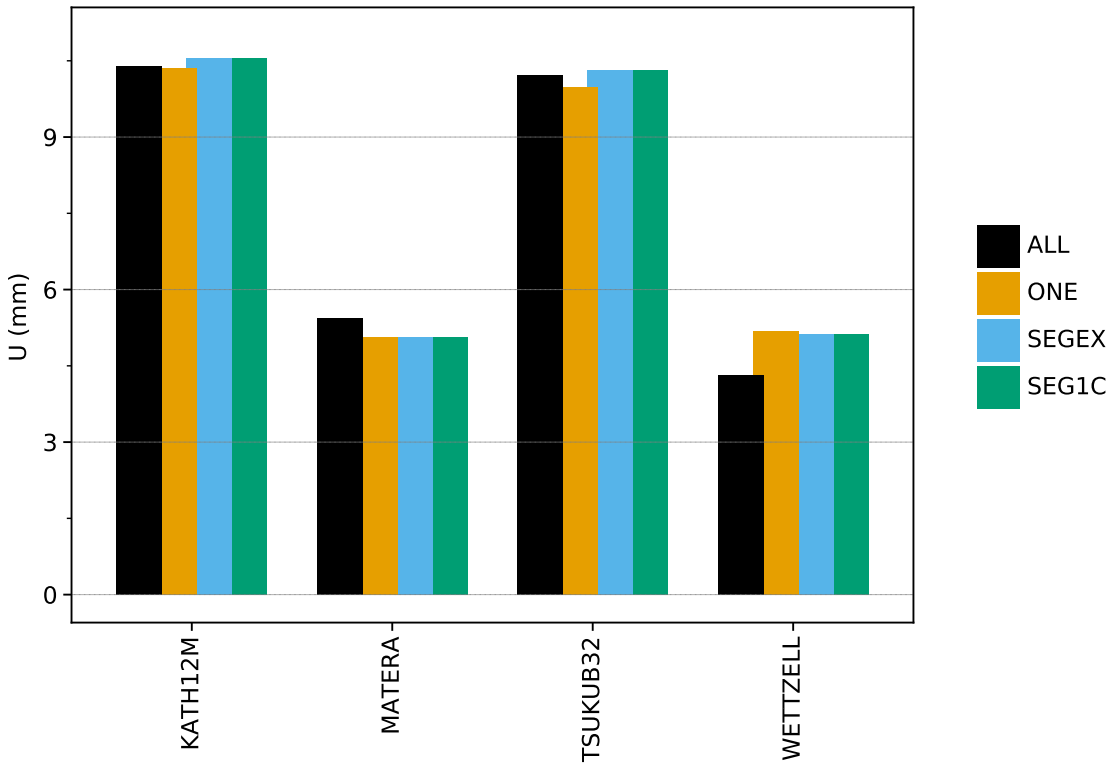

(a) The up coordinate repeatability of VLBI telescopes.

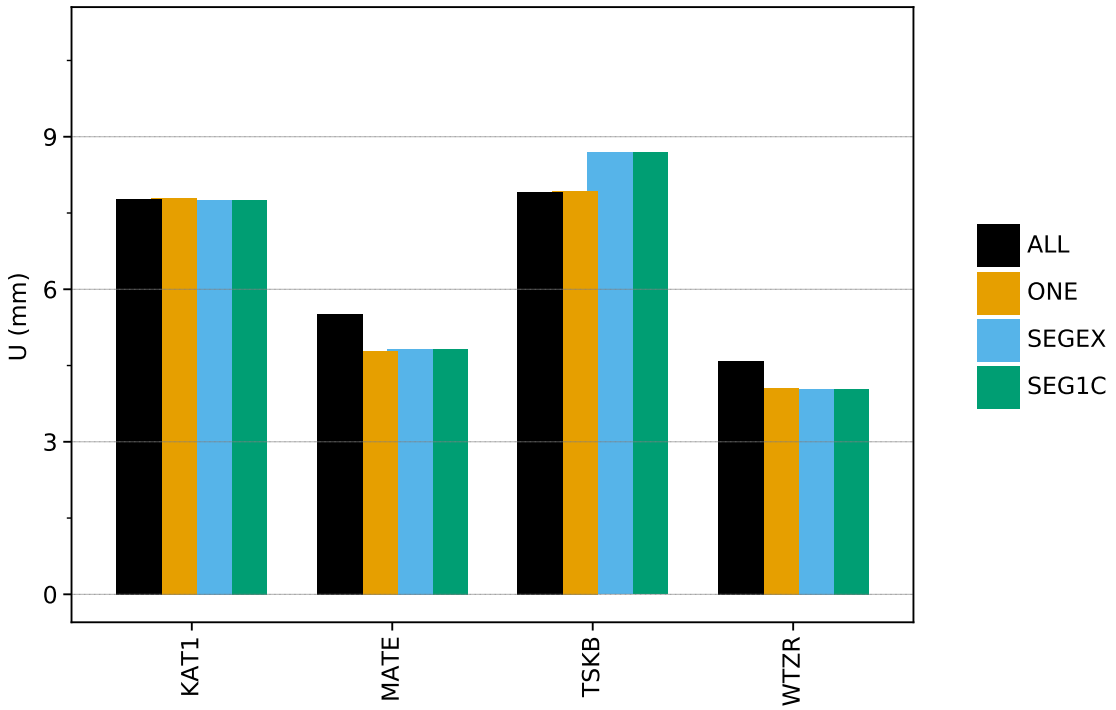

(b) The up coordinate repeatabilities of GNSS stations.

Figure 5.6: Up coordinate repeatabilities of four selected co-location sites derived from a station-wise combination employing tropospheric ties with two different temporal resolutions, as well as excluding and applying with loose weight for a questionable epoch of troposphere parameters.

correction. Additionally, applying tropospheric ties with instrumental bias correction improved the agreement between combined station coordinate differences and the expected coordinate

differences from local ties in the up component. This indicates that instrumental bias correction mitigates the systematic effect that might occur in the height station coordinates or troposphere parameters due to their high correlation in the combination of VLBI and GNSS.

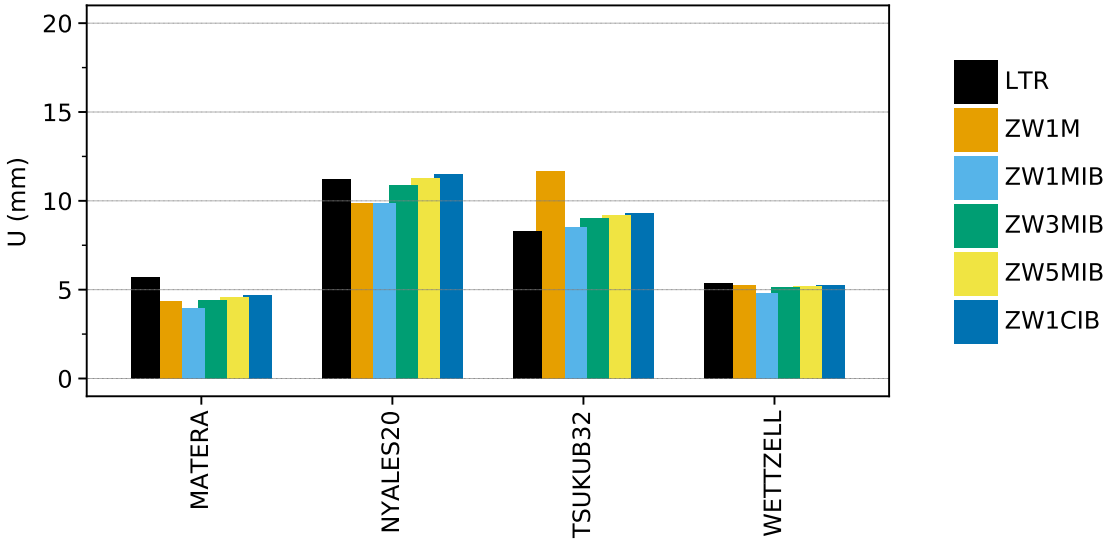

(a) The up coordinate repeatabilities of VLBI telescopes.

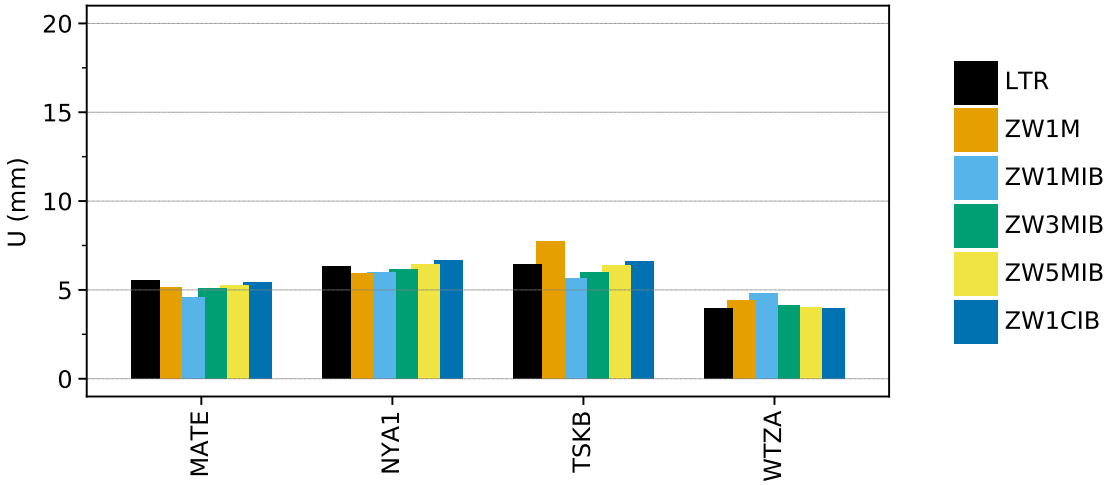

(b) The up coordinate repeatabilities of GNSS stations.

Figure 5.7: Up coordinate repeatabilities of four selected co-location sites derived from a station-wise combination employing tropospheric ties and instrumental bias correction with four different weightings, as well as the reference solution (LTR) and applying tropospheric ties without instrumental bias correction and using a standard deviation of 1 mm as the weight.

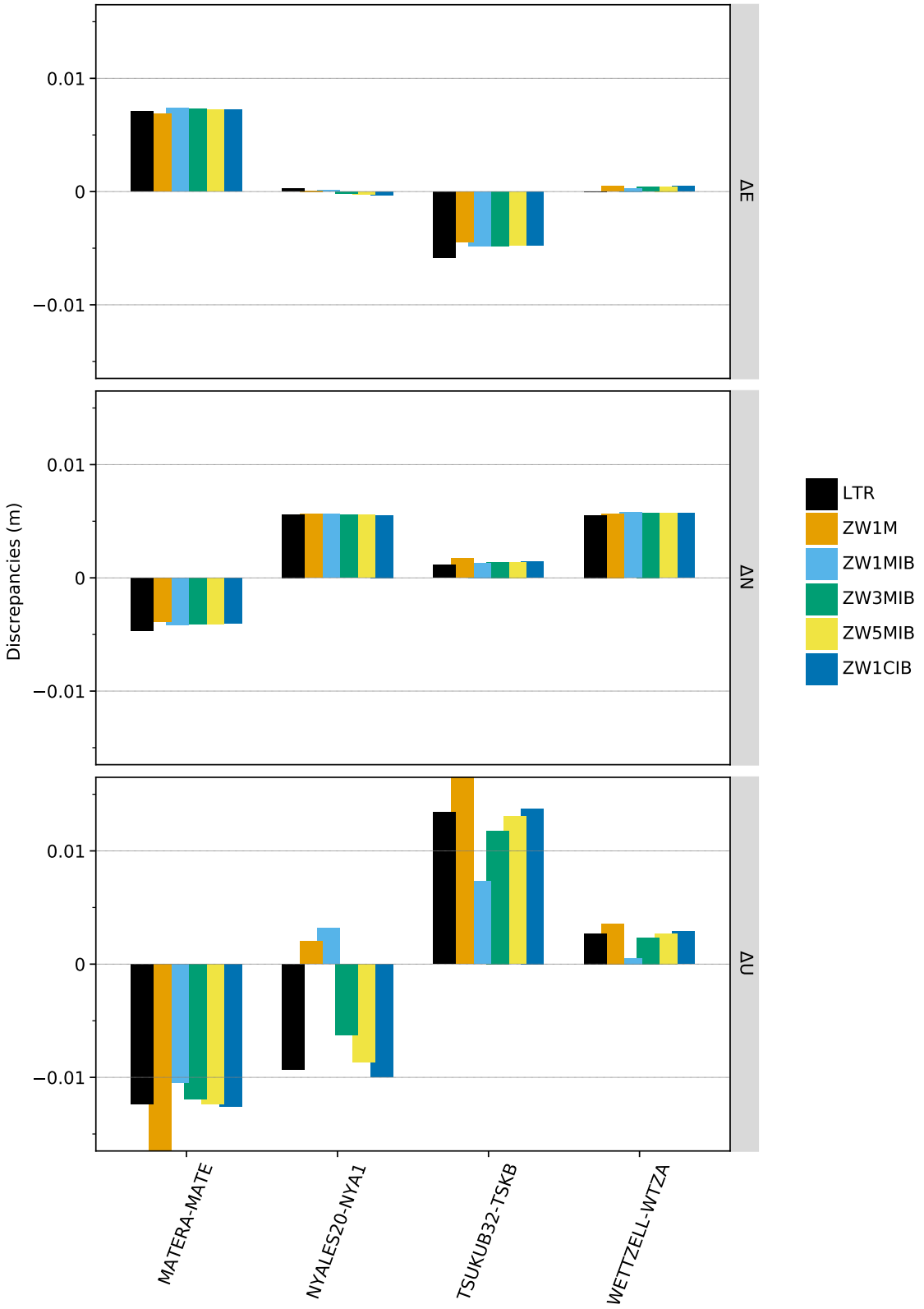

Figure 5.8: The discrepancies between local ties and station coordinate differences determined by a station-wise combination of four selected co-location sites employing tropospheric ties and instrumental bias correction with four different weightings, as well as the reference solution (LTR) and employing tropospheric ties without instrumental bias correction and a standard deviation of 1 mm as weight.

5.2 Impact on troposphere parameters

This section evaluates the combined tropospheric parameters obtained through a combination of VLBI and GNSS. The combined tropospheric parameters are compared to the ray-traced tropospheric parameters derived from NWM, as outlined in section 4.2.3.1. The results of the five experimental scenarios described in section 4.2.3.2 are presented.

The first scenario demonstrated the impact of combining VLBI with tropospheric ties on tropospheric parameters during CONT14. Table 5.1 lists the mean bias and WRMS of the ZTD parameters for the Hobart co-located telescopes w.r.t. the ERA5 NWM during CONT14. The HOBART12 telescope showed an improvement of 2 mm in the mean bias in the ZW1M w.r.t. SING solution. Moreover, ZW3M and ZW5M scenarios demonstrated an improvement of 1 mm in the mean bias, meanwhile, an improvement of 2 mm was found in WRMS. ZW1C showed a marginal improvement w.r.t. SING solution. The HOBART26 telescope demonstrated a dramatic improvement in troposphere parameters, unlike the station coordinate. The mean bias was reduced by 2 mm in the ZW1M w.r.t. SING solution. In addition, ZW3M and ZW5M improved the mean bias by 1 mm w.r.t. SING solution. Similar to HOBART12, ZW1C showed only a small improvement w.r.t. SING solution.

The results suggest that applying tropospheric ties improve an agreement between combined ZTD and ERA5 NWM. This improvement is caused by an improvement in the combined observation geometry of the Hobart co-located telescopes resulting in an improvement in ZTD parameter estimation. Moreover, using strong weight demonstrates the most benefit when applying tropospheric ties, as shown by the ZW1M scenario.

Station	SING	ZW1M	ZW3M	ZW5M	ZW1C
HOBART26	-2.92 (9.22)	-0.18 (7.31)	-1.07 (7.36)	-1.63 (7.47)	-2.21 (7.73)
HOBART12	2.23 (8.2)	0.96 (7.97)	1.53 (8.0)	1.85 (8.06)	2.11 (8.14)

Table 5.1: Comparison of ZTD parameters obtained from two Hobart telescopes with respect to the ERA5 Numerical Weather Model (NWM) for five different solutions. The results are presented in units of millimeters and expressed in the format of WM (WRMS).

In the second scenario, the assessment of combining VLBI tropospheric parameters using tropospheric ties during CONT17 was conducted by extending the study carried out by Kitpracha et al. (2022), which combined the parallel VLBI networks during CONT17 using tropospheric ties. The ZTD parameters from the combined two VLBI networks during CONT17 were evaluated. According to the results, the combined ZTD at co-located telescopes (Wettzell) showed an improvement compared to GNSS-derived ZTD and ERA5 NWM. According to the results, the combined ZTD at co-located telescopes (Wettzell) showed an improvement w.r.t. GNSS-derived ZTD and ERA5 NWM. The detailed results can be found in Kitpracha et al. (2022).

Furthermore, this scenario addresses the potential of tropospheric ties to replace local ties in the datum transfer in the combination of space geodetic techniques, which was also assessed in tropospheric parameters. Similar to the station coordinate results, numerical problems occurred during the inversion of NEQ; therefore, the results can be omitted from the discussion.

The third scenario addresses the question of whether replacing questionable local ties with tropospheric ties also improves the combined tropospheric parameters. Figure 5.9 shows the WRMS of combined ZTD parameters with respect to the ERA5 NWM for each scenario during CONT14. The HOBART12 telescope demonstrated an improvement of 1 mm in ZW1M with respect to LTR, similar to the station coordinate. On the other hand, ZW3M, ZW5M, and ZW1C showed a small improvement compared to ZW1M for the HOBART12 telescope. However, its co-located GNSS station, HOB2, showed only a small improvement in ZW1M, whereas ZW3M, ZW5M, and ZW1C remained unchanged with respect to LTR. This situation also applied to other co-location sites, such as Matera, Tsukuba, Onsala, Warkworth, and Westford. The Wettzell co-location site, where the local ties are of good quality, also demonstrated an improvement in WETTZELL telescopes, whereas WTZR remained unchanged. This also applied to the Yarragade co-location site. Moreover, the NYALES20 telescope also showed an improvement of 2 mm for ZW1M with respect to LTR. In addition, NYA1 showed a small improvement in ZW1M, whereas ZW3M, ZW5M, and ZW1C remained unchanged compared to LTR.

Furthermore, the impact of replacing questionable horizontal components of local ties with gradient ties was also assessed in terms of horizontal gradient parameters. According to Figure 5.10, all VLBI telescopes benefited from replacing the horizontal components of local ties with gradient ties. A major improvement of roughly 0.2 mm was observed in both east and north gradients for co-location sites where their local ties are biased in this study. However, in GW1M and GW01, a few telescopes demonstrated a small deterioration, such as MATERA in the east gradients and TSUKUB32 in the north gradients. Nevertheless, MATERA telescopes demonstrated an improvement in TGS. In contrast, TSUKUB32 remained unaffected. Moreover, TGS showed the best improvement compared to GW1M and GW01 in this study. On the other hand, Figure 5.11 shows the WRMS of combined horizontal gradient parameters with respect to the ERA5 NWM for GNSS stations. The results showed that replacing the problematic horizontal components of local ties did not affect GNSS stations. GW1M and GW01 remained unchanged with respect to LTR in this study. On the other hand, TGS demonstrated a deterioration of roughly 0.2 mm for every GNSS station.

The results of this study indicate that replacing the problematic component of local ties with tropospheric ties not only improves the station coordinate but also troposphere parameters, particularly ZTD parameters. The co-location sites of Hobart, Matera, Westford, and Warkworth, where the height component of local ties is biased (see Table 4.11), show improvement from the application of tropospheric ties as a replacement on VLBI telescopes. Other co-location sites, where the height component of local ties is of good quality, demonstrate only a small improvement from using tropospheric ties as a replacement. The results suggest that using strong weight when applying tropospheric ties leads to the best outcome in this study, as demonstrated by ZW1M. However, in this study, GNSS stations show only a small improvement in ZW1M, while other scenarios remain unchanged. This is because the GNSS observation geometry already has good sky coverage (see Figure 5.5), providing a better estimation of troposphere parameters compared to VLBI. Hence, GNSS tends to receive less benefit from tropospheric ties compared to VLBI. Furthermore, applying gradient ties as a replacement for horizontal components of local ties indicates a benefit in horizontal

gradient parameters, similar to ZTD parameters. The main benefit was demonstrated in VLBI telescopes in the east and north gradients in this study. However, MATERA showed a small deterioration in GW1M and GW01 in the east gradients due to the good quality of the east component of local ties, as shown in Table 4.11. This also applied to TSUKUB32 telescopes. Similar to ZTD parameters, applying gradient ties with strong weight indicates the best improvement in this study. Concerning GNSS stations, applying gradient ties as a replacement for horizontal components of local ties does not show any improvement in this study. As previously mentioned, GNSS has good sky coverage, which provides a better estimation of troposphere parameters. Therefore, GNSS does not benefit from applying gradient ties compared to VLBI.

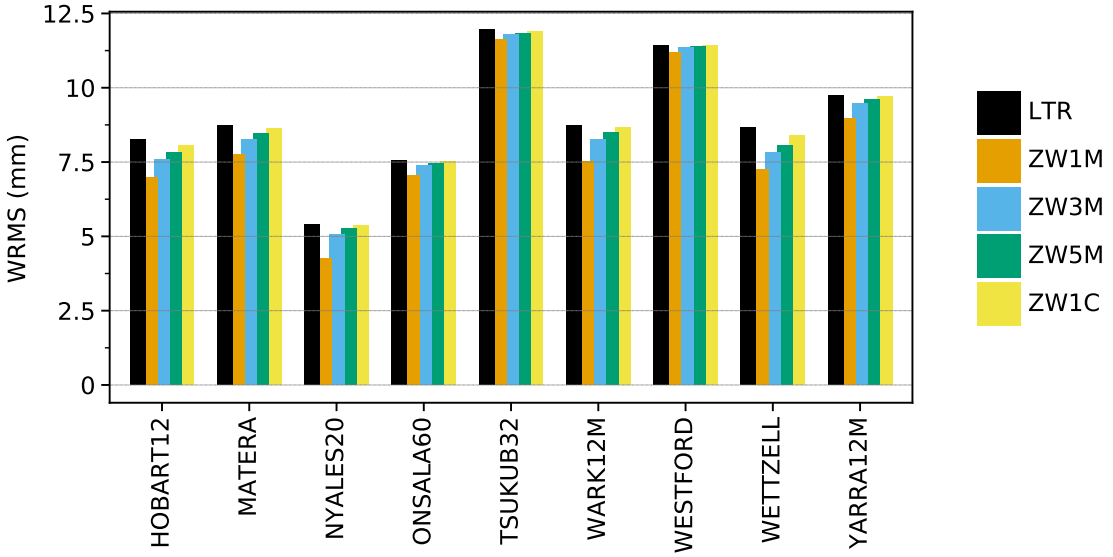

(a) WRMS of ZTD parameters w.r.t. ERA5 NWM of VLBI telescopes.

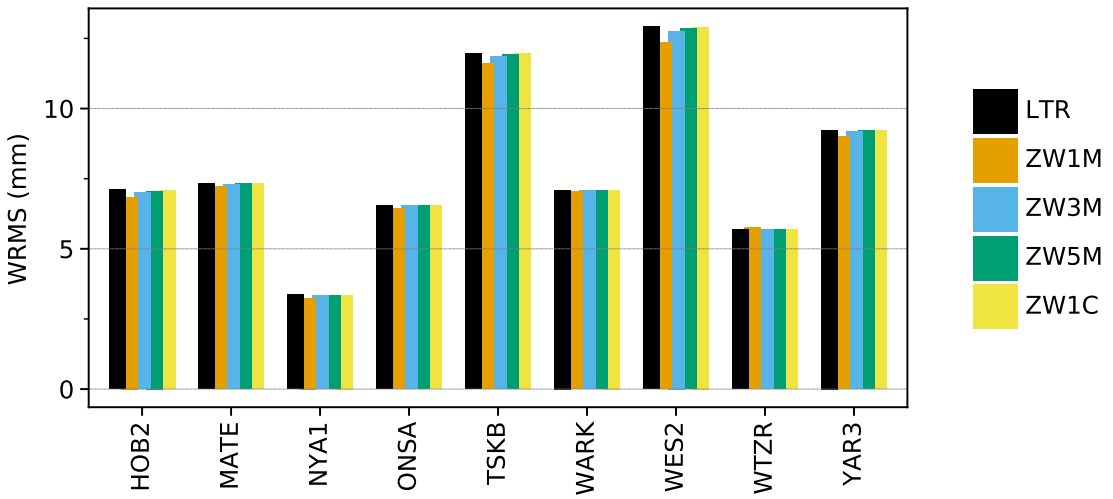

(b) WRMS of ZTD parameters w.r.t. ERA5 NWM of GNSS stations.

Figure 5.9: WRMS of ZTD parameters w.r.t. ERA5 NWM of co-location sites where the up component of local ties is questionable, as well as two co-location sites (Wettzell and Yarragade) where the up component of local ties is of good quality, derived from a station-wise combination utilizing tropospheric ties with four different weightings with respect to the reference solution (LTR).

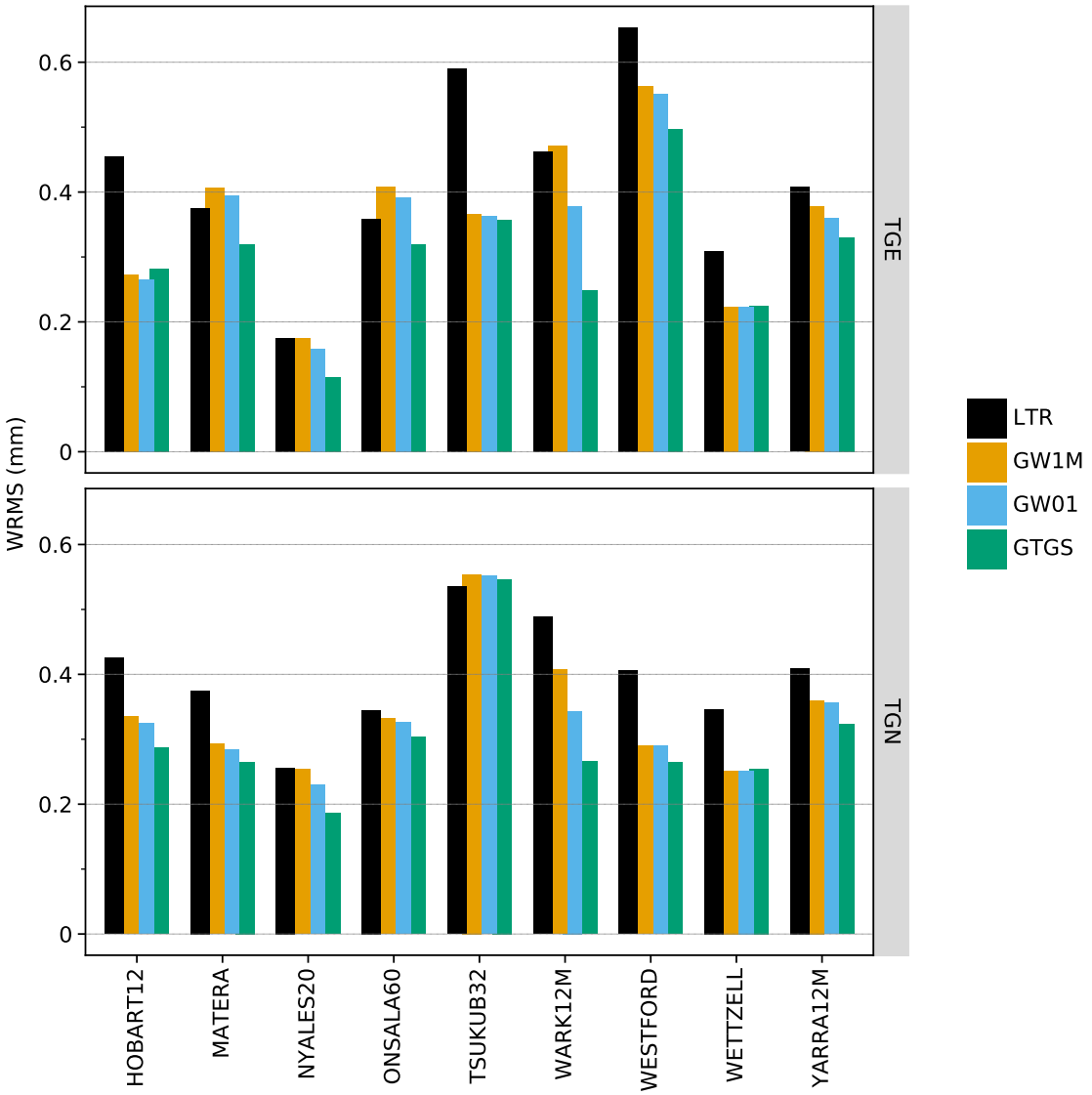

Figure 5.10: WRMS of horizontal gradient parameters w.r.t. ERA5 NWM of VLBI co-location sites where the up component of local ties is questionable, as well as two co-location sites (Wettzell and Yarragade) where the up component of local ties is of good quality, derived from a station-wise combination utilizing gradient ties with three different weightings with respect to the reference solution (LTR).

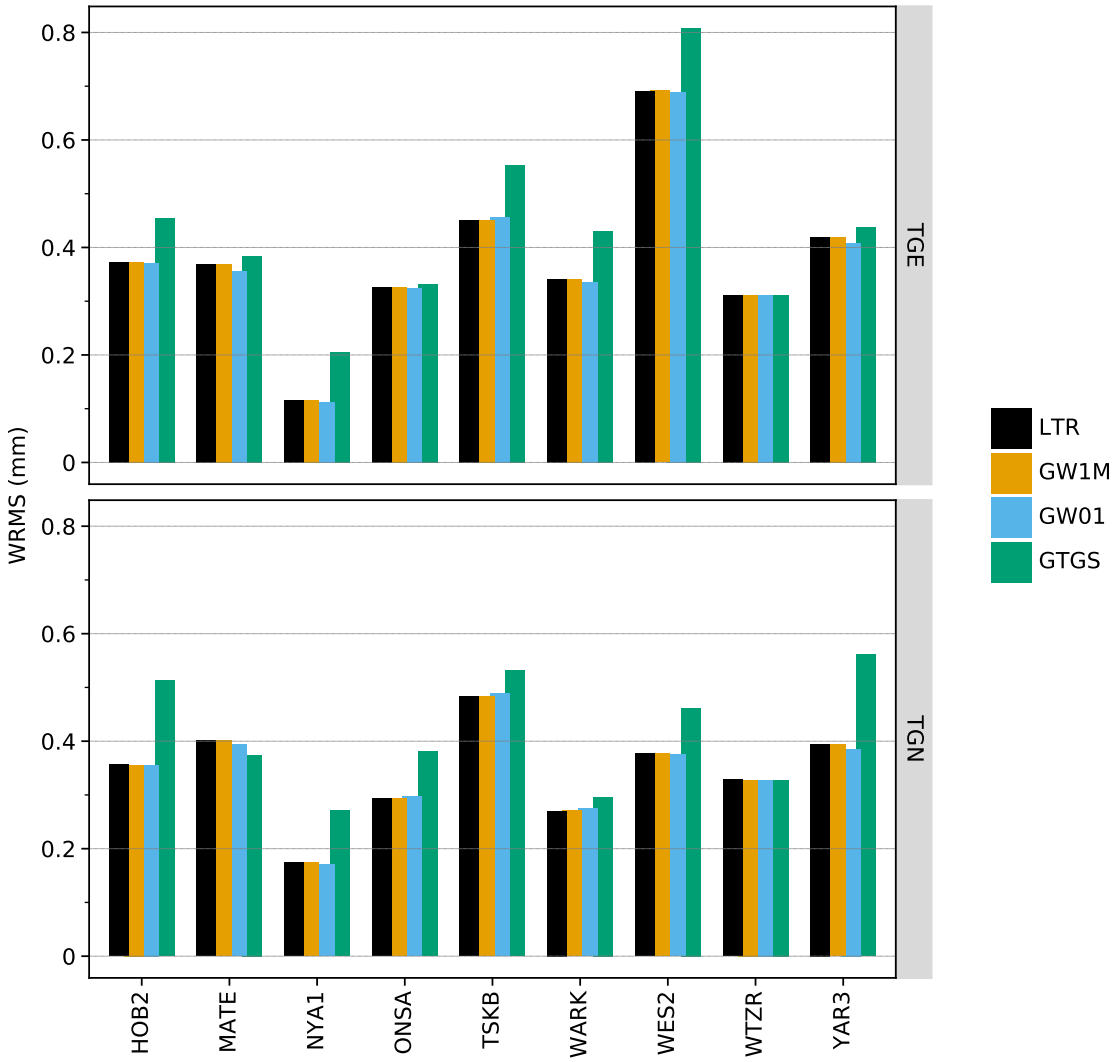

Figure 5.11: WRMS of horizontal gradient parameters w.r.t. ERA5 NWM of GNSS co-location sites where the up component of local ties is questionable, as well as two co-location sites (Wettzell and Yarragade) where the up component of local ties is of good quality, derived from a station-wise combination utilizing gradient ties with four three weightings with respect to the reference solution (LTR).

The fourth scenario investigates the application of different temporal tropospheric ties for ZTD parameters. Table 5.2 presents the mean bias and WRMS of ZTD parameters for each scenario with respect to ERA5 NWM. The majority of stations exhibited similar results in mean bias and WRMS across all scenarios. However, some stations demonstrated marginal changes in mean bias. For instance, the mean bias for MATE varied by approximately 1.3 mm in ONE, SEGEX, and SEG1C compared to ALL, while MATERA degraded by 1.3 mm for ONE, SEGEX, and SEG1C compared to ALL. Nevertheless, the WRMS showed no significant change. Similar changes were observed at the Wettzell co-location site compared to the Matera co-location site.

The study finds that using tropospheric ties with different temporal resolutions yields similar results, as there was no significant temporal variation during CONT14. However, this may not be the case for multi-year combinations due to seasonal variation. Excluding

problematic epochs has no significant impact, as the number of problematic epochs is small, as shown in Figure 4.10.

Station	ALL	ONE	SEGEX	SEG1C
KATH12M	4.56 (9.75)	4.64 (9.72)	4.54 (9.93)	4.54 (9.93)
MATERA	0.94 (7.85)	2.45 (7.87)	2.49 (7.83)	2.5 (7.83)
TSUKUB32	-0.49 (13.48)	-0.46 (13.49)	-0.47 (13.5)	-0.47 (13.5)
WETTZELL	-0.69 (6.62)	0.52 (6.6)	0.45 (6.97)	0.44 (6.91)
KAT1	7.03 (10.75)	6.9 (10.75)	7.07 (10.71)	7.07 (10.72)
MATE	1.86 (7.67)	0.52 (7.56)	0.47 (7.63)	0.47 (7.63)
TSKB	3.41 (11.75)	3.01 (11.75)	3.42 (11.77)	3.42 (11.77)
WTZR	0.01 (5.88)	-0.9 (5.74)	-0.83 (5.74)	-0.83 (5.74)

Table 5.2: Comparison of ZTD parameters w.r.t. the ERA5 NWM of four selected co-location sites derived from a station-wise combination employing tropospheric ties with two different temporal resolutions, as well as excluding and applying with loose weight for a questionable epoch of troposphere parameters. The results are presented in WM (WRMS) format. The values are given in units of millimeters.

In the fifth scenario, the impact of using instrumental bias correction on tropospheric ties was investigated for the combined troposphere parameters. Figure 5.12 shows the WRMS of ZTD parameters for four selected co-location sites with respect to ERA5 NWM for each scenario. The results show that using ZW1MIB and ZW1M scenarios resulted in similar WRMS. On the other hand, using ZW3MIB, ZW5MIB, and ZW1CIB caused a degradation in VLBI telescopes but had no effect on GNSS stations. Furthermore, using ZW1M and ZW1MIB resulted in a 1 mm improvement with respect to LTR for VLBI telescopes.

The results suggest that applying instrumental bias in tropospheric ties does not improve the combined ZTD parameters significantly. This is because the impact of instrumental bias mainly stems from instrument deficiencies such as GNSS antenna phase center modeling, which directly affects station coordinates rather than troposphere parameters. Moreover, applying tropospheric ties scenarios does not significantly affect GNSS since it already has good sky coverage.

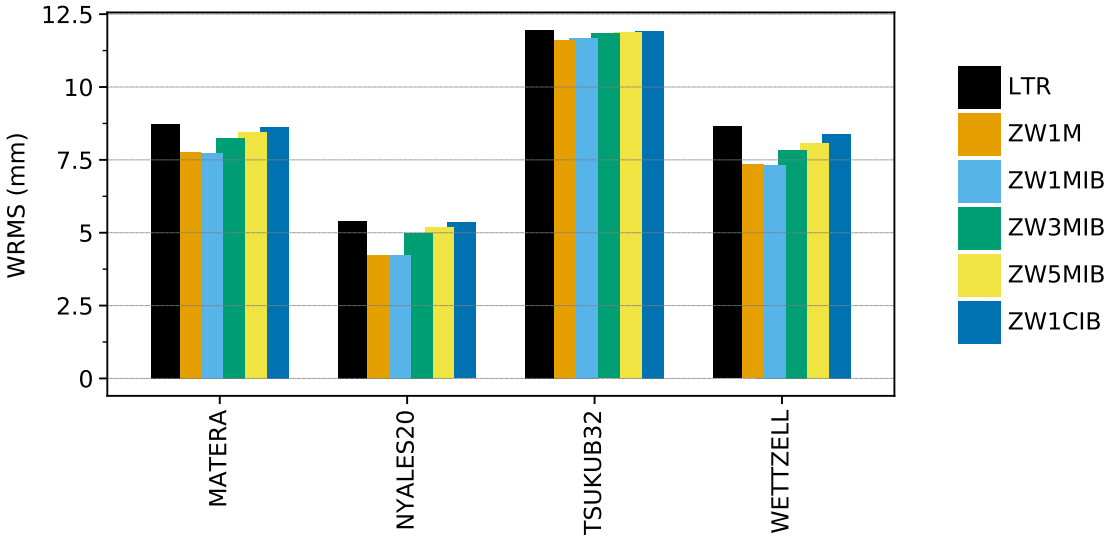

(a) WRMS of ZTD parameters w.r.t. ERA5 NWM of VLBI telescopes.

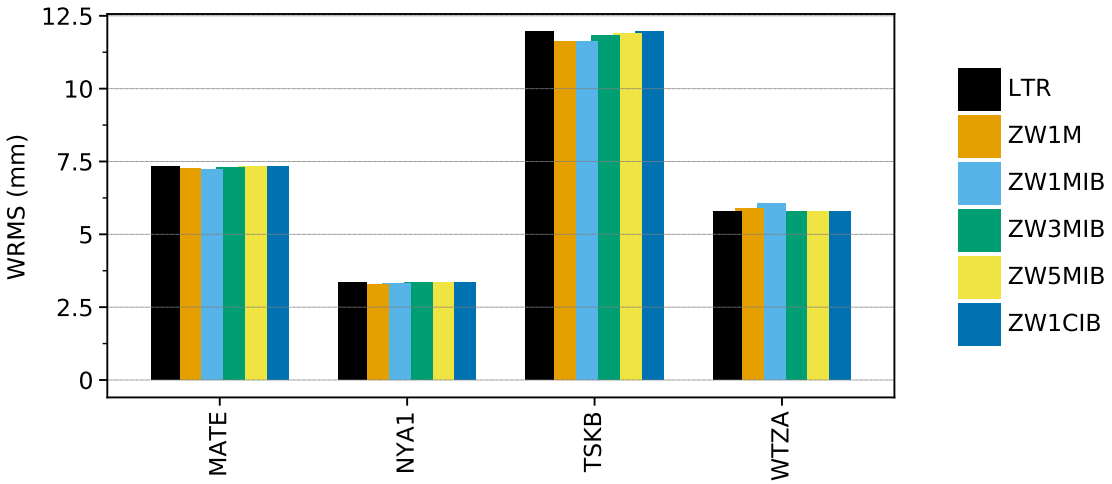

(b) WRMS of ZTD parameters w.r.t. ERA5 NWM of GNSS stations.

Figure 5.12: WRMS of ZTD parameters w.r.t. ERA5 NWM of four selected co-location sites derived from a station-wise combination employing tropospheric ties and instrumental bias correction with four different weightings, as well as the reference solution (LTR) and applying tropospheric ties without instrumental bias correction and using 1 mm STD as the weight.

6

Conclusions and outlooks

In this final section of the thesis, the explanations for the major results are provided. The novelty of the work conducted here lies in addressing the characteristics of each tropospheric tie model, discrepancies between these models and those derived from space geodetic techniques, as well as the strengths and limitations of tropospheric ties in the combination of space geodetic techniques, particularly VLBI and GNSS. Section 6.1 presents the key conclusions drawn from this study, while Section 6.2 outlines plans for future research.

6.1 Conclusions

This thesis provides a comprehensive investigation of the characteristics and applications of tropospheric ties. One of the key findings of this study is that tropospheric ties can be derived from either analytical models or ray-tracing techniques. Furthermore, the analysis reveals that tropospheric ties contain a mean offset due to height differences, primarily in the dry part, while the variation strongly exhibits in the wet part than the dry part and depends on the humidity at the site as well as height differences.

Sub-daily variations of tropospheric ties were also investigated and found to depend on meteorological data. Meteorological data from meteorological sensors and NWM show sub-daily variation, whereas the meteorological data obtained from empirical models, such as GPT3, shows no sub-daily variation. Another significant finding of this study is that tropospheric ties from analytical models and ray-tracing show similar performance when the weather condition is calm. However, in humid or extreme weather conditions, such as in the summer, tropospheric ties from analytical models based on meteorological models from empirical models and NWM show different performance compared to ray-traced tropospheric ties and tropospheric ties from analytical models based on meteorological sensors. In addition, the advantage of an analytical model is its capability to provide data at any temporal resolution since it depends solely on the temporal resolution of meteorological information. On the other hand, the temporal resolution of ray-traced tropospheric ties is limited by the temporal resolution of NWM despite showing similar performance to tropospheric ties from analytical models based on meteorological sensors.

The uncertainties of tropospheric ties are also investigated in this work. The findings demonstrate that the uncertainties of tropospheric ties are below the sub-millimeter level. The magnitudes of uncertainties for each component differ by various meteorological parameters. The ZHD component is primarily affected by the uncertainties of atmospheric pressure, whereas the ZWD component is influenced by the uncertainties of water vapor pressure. Additionally, this work investigates the effect of the uncertainties in the height differences between two reference point positions on tropospheric ties. The findings demonstrate no significant impact on the uncertainty of tropospheric ties resulting from the uncertainty in the height difference. It is important to note that this study was exclusively conducted with tropospheric ties derived from an analytical model using meteorological information obtained from meteorological sensors, owing to the availability of uncertainties in meteorological data.

The characteristics of gradient ties were also investigated in this study. Unlike tropospheric ties, which can be derived using various methods, gradient ties rely solely on ray-tracing in this study. The gradient ties, similar to tropospheric ties, are time-dependent. However, the mean offsets of gradient ties show no correlation with the horizontal distance between stations. Remarkably, the mean offsets remain at the sub-millimeter level across all co-location sites, regardless of their varying horizontal differences. On the other hand, the variation of gradient ties is found to be influenced by the height differences between stations, with higher variations observed during humid atmospheric conditions, particularly in summer. Nevertheless, even with varying height differences and atmospheric conditions, the magnitude of gradient ties remains consistently at the sub-millimeter level for all co-location sites.

The comparison study revealed that the instrumental bias in GNSS causes a discrepancy between observed ZTD differences and the tropospheric ties. However, the multipath effect at low elevation observations causes a bias in observed gradient differences. Equipment deficiencies, such as problems in the antenna amplifier, can also degrade the tropospheric parameters. On the other hand, instrumental bias was not observed in VLBI in this study. It is important to note that long-term observations of co-located VLBI radio telescopes are available for one site in this thesis.

To address instrumental bias, two experiments were conducted, designated A20 and A17. The A20 experiment demonstrated that instrumental bias can occur due to the use of different instruments, such as antennas or radomes, at different GNSS stations. It also found that tropospheric ties derived from analytical models and ray-tracing exhibited similar performance. In contrast, the A17 experiment successfully minimized the height shift that occurs during antenna changes to within a millimeter level, and determined the instrumental bias in GNSS-derived tropospheric parameters using the double-differencing approach. However, it found that employing the same antenna type again in this experiment produced an offset that was comparable to using different antenna types, as determined from the double-differencing approach. Additionally, the experiment demonstrated that severe weather events can cause a significant shift in GNSS-derived tropospheric parameters. Furthermore, there is no significant discrepancy founded in tropospheric parameter from using different GNSS receivers in this experiment.

The study reveals that utilizing tropospheric ties can result in an improvement in station coordinates and tropospheric parameters. Additionally, tropospheric ties can serve

as supplementary ties when the local tie is questionable, provided that at least one local tie is required at any co-location site during the combination. The study shows that the main improvements are found in station coordinates and tropospheric parameters. Furthermore, utilizing tropospheric ties with different temporal resolutions provides similar results, and the exclusion of questionable epochs of tropospheric ties does not show benefits in this study. Therefore, further investigation is required for the multi-year combination of VLBI and GNSS using tropospheric ties due to seasonality and the number of questionable epochs of tropospheric parameters, which may affect the temporal resolution of the combination solution. It is also important to emphasize that while tropospheric ties can be helpful, they cannot replace local ties in transferring datum information.

Additionally, the study suggests that correcting tropospheric ties using instrumental bias correction can improve station coordinates. However, the improvement in tropospheric parameters was not observed. Applying instrumental bias as a correction to tropospheric ties significantly reduces the discrepancy between combined station coordinate differences and local ties. Therefore, the study recommends applying tropospheric ties with strong weight along with instrumental bias correction in the combination of VLBI and GNSS, as it provides the best benefit from tropospheric ties. However, it is important to note that the instrumental bias obtained in this thesis may not be accurate, as some co-location sites showed deterioration when using strong weight, but an improvement when using loose weight. This study assumed that there is no instrumental bias in VLBI. Further improvements, such as the implementation of absolute calibration, are necessary to calibrate instrumental bias accurately.

6.2 Outlook

The current assumption regarding tropospheric ties is solely based on height differences between the reference point positions of space geodetic techniques. However, there is no consideration of horizontal differences between the reference point positions of space geodetic techniques in the current definition of tropospheric ties. Therefore, further investigation in this perspective is recommended, as it will elucidate the maximum horizontal separation between reference point positions of space geodetic techniques applicable for tropospheric ties.

The comparison of tropospheric ties is extensively studied in this work. However, a further comparison between ray-traced tropospheric ties and tropospheric ties derived from an analytical model with meteorological information using different NWMs, e.g., ERA5, is deemed valuable. This study exclusively utilized ECMWF operational NWM through VMF3 for obtaining the ray-traced ties and tropospheric ties derived from the analytical model. This will also facilitate the investigation of gradient ties, as gradient ties can only be derived from ray-tracing.

The uncertainties of tropospheric ties are solely investigated for the analytical model with meteorological information from in situ measurements, as it is not feasible to extract the uncertainties of meteorological information from NWMs and empirical models, e.g., GPT3, in this study. Understanding the uncertainty of tropospheric ties is crucial, as it provides a realistic weighting for tropospheric ties in the combination of space geodetic techniques. Therefore, it is worthwhile to further investigate the uncertainties of other tropospheric tie

models by extracting the uncertainty information from NWMs or empirical models, particularly in cases where the meteorological sensor is not calibrated, or the relative position between the reference points of the meteorological sensor and the geodetic instrument is not available for all co-location sites (Heinkelmann et al., 2011).

The instrumental bias in tropospheric parameters, which causes discrepancies between observed tropospheric parameter differences and tropospheric ties, is primarily observed in GNSS. Conversely, there is no conclusive evidence of instrumental bias observed in VLBI, as the comparison of co-located VLBI radio telescopes was conducted for only one co-location site due to data availability. Therefore, it is recommended for future studies to examine other co-located VLBI telescopes to verify the instrumental bias in VLBI.

As mentioned earlier, the definition of tropospheric ties in terms of maximum horizontal distance between reference point positions of space geodetic techniques has not yet been established. Therefore, the A20 experiment can be extended to further investigate this aspect, as unexpected systematic effects, such as instrumental bias, are mitigated by the experiment's setup. Moreover, the instrumental bias correction extraction for tropospheric ties approach in the A17 experiment is an empirical approach that relies on the assumption of no height-dependent effects in observed tropospheric parameters. Additionally, it is a relative approach that necessitates a reference station with high stability over a long time span. Given that the instrumental bias correction for tropospheric ties is crucial to enhance the accuracy of the geodetic parameters provided by the combination of VLBI and GNSS, further development of the absolute calibration approach is imperative.

The benefit of utilizing tropospheric ties in the combination of VLBI and GNSS is demonstrated solely on the station coordinates and tropospheric parameters in this work. Investigating its impact on other geodetic parameters, such as EOP and geocenter, is merited. Furthermore, this work is mainly carried out on a special observation campaign, e.g., CONT14, which spans only two weeks. It is limited to generalize the benefit of using tropospheric ties in combination of VLBI and GNSS. Therefore, a multi-year combination study is recommended, as it can delve into the impact on station velocity, as well as determine an appropriate temporal resolution for applying tropospheric ties. Moreover, the impact of weighting of tropospheric ties was studied and interesting results were found. However, this study only considered the variance component. Therefore, to further improve the stochastic model of tropospheric ties, resulting in an improvement in the geodetic parameters obtained from the combination of VLBI and GNSS with tropospheric ties, a further study on the realistic stochastic model used full variance-covariance information for tropospheric ties is recommended.

Furthermore, a potential extension of this thesis involves the inclusion of the third microwave technique, namely DORIS. This technique also possesses the capacity to provide tropospheric parameters. Since this technique may exhibit distinct systematic effects compared to GNSS or VLBI, which can result in discrepancies between observed tropospheric parameter differences and tropospheric ties. The comparison of tropospheric parameters with DORIS was demonstrated by Heinkelmann et al. (2016), revealing that the factor contributing to the disagreement between DORIS-derived tropospheric parameter differences and tropospheric ties is the observation geometry. This factor can introduce discrepancies similar to an instrumental bias in GNSS founded in this thesis. Therefore, further investigation is required, including

a combined study with DORIS employing tropospheric ties. Moreover, an extension study employing an optical technique, namely SLR, holds value. The potential of combining VLBI, GNSS, and SLR was demonstrated by Balidakis et al. (2023), offering an opportunity for additional research, such as the development of a tropospheric tie model between microwave and optical techniques. The current tropospheric tie models are currently applicable to microwave techniques. Additionally, comparing tropospheric parameters between microwave and optical techniques is of interest, as it may reveal distinct systematic effects unique to microwave techniques. Furthermore, a thorough investigation of an appropriate observation model and stochastic model is imperative due to the differing magnitudes of tropospheric parameters between microwave and optical techniques.

References

O. A. Alduchov and R. E. Eskridge. Improved Magnus form approximation of saturation vapor pressure. *J APPL METEOROL*, 35(4):601–609, 1996.

M. M. Alizadeh, D. D. Wijaya, T. Hobiger, R. Weber, and H. Schuh. Ionospheric effects on microwave signals. In *Atmospheric Effects in Space Geodesy*, pages 35–71. Springer, 2013.

Z. Altamimi, P. Rebischung, L. Métivier, and X. Collilieux. ITRF2014: A new release of the International Terrestrial Reference Frame modeling nonlinear station motions. *Journal of Geophysical Research: Solid Earth*, 121(8):6109–6131, 2016.

Z. Altamimi, P. Rebischung, X. Collilieux, L. Metivier, and K. Chanard. ITRF2020: main results and key performance indicators. 2022. doi: 10.5194/egusphere-egu22-3958. URL `https://doi.org/10.5194/egusphere-egu22-3958`.

K. Balidakis, S. Glaser, F. Zus, T. Nilsson, and H. Schuh. On the multi-technique combination with atmospheric ties. In *EGU General Assembly 2020*, 2020.

K. Balidakis, C. Kitpracha, K. Sosnica, J. Wang, S. Glaser, R. Heinkelmann, H. Dobslaw, and D. Thaller. Combination of GNSS, VLBI, and SLR at the Normal Equation Level with Local, Global, and Atmospheric Ties. In *XXVIII General Assembly of the International Union of Geodesy and Geophysics (IUGG)*. GFZ German Research Centre for Geosciences, 2023.

C. Bizouard, S. Lambert, C. Gattano, O. Becker, and J.-Y. Richard. The IERS EOP 14C04 solution for Earth orientation parameters consistent with ITRF 2014. *Journal of Geodesy*, 93(5):621–633, 2019.

G. Blewitt. GPS and Space-Based Geodetic Methods. *Treatise on Geophysics: Second Edition*, 3:307–338, 1 2015. doi: 10.1016/B978-0-444-53802-4.00060-9.

O. Bock, P. Willis, M. Lacarra, and P. Bosser. An inter-comparison of zenith tropospheric delays derived from DORIS and GPS data. *Advances in Space Research*, 46:1648–1660, 12 2010. ISSN 02731177. doi: 10.1016/j.asr.2010.05.018.

J. Boehm, B. Werl, and H. Schuh. Troposphere mapping functions for GPS and very long baseline interferometry from European Centre for Medium-Range Weather Forecasts operational analysis data. *Journal of Geophysical Research: Solid Earth*, 111, 2 2006. ISSN 21699356. doi: 10.1029/2005JB003629.

J. Böhm, D. Salstein, M. M. Alizadeh, and D. D. Wijaya. Geodetic and atmospheric background. In *Atmospheric effects in space geodesy*, pages 1–33. Springer, 2013.

E. Brockmann, D. Ineichen, M. Kistler, U. Marti, S. Schaer, A. Schlatter, B. Vogel, A. Wiget, and U. Wild. National Report of Switzerland. In *EUREF-Symposium, San Sebastian, Spain*, pages 25–27, 2016.

F. Brunner and J. Rüeger. Theory of the local scale parameter method for EDM. *Bulletin géodésique*, 66(4): 355–364, 1992.

W. Cannon. Overview of VLBI. *International VLBI service for geodesy and astrometry*, pages 13–17, 1999.

P. Charlot, C. Jacobs, D. Gordon, S. Lambert, A. De Witt, J. Böhm, A. Fey, R. Heinkelmann, E. Skurikhina, O. Titov, et al. The third realization of the International Celestial Reference Frame by very long baseline interferometry. *Astronomy & Astrophysics*, 644:A159, 2020.

G. Chen and T. Herring. Effects of atmospheric azimuthal asymmetry on the analysis of space geodetic data. *Journal of Geophysical Research: Solid Earth*, 102(B9):20489–20502, 1997.

R. Dach, S. Lutz, P. Walser, and P. Fridez. *Bernese GNSS software version 5.2.* University of Bern, Bern Open Publishing, 2015.

S. De Haan, E. Pottiaux, J. Sánchez-Arriola, M. Bender, J. Berckmans, H. Brenot, C. Bruyninx, L. De Cruz, G. Dick, N. Dymarska, et al. Use of GNSS Tropospheric Products for High-Resolution, Rapid-Update NWP and Severe Weather Forecasting (Working Group 2). In *Advanced GNSS Tropospheric Products for Monitoring Severe Weather Events and Climate: COST Action ES1206 Final Action Dissemination Report*, pages 203–265. Springer, 2019.

S. D. Desai and A. E. Sibois. Evaluating predicted diurnal and semidiurnal tidal variations in polar motion with GPS-based observations. *Journal of Geophysical Research: Solid Earth*, 121(7):5237–5256, 2016. doi: https://doi.org/10.1002/2016JB013125. URL `https://agupubs.onlinelibrary.wiley.com/doi/abs/10.1002/2016JB013125`.

P.-K. Diamantidis, G. Kłopotek, and R. Haas. VLBI and GPS inter-and intra-technique combinations on the observation level for evaluation of TRF and EOP. *Earth, Planets and Space*, 73:1–16, 2021. ISSN 1880-5981.

J. Douša, G. Dick, Y. Altiner, F. Alshawaf, J. Bosy, H. Brenot, E. Brockmann, R. Brožková, Z. Deng, W. Ding, K. Eben, M. Eliaš, R. Fernandes, A. Ganas, A. Geiger, G. Guerova, T. Hadaś, C. Hill, P. Hordyniec, F. Hurter, J. Jones, M. Kačmařík, K. Kaźmierski, J. Kaplon, P. Krč, D. Landskron, X. Li, C. Lu, J. P. Martins, G. Möller, L. Morel, G. Ófeigsson, R. Pacione, C. Pikridas, E. Pottiaux, J. Resler, W. Rohm, A. Sá, J. Sammer, T. Simeonov, W. Söhne, A. Stoycheva, A. Stürze, S. Rozsa, F. N. Teferle, S. Thorsteinsson, P. Václavovic, H. Valentim, B. Van Schaeybroeck, P. Viterbo, K. Wilgan, L. Yang, L. Zhao, N. Zinas, and F. Zus. Advanced GNSS Processing Techniques (Working Group 1). In J. Jones, G. Guerova, J. Douša, G. Dick, S. de Haan, E. Pottiaux, O. Bock, R. Pacione, and R. van Malderen, editors, *Advanced GNSS Tropospheric Products for Monitoring Severe Weather Events and Climate*, pages 33–201, Cham, 2020. Springer International Publishing. ISBN 978-3-030-13901-8.

G. Elgered and J. Wickert. *Monitoring of the Neutral Atmosphere*, pages 1109–1138. Springer International Publishing, Cham, 2017. ISBN 978-3-319-42928-1. doi: 10.1007/978-3-319-42928-1_38. URL `https://doi.org/10.1007/978-3-319-42928-1_38`.

S. Glaser, R. König, K. H. Neumayer, T. Nilsson, R. Heinkelmann, F. Flechtner, and H. Schuh. On the impact of local ties on the datum realization of global terrestrial reference frames. *Journal of Geodesy*, 93:655–667, 5 2019. ISSN 14321394. doi: 10.1007/s00190-018-1189-0.

R. Gross, G. Beutler, and H.-P. Plag. *Integrated scientific and societal user requirements and functional specifications for the GGOS*, pages 209–224. Springer Berlin Heidelberg, Berlin, Heidelberg, 2009. ISBN 978-3-642-02687-4. doi: 10.1007/978-3-642-02687-4_7. URL `https://doi.org/10.1007/978-3-642-02687-4_7`.

R. Heinkelmann, J. Böhm, S. Bolotin, G. Engelhardt, R. Haas, R. Lanotte, D. MacMillan, M. Negusini, E. Skurikhina, O. Titov, et al. VLBI-derived troposphere parameters during CONT08. *Journal of Geodesy*, 85(7):377–393, 2011.

R. Heinkelmann, P. Willis, Z. Deng, G. Dick, T. Nilsson, B. Soja, F. Zus, J. Wickert, and H. Schuh. Multi-technique comparison of atmospheric parameters at the DORIS co-location sites during CONT14. *Advances in Space Research*, 58:2758–2773, 12 2016. ISSN 18791948. doi: 10.1016/j.asr.2016.09.023.

T. Herring. Modeling atmospheric delays in the analysis of space geodetic data. *Proceedirws of Refraction of Transatmospheric simals in Geodesy, eds. JC De Munck and TA Spoelstra, Netherlands Geodetic Commission Publications on Geodesy*, 36(4), 1992.

H. Hersbach, B. Bell, P. Berrisford, S. Hirahara, A. Horányi, J. Muñoz-Sabater, J. Nicolas, C. Peubey, R. Radu, D. Schepers, A. Simmons, C. Soci, S. Abdalla, X. Abellan, G. Balsamo, P. Bechtold, G. Biavati, J. Bidlot, M. Bonavita, G. D. Chiara, P. Dahlgren, D. Dee, M. Diamantakis, R. Dragani, J. Flemming, R. Forbes, M. Fuentes, A. Geer, L. Haimberger, S. Healy, R. J. Hogan, E. Hólm, M. Janisková, S. Keeley, P. Laloyaux, P. Lopez, C. Lupu, G. Radnoti, P. de Rosnay, I. Rozum, F. Vamborg, S. Villaume, and J.-N. Thépaut. The ERA5 global reanalysis. *Quarterly Journal of the Royal Meteorological Society*, 146:1999–2049, 2020. doi: https://doi.org/10.1002/qj.3803. URL `https://rmets.onlinelibrary.wiley.com/doi/abs/10.1002/qj.3803`.

T. Hobiger and N. Jakowski. *Atmospheric Signal Propagation*, pages 165–193. Springer International Publishing, Cham, 2017. ISBN 978-3-319-42928-1. doi: 10.1007/978-3-319-42928-1_6. URL `https://doi.org/10.1007/978-3-319-42928-1_6`.

H. Hopfield. Two-Quartic Tropospheric Refractivity Profile for Correcting Satellite Data. *Journal of Geophysical research*, 74, 1969. doi: 10.1029/JC074i018p04487.

J. Jones. Scientific Background. In J. Jones, G. Guerova, J. Douša, G. Dick, S. de Haan, E. Pottiaux, O. Bock, R. Pacione, and R. van Malderen, editors, *Advanced GNSS Tropospheric Products for Monitoring Severe Weather Events and Climate*, pages 1–15, Cham, 2020. Springer International Publishing. ISBN 978-3-030-13901-8.

C. Kitpracha, K. Balidakis, R. Heinkelmann, and H. Schuh. Assessment on atmospheric parameters at co-location sites. *EGU2020*, 3 2020. doi: 10.5194/EGUSPHERE-EGU2020-6517. URL `https://meetingorganizer.copernicus.org/EGU2020/EGU2020-6517.html`.

C. Kitpracha, T. Nilsson, R. Heinkelmann, K. Balidakis, S. Modiri, and H. Schuh. The impact of estimating common tropospheric parameters for co-located VLBI radio telescopes on geodetic parameters during CONT17. *Advances in Space Research*, 2022. ISSN 18791948. doi: 10.1016/j.asr.2022.02.013.

C. Kitpracha, R. Heinkelmann, M. Ramatschi, K. Balidakis, B. Männel, and H. Schuh. Validation of tropospheric ties at the test setup GNSS co-location site in Potsdam. Submitted to Journal of Earth, Planets and Space, submitted.

J. Kouba and P. Héroux. Precise Point Positioning Using IGS Orbit and Clock Products. *GPS Solutions*, 5(2): 12–28, 2001. ISSN 1080-5370. doi: 10.1007/PL00012883. URL `http://dx.doi.org/10.1007/PL00012883`.

M. Krügel, D. Thaller, V. Tesmer, M. Rothacher, D. Angermann, and R. Schmid. Tropospheric parameters: combination studies based on homogeneous VLBI and GPS data. *Journal of Geodesy*, 81(6):515–527, 2007. ISSN 1432-1394. doi: 10.1007/s00190-006-0127-8. URL `http://dx.doi.org/10.1007/s00190-006-0127-8`.

H. Krásná, J. Böhm, and H. Schuh. Tidal Love and Shida numbers estimated by geodetic VLBI. *Journal of Geodynamics*, 70:21–27, 10 2013. ISSN 0264-3707. doi: 10.1016/J.JOG.2013.05.001.

K. Lagler, M. Schindelegger, J. Böhm, H. Krásná, and T. Nilsson. Gpt2: Empirical slant delay model for radio space geodetic techniques), gpt2: Empirical slant delay model for radio space geodetic techniques. *Geophys. Res. Lett*, 40:1069–1073, 2013. doi: 10.1002/grl.50288. URL `https://agupubs.onlinelibrary.wiley.com/doi/10.1002/grl.50288`.

D. Landskron and J. Böhm. VMF3/GPT3: refined discrete and empirical troposphere mapping functions. *Journal of Geodesy*, 92:349–360, 4 2018. ISSN 14321394. doi: 10.1007/s00190-017-1066-2.

R. B. Langley, P. J. Teunissen, and O. Montenbruck. *"Introduction to GNSS"*, pages 3–23. "Springer International Publishing", Cham, 2017. ISBN 978-3-319-42928-1. doi: 10.1007/978-3-319-42928-1_1. URL `https://doi.org/10.1007/978-3-319-42928-1_1`.

R. Leandro, M. Santos, and R. Langley. Unb neutral atmosphere models: development and performance. In *Proceedings of the 2006 national technical meeting of the institute of navigation*, pages 564–573, 2006.

N. R. Lomb. Least-squares frequency analysis of unequally spaced data. *Astrophysics and Space Science*, 39(2): 447–462, 1976.

D. MacMillan. Atmospheric gradients from very long baseline interferometry observations. *Geophysical Research Letters*, 22(9):1041–1044, 1995.

D. MacMillan and C. Ma. Atmospheric gradients and the VLBI terrestrial and celestial reference frames. *Geophysical Research Letters*, 24(4):453–456, 1997.

J. W. Marini. Correction of satellite tracking data for an arbitrary tropospheric profile. 7:223–231, 1972. doi: 10.1029/RS007i002p00223. URL `https://agupubs.onlinelibrary.wiley.com/doi/10.1029/RS007i002p00223`.

T. Nilsson, J. Böhm, D. D. Wijaya, A. Tresch, V. Nafisi, and H. Schuh. *Path Delays in the Neutral Atmosphere*, pages 73–136. Springer Berlin Heidelberg, Berlin, Heidelberg, 2013. ISBN 978-3-642-36932-2. doi: 10.1007/978-3-642-36932-2_3. URL `https://doi.org/10.1007/978-3-642-36932-2_3`.

T. Nilsson, M. Karbon, B. Soja, R. Heinkelmann, C. Lu, and H. Schuh. Atmospheric modeling for co-located VLBI antennas and twin telescopes. *Journal of Geodesy*, 89:655–665, 2015. ISSN 1432-1394.

A. Nothnagel. Conventions on thermal expansion modelling of radio telescopes for geodetic and astrometric VLBI. *Journal of Geodesy*, 83(8):787–792, 2009.

D. Odijk. *Positioning Model*, pages 605–638. Springer International Publishing, Cham, 2017. ISBN 978-3-319-42928-1. doi: 10.1007/978-3-319-42928-1_21. URL `https://doi.org/10.1007/978-3-319-42928-1_21`.

G. Petit and B. Luzum. IERS conventions (2010). Technical report, Bureau International des Poids et mesures sevres (france), 2010.

B. Petrachenko, A. Niell, D. Behrend, B. Corey, J. Böhm, P. Chralot, A. Collioud, J. Gipson, R. Haas, T. Hobiger, et al. Design aspects of the VLBI2010 system-Progress report of the IVS VLBI2010 committee. Technical report, 2009.

L. Petrov and J.-P. Boy. Study of the atmospheric pressure loading signal in very long baseline interferometry observations. *Journal of Geophysical Research: Solid Earth*, 109(B3), 2004. doi: https://doi.org/10.1029/2003JB002500. URL `https://agupubs.onlinelibrary.wiley.com/doi/abs/10.1029/2003JB002500`.

H.-P. Plag, M. Rothacher, M. Pearlman, R. Neilan, and C. Ma. The global geodetic observing system. In *Advances in Geosciences: Volume 13: Solid Earth (SE)*, pages 105–127. World Scientific, 2009.

M. Poutanen and S. Rózsa. The Geodesist's Handbook 2020. *Journal of Geodesy*, 94, 11 2020. ISSN 14321394. doi: 10.1007/s00190-020-01434-z.

V. Puente, E. Azcue, Y. Gomez-Espada, and S. Garcia-Espada. Comparison of common VLBI and GNSS estimates in CONT17 campaign. *Journal of Geodesy*, 95, 11 2021. ISSN 14321394. doi: 10.1007/s00190-021-01565-x.

M. Rothacher. Combination of space-geodetic techniques. In *NASA CONFERENCE PUBLICATION*, pages 33–44. NASA; 1998, 2002.

M. Rothacher, D. Angermann, T. Artz, W. Bosch, H. Drewes, M. Gerstl, R. Kelm, D. König, R. König, B. Meisel, H. Müller, A. Nothnagel, N. Panafidina, B. Richter, S. Rudenko, W. Schwegmann, M. Seitz, P. Steigenberger, S. Tesmer, V. Tesmer, and D. Thaller. GGOS-D: Homogeneous reprocessing and rigorous combination of space geodetic observations. *Journal of Geodesy*, 85:679–705, 10 2011. ISSN 09497714. doi: 10.1007/s00190-011-0475-x.

J. Saastamoinen. Atmospheric correction for the troposphere and stratosphere in radio ranging satellites. *The use of artificial satellites for geodesy*, 15:247–251, 1972.

J. D. Scargle. Studies in astronomical time series analysis. ii-statistical aspects of spectral analysis of unevenly spaced data. *The Astrophysical Journal*, 263:835–853, 1982.

H. Schuh and D. Behrend. VLBI: A fascinating technique for geodesy and astrometry, 10 2012. ISSN 02643707.

H. Schuh and J. Böhm. Very long baseline interferometry for geodesy and astrometry. In *Sciences of Geodesy-II*, pages 339–376. Springer, 2013.

H. Schuh and J. Böhm. Very Long Baseline Interferometry for Geodesy and Astrometry. *Sciences of Geodesy - II: Innovations and Future Developments*, pages 339–376, 1 2013. doi: 10.1007/978-3-642-28000-9_7. URL `https://link.springer.com/chapter/10.1007/978-3-642-28000-9_7`.

H. Schuh, R. Heinkelmann, G. Beyerle, J. M. Anderson, K. Balidakis, S. Belda, S. Dhar, S. Glaser, O. Jenie, M. Karbon, et al. The Potsdam Open Source Radio Interferometry Tool (PORT). *Publications of the Astronomical Society of the Pacific*, 133(1028):104503, 2021.

I. Selmke, R. Dach, D. Arnold, L. Prange, S. Schaer, D. Sidorov, P. Stebler, A. Villiger, A. Jäggi, and U. Hugentobler. CODE repro3 product series for the IGS. 2020. doi: 10.7892/BORIS.135946. URL `https://boris.unibe.ch/135946/`.

K. Sośnica. *Determination of precise satellite orbits and geodetic parameters using satellite laser ranging*. Astronomical Institute, University of Bern, Switzerland, 2014.

O. J. Sovers, J. L. Fanselow, and C. S. Jacobs. Astrometry and geodesy with radio interferometry: Experiments, models, results. *Reviews of Modern Physics*, 70:1393–1454, 1998. ISSN 00346861. doi: 10.1103/REVMODPHYS.70.1393.

P. Steigenberger, V. Tesmer, M. Krügel, D. Thaller, R. Schmid, S. Vey, and M. Rothacher. Comparisons of homogeneously reprocessed GPS and VLBI long time-series of troposphere zenith delays and gradients. *Journal of Geodesy*, 81(6):503–514, 2007. ISSN 1432-1394. doi: 10.1007/s00190-006-0124-y. URL `http://dx.doi.org/10.1007/s00190-006-0124-y`.

J. Subirana, J. Zornoza, and M. Hernández-Pajares. GNSS DATA PROCESSING: Volume I: Fundamentals and Algorithms (ESA TM-23/1, May 2013). *ESA Communications ESTEC, the Netherlands*, 2013a.

J. S. Subirana, J. M. J. Zornoza, and M. Hernández-Pajares. GNSS DATA PROCESSING Volume I: Fundamentals and Algorithms Acknowledgements. 2013b. URL `www.esa.int`.

K. Teke, J. Böhm, T. Nilsson, H. Schuh, P. Steigenberger, R. Dach, R. Heinkelmann, P. Willis, R. Haas, S. García-Espada, T. Hobiger, R. Ichikawa, and S. Shimizu. Multi-technique comparison of troposphere zenith delays and gradients during CONT08. *Journal of Geodesy*, 85:395–413, 7 2011. ISSN 09497714. doi: 10.1007/s00190-010-0434-y.

P. J. Teunissen and O. Montenbruck. *Springer handbook of global navigation satellite systems*, volume 10. Springer, 2017.

D. Thaller. *Inter-technique combination based on homogeneous normal equation systems including station coordinates, Earth orientation and troposphere parameters*. PhD thesis, Technische Universität München, 2008.

A. Villiger, R. Dach, S. Schaer, L. Prange, F. Zimmermann, H. Kuhlmann, G. Wübbena, M. Schmitz, G. Beutler, and A. Jäggi. GNSS scale determination using calibrated receiver and Galileo satellite antenna patterns. *Journal of geodesy*, 94:1–13, 2020.

J. Wang, M. Ge, S. Glaser, K. Balidakis, R. Heinkelmann, and H. Schuh. Improving VLBI analysis by tropospheric ties in GNSS and VLBI integrated processing. *Journal of Geodesy*, 96:1–15, 4 2022. ISSN 14321394. doi: 10.1007/S00190-022-01615-Y/FIGURES/8. URL `https://link.springer.com/article/10.1007/s00190-022-01615-y`.

A. R. Whitney. How Do VLBI Correlators Work? In *International VLBI Service for Geodesy and Astrometry 2000 General Meeting Proceedings*, pages 187–205, 2000.

G. Xu and Y. Xu. *GPS: Theory, algorithms and applications, third edition*. Springer Berlin Heidelberg, 1 2016. ISBN 9783662503676. doi: 10.1007/978-3-662-50367-6.

F. Zus, M. Bender, Z. Deng, G. Dick, S. Heise, M. Shang-Guan, and J. Wickert. A methodology to compute GPS slant total delays in a numerical weather model. *Radio Science*, 47:2018, 4 2012. ISSN 1944-799X. doi: 10.1029/2011RS004853. URL https://onlinelibrary.wiley.com/doi/full/10.1029/2011RS004853https://onlinelibrary.wiley.com/doi/abs/10.1029/2011RS004853https://agupubs.onlinelibrary.wiley.com/doi/10.1029/2011RS004853.

F. Zus, G. Dick, J. Douša, S. Heise, and J. Wickert. The rapid and precise computation of GPS slant total delays and mapping factors utilizing a numerical weather model. *Radio Science*, 49:207–216, 2014. ISSN 1944-799X.